Fermi National Accelerator Laboratory

FERMILAB-Conf-90/254-E
[E-741/CDF]

Recent Results from Hadron Colliders *

The CDF Collaboration

presented by

Henry J. Frisch
University of Chicago
Chicago, Illinois 60637

December 10, 1990

* Invited talk presented at the XIIth International Conference on Particles and Nuclei (PANIC 90), Cambridge, Massachusetts, June 25-29, 1990.

Operated by Universities Research Association Inc. under contract with the United States Department of Energy

EFI 90-83
Fermilab-CONF-90/254-E
CDF/PUB/CDF/PUBLIC/1326
December 10, 1990

Recent Results from Hadron Colliders

Henry J. Frisch
The Enrico Fermi Institute and Physics Department
University of Chicago

Invited Talk at PANIC XII, MIT, June 25-29, 1990

Abstract

This is a summary of some of the many recent results from the CERN and Fermilab colliders, presented for an audience of nuclear, medium-energy, and elementary particle physicists. The topics are jets and QCD at very high energies, precision measurements of electroweak parameters, the remarkably heavy top quark, and new results on the detection of the large flux of B mesons produced at these machines. A summary and some comments on the bright prospects for the future of hadron colliders conclude the talk.

1 Introduction

This talk is for the non-specialist, as I know that many of you, while expert in related fields, are not high-energy elementary particle physicists. It tries to convey the remarkable progress in exploring the highest available energies in the last two years. We know now that the top quark mass is at least as large as the masses of the vector bosons. We also now have seen constituent scatterings at a center-of-mass energy of 1 TeV. It is at these very high energies as well as in precision measurements at lower energies that we look for surprises.

Hadron-hadron colliders are the source of our highest available energies. The Tevatron with a 1-km radius has a center of mass energy of 1.8 TeV; the SSC will have 40 TeV. In contrast the premier electron machine, LEP, with a radius more than four times larger than that of the Tevatron, can achieve on the order of 100 GeV, and, after an upgrade, will be able to go to 200 GeV. The SLAC *R&D* project SLC, being a linear collider, can also achieve 90 GeV in its 2-mile length, although so far at much lower luminosity.

The strength of the hadron machines is in the ability to explore the highest energy regime. New phenomena such as the top quark, supersymmetry, the lowest state of technicolor, and new heavy W and Z bosons can best be searched for at a hadron collider. It is an advantage for exploration that the initial state is not well-defined in its energy or other quantum numbers such as charge, being a sum of

gluons and the many flavors of quarks. The production of (charged) W bosons, and of B mesons from gluon collisions are two examples. Hadron machines and lepton colliders complement each other remarkably well; a future TeV e^+e^- collider may well be the tool to make precision measurements of phenomena discovered at the LHC or SSC.

Because one is seeing collisions of the constituents of the hadrons the full beam energy is in general not available in the parton-parton center-of-mass. There is an often quoted rule-of-thumb that a hadron collider is equivalent to an electron machine at one third the energy. This is also overly simplistic– there are parton-parton collisions at energies all the way up to the full energy, but the effective luminosity falls with increasing energy. One consequently has to compare the available energy in hadron machines and electron machines at a given luminosity. Hadron colliders can achieve very high luminosities, and consequently the 'reach' can extend out to values far beyond the third of the simple rule-of-thumb. Moreover different processes may have different cross-sections, some being much larger than the electroweak cross-sections. At the present Tevatron in $\bar{p}p$ collisions, for example, one already observes parton-parton collisions with a center-of-mass energy over half the available energy. The luminosity is expected to increase substantially in the future, extending the reach well beyond the current limits. For example, with an integrated luminosity of $1 fb^{-1}$ at 2 TeV one should be able to discover a strongly interacting resonance with a mass of 1 TeV if it exists (the dijet mass spectrum extends appreciably further). A similar exposure would discover a Z-prime with a mass of 800 GeV, or a W-prime at 1 TeV. Higher luminosities, such as would be available in proton-proton machines, extend the energy reach even further for some processes. These kinds of measurements, in particular measurements of jets at very high energies and very high Q^2 tests of QCD, are the subjects of the first physics section (Section 3) of this talk, following a brief introduction to the detectors in Section 2.

It has surprised some people that one can do precision measurements at a hadron collider (though probably it does not surprise any experimentalist in this audience.) The measurement of the Z mass by the CDF collaboration [1] established the power of a first-rate magnetic spectrometer, and although the measurements at LEP [2] and SLC [3] made by scanning the beam energy rather than analyzing the energies of the decay products are now much more precise, the point that the events are clean and emminently analyzable is well established. The CDF collaboration [4] estimates that with an integrated luminosity of 500 pb^{-1}, if the systematic errors continue to scale with statistics, an uncertainty on the W mass of 50 MeV (out of 80 GeV) may be possible. This measurement would be competitive with that from LEP200. The status of measurements of electroweak parameters is the subject of the fourth section of this talk, with special emphasis on the W mass and width.

The search for the top quark, which only recently is known to be much heavier than any of the other quarks or the leptons, and is at least as heavy as the

W and Z bosons themselves, is described in the fifth section. That the top quark is so heavy is in itself an immensely interesting recent result.

The last section before the summary presents the recent work on the identification of B mesons in $\bar{p}p$ collisions. The cross-section for b quark production is large, being 45 microbarns or so at a center-of-mass energy ($\sqrt{s}$) of 1.8 TeV. The Tevatron running at its present peak luminosity of $2 \times 10^{30} cm^{-2} sec^{-1}$ thus produces 90 b quarks per second. The challenge for the experimenter is to be able to see them. It is an interesting contrast to the e^+e^- B factory proposals, where the experimenting is easier, but building a machine with sufficient luminosity is the challenge. For some cases, such as the rare decay $B \rightarrow \mu\mu$ and $B \rightarrow \psi K$ the signature is very clean, and the hadron colliders should be able to exploit the large B cross-sections.

These past two years have seen a sea-change for hadron collider experiments. The two CERN experiments have increased their data sample by almost a factor of ten. In this country the Tevatron performed at a luminosity a factor of 10 higher than predicted, and consequently the CDF experiment accumulated a large data set. The higher energy at Fermilab leads to W and Z boson cross-sections about a factor of 3 higher than those at CERN, and the cross-sections for a heavy top quark, for example, are much larger yet (a factor of 30 at a mass of 100 GeV, for example).

One last introductory comment. Future accelerators- the upgraded Tevatron, the LHC, and the SSC - will be difficult to use, and we need to learn how to exploit them. The most important new result from the present hadron colliders is perhaps the realization, based on the new very large data sets accumulated at CERN and Fermilab, of the potential not only for exploration at the highest energies, but also for precision measurements such as the W mass and the detailed spectroscopy and exploration of T and B mesons at a remarkable level of sensitivity. We have just begun.

2 Detectors - UA1, UA2, and CDF

The detectors built by the UA1[5], UA2[6], and CDF[7] collaborations are all large detectors with tracking chambers and large solid angle calorimeters. The detectors themselves are well documented– I will limit myself to a few brief remarks on their respective strengths and weaknesses.

The UA1 detector is shown in Figure 1a in plan view. For the new data run, its main strength is in its large-solid angle muon coverage, and its beautiful tracking chamber imbedded in a dipole magnet. Its main weakness is in its much-diminished calorimeter capability. For this run the electromagnetic calorimeters shown in Figure 1a were absent, and only the hadron calorimeters were in place. This was the unhappy result of an intended upgrade to warm-liquid calorimeters which, if successful, would have resulted in much improved calorimetry.

The upgraded UA2 detector used in the last data taking is shown in Figure 1b. Its strengths are in its electron and jet identification, and good calorimetry over

a large solid angle. The central calorimeters in particular are well understood as a result of years of extensive work with test beams. Seen from my vantage point of CDF, some analyses are hindered by the lack of a magnet. There is no muon coverage in the new configuration.

The CDF detector (Figure 1c) strengths are the precision momentum measurement of charged tracks with a solenoidal magnet in the central region, good electron identification, good muon identication over a limited region, decent calorimetry over large solid angle, and the higher energy of the Fermilab Tevatron. A weakness is the limited muon coverage, which is being fixed as an upgrade to the detector.

3 Jets and QCD - Very High Q^2 Tests

Jet physics has gone from the days when it was arguable whether or not jets existed [8] to being a rather precise experimental science. A jet is defined by the UA2 collaboration [9], for example, as a cluster of calorimeter towers with energy greater than 400 MeV with a common tower side to a tower that is a local maximum in transverse energy ($E_{\rm T}$). In CDF, the jet algorithm is a cone algorithm: a circle with radius 0.7 in rapidity-azimuth ($\eta - \phi$) space is drawn about any tower with at least 1 GeV in transverse energy ($E_{\rm T}$). Towers with transverse energy greater than 0.2 GeV are added to the seed tower, the energy-weighted centroid is calculated, and a new circle is formed. The process is repeated until the list of towers in the circle remains unchanged. If two such clusters overlap such that one shares more than 50% the two are merged into one jet; otherwise the common towers are assigned to the nearest cluster. In both cases corrections must be made for energy leakage out of the cluster or cone, for energy from the 'underlying event' that leaks in, and for the detector's dimished response to low energy particles as well as energy lost in cracks.

3.1 The Jet Invariant Mass and Pt Spectra

The invariant mass spectrum for two jets as measured by the UA2 collaboration at a c.m energy ($\sqrt{s}$) of 630 GeV is shown in Figure 2. The UA2 collaboration has made a remarkable analysis of the mass spectrum in the region of the W mass, and sees a clear peak above the falling QCD spectrum from the (two-body) decay of the W into two jets. This is shown in Figure 3; the peak has 5620 ± 1130 events. From the measured $W \rightarrow e\nu$ rate and the Standard Model couplings the predicted number of events is 4250 ± 150 events, in good agreement (a measurement from a previous data run with much poorer statistics had seen about twice the number expected, but the discrepancy was not statistically significant.) The fitted mass is 78.9 ± 1.5 GeV, in good agreement with the world value from the lepton decay mode measurements. The width of the peak is completely dominated by the resolution, and has a σ of 9.3 ± 2.0 GeV. The total decay width of the W has recently been measured to better

than 10% (see Section 4 below) and is in very good agreement with the Standard Model prediction, so that one would be very surprised if the quark decays of the W were at a different rate from expected. However the measurement strikingly demonstrates both the resolution and the calibration of the UA2 calorimeters.

The same quantity, the dijet invariant mass distribution, as measured by the CDF collaboration at $\sqrt{s} = 1800\ GeV$ is shown in Figure 4. A cone of radius 0.7 in $\eta - \phi$ space is used to find the jets. For this spectrum the two highest E_T jets are required to be in the central region, $|\eta| < 0.7$, and to be back-to-back in azimuth ($\Delta\phi = 180 \pm 30\,\mathrm{deg}$). The data are preliminary, and the corrections for resolution effects have not been included (but are not enormous) in this plot. The average systematic uncertainty from the energy scale and other effects is shown in the lower left. Also shown is a band representing a range of typical theoretical predictions obtained by varying the Q^2 scale from twice P_T^2 to half P_T^2, and varying the choice of parton distribution funcitions among ELHQ1, EHLQ2, DO1, and DO2[10]. The agreement is remarkable; in Figure 5 the rato of data minus prediction to prediction is plotted on a *linear* scale although the spectrum falls 6 orders of magnitude with increasing mass. The normalization in Figures 4 and 5 is absolute (in itself remarkable).

3.2 Do Partons Themselves Have Structure?

Suppose that the partons themselves have a size. Then at some momentum transfer, and hence wavelength of the probe, one will see the cross-section for parton-parton scattering stop falling inversely as the c.m energy and become purely geometrical. The interaction is thus characterized by a new energy scale, which we will denote as Λ. A more sensitive search for such a 'contact' term can be done at the Tevatron than at CERN because of the three times higher energy.

Figure 6 shows the measured invariant mass spectrum from CDF, with the QCD prediction alone, and also with a specific form for the contact term [11] added. At 95% *C.L.*, CDF finds a limit of $\Lambda > 950$ GeV. Crudely speaking, this means that the quarks and gluons are pointlike down to distances of about $2 \times 10^{-4}\ fm$.

3.3 MultiJet Events

In hadron colliders the energies are high enough so that there is a lot of 'room' (in phase space) for many jets in a single event. Figure 7a shows the 'Lego' plot of transverse energy in $\eta - \phi$ space for a typical 3-jet event in the CDF detector. In Figure 7b the tracking chamber display for this event is shown in the r-ϕ view, showing clearly the jet structure of the two jets that are in the central region.

The UA2 experiment has compared the structure of 4-jet events to leading-order calculations of Kunszt and Stirling [12]. Events with the two highest E_T jets greater than 30 GeV and with an azimuthal separation of at least 143^0 are selected.

The third and fourth largest jets are required to be greater than 15 GeV in E_T. All jets must be within $|\eta| < 2$. These requirements leave 857 events in an exposure of 3.1 pb^{-1}. Figure 8 shows distributions in the 4-jet mass, sphericity, and the angles between the respective jets compared to the theoretical predictions. The theory agrees very well with the measurements.

The CDF experiment has made similar comparisons of 3-jet events to the Papageno QCD program predictions in leading order [13]. Each jet is required to have E_T greater than 10 GeV, and to be within $|\eta| < 3.5$. In addition, the three-jet invariant mass must be larger than 200 GeV. There are 4973 events in a 2.2 pb^{-1} sample. Figure 9a shows the distribution of the number of events versus the fraction of the 3-jet mass carried by the leading (highest E_T) jet[14]. The solid line is the Papageno program QCD prediction; the dashed line is phase space. Figure 9b shows the similar distribution for the next highest E_T jet. Again the QCD prediction is the solid line; it agrees well with the data. The dashed line represents the prediction from phase space only (no matrix elements), and is in poor agreement with the data.

4 Electroweak Parameters

The masses of the W and Z bosons are fundamental quantities in the Standard Model [15]. Ignoring radiative corrections, they are both proportional to the vacuum expectation value of the Higgs field V:

$$M_W = \frac{1}{2}gV \tag{1}$$

and

$$M_Z = \frac{1}{2}\sqrt{g^2 + g'^2}V, \tag{2}$$

where g is the coupling constant of the $SU(2)_L$ isotriplet bosons $W^{1,2,0}$ to the left-handed weak currents and g' is the coupling for the U(1) of the isosinglet B to the hypercharge current. The weak mixing angle $\sin\theta_W$ is thus determined directly by the ratio of the W and Z masses by:

$$\cos\theta_W = M_W/M_Z \tag{3}$$

Radiative corrections change these predictions for the W and Z masses[16]. There is a self-energy loop diagram for the W where the W couples to a virtual $t\bar{b}$ pair. The Z has a similar diagram for a $t\bar{t}$. The contributions of these diagrams increases with top mass as m_t^2/m_W^2. One can thus put an upper limit on the top mass from a comparison of θ_W measured from the W and Z masses and from low energy determinations of the couplings from measurements of neutrino scattering, α, and G_{Fermi}, or measurements of the g and g' couplings directly from the Z [17]. A similar limit applies to new heavy generations of quarks provided the 'top' and 'bottom' quarks are very different in mass as in the top and bottom cases [18].

At present measurements of W bosons are the sole province of the hadron colliders at CERN and Fermilab.

4.1 The W Boson Mass

The measurement of the W boson mass depends on the fact that the decay $W \rightarrow e\nu$ is a two-body decay. The transverse momentum spectrum of the leptons consequently peaks at half the mass of the W. As the W is heavy the signature of a high P_T monochromatic electron should be striking, and the mass of the W then can in principle be determined easily from the electron spectrum as being twice the energy of the electron [19].

This seemingly neat experimental picture is, however, more complicated. First, the W is not made at rest, either in the longitudinal (along the beam) direction or in the transverse. The transverse momentum of the W, P_T^W, which we believe arises largely from radiation of gluons from the incoming quarks [20], 'smears' the line-shape of the electron momentum. The longitudinal momentum of the W, which results from the fact that the experiment is not in the c.m. frame of the quark and anti-quark that annihilate into the W, contributes to the longitudinal momentum of the electron. Because of both effects, the electron is consequently not at-all monochromatic, and the sharp cut-off in the transverse components at half the mass of the W is appreciably blurred.

Second, the other particle in the two-body W decay is a neutrino. One consequently cannot directly reconstruct the invariant mass of the two leptons.

The solutions to these problems, such as they are, go as follows. One forgets the longitudinal components of momentum, as so much of the original beam momenta go down the vacuum pipe and are unmeasurable. One uses the large-solid-angle calorimeter to measure the *transverse* components of momentum of whatever recoils against the P_T of the W. This gives the transverse momentum of the neutrino from conservation of the transverse components:

$$P_T(\nu) + P_T(e) + P_T(hadrons) = 0 \tag{4}$$

$$P_T(\nu) = -(P_T(e) + P_T(hadrons)) \tag{5}$$

The invariant mass using just these transverse momentum components (called the transverse mass) is then calculated:

$$M_T^2 = 2E_T^e E_T^\nu (1 - cos(\Delta\phi)) \tag{6}$$

The spectrum in this measured quantity is then compared to Monte Carlo predictions with different input masses. The Monte Carlo programs must treat correctly the W pt spectrum, the detector resolution for both the lepton and the underlying hadronic event which gives the neutrino momentum, and the production

characteristics of the W's. Uncertainties in these quantities lead to systematic uncertainties in the W mass. The measurement is thus strongly dependent on one's understanding of the response of the detector both to the leptons and to the many particles which come out in the underlying event.

Figure 10 shows the spectra of electron transverse momentum, neutrino transverse momentum, and transverse mass, as measured by the UA2 collaboration [21]. The curve represents the Monte Carlo prediction for the best fit W mass. The W sample consists of 1203 $W \rightarrow e\nu$ events where the electron hits their central detector (Figure 1b), and the event has $20 < P_T^e < 60\ GeV$, $20 < P_T^\nu < 60\ GeV$, and $40 < m_T < 120\ GeV$. The shape is a fairly good fit in transverse mass, especially on the low side of the peak (however,the maximum information on the W mass is in the falling high-side edge.)

Table I is the UA2 summary [21] of their fits to different W distributions. One sees that the fits are statistically very good, and do not drift far when the W width is left free to float in the fit (a good sign, meaning that the resolutions and WP_T distributions are understood). Table II gives the UA2 summary of the corrections and systematic uncertainties in their mass determination. The total systematic uncertainty, excluding the overall energy scale, which is tied to the Z mass, is remarkably small– 0.2% on a measurement with a missing neutrino. When they adjust the overall energy scale so that their Z mass agrees with that measured at LEP, they find

$$M_W^{UA2} = 80.48 \pm 0.42(stat) \pm 0.24(syst.)\ GeV \tag{7}$$

The corresponding spectra in transverse mass for the CDF collaboration's measurement of the W mass are shown in Figure 11a for electrons and Figure 11b for muons. The momentum spectra for the electrons, muons, and neutrinos are shown in Figure 12.

In the CDF case the calibration of the energy scale of the calorimeters is done *in situ* using the magnetic spectrometer to measure the momentum of electrons. Tower-to-tower calibrations are made using a sample of 17,000 inclusive electrons, and the final overall scale is set by matching E (measured with the calorimeter) to P (measured with the tracking chamber and magnetic field) for electrons from W decay [22]. The W mass consequently is measured without referencing to the Z mass.

The results are:
muon channel:

$$M_W^{\mu CDF} = 79.90 \pm 0.53(stat) \pm 0.32(syst.) \pm 0.08(scale)\ GeV \tag{8}$$

electron channel:

$$M_W^{eCDF} = 79.91 \pm 0.35(stat) \pm 0.24(syst.) \pm 0.19(scale)\ GeV \tag{9}$$

They are embarrassingly close. When the two numbers are combined, treating common systematics correctly, the result is

$$M_W^{CDF} = 79.91 \pm 0.39\ GeV \tag{10}$$

The measurement of $\sin^2(\theta_W)$ depends only on the measurements of the W and Z masses. UA2 and CDF treat the measurement differently, a result of the different detector strengths. The energy scale is the dominant UA2 experimental uncertainty. UA2 consequently uses the ratio of their own measurements of the W mass and Z mass, in which the scale error cancels out, to get a measurement [21] of $\sin^2(\theta_W)$:

$$\sin^2(\theta_W)^{UA2} = 0.2202 \pm 0.0084(stat) \pm .0045(syst) \tag{11}$$

This gives an upper limit [21] on the top mass, assuming the Standard Model, of:

$$M_{Top} < 289\ GeV\ at\ 95\%\ Confidence\ Level \tag{12}$$

The relationship of M_W, M_Z and M_T and the UA2 results are shown in Figure 13.

CDF in contrast, uses the magnetic spectrometer to set an absolute energy scale. A summary of their systematic uncertainties is given in Table III. The overall uncertainty on $\sin^2(\theta_W)$ is smaller including the scale error on the W mass and using the precision measurement of the Z mass from LEP [2] than it would be taking the ratio of W and Z masses from CDF including the statistical error on the Z mass. CDF finds [22]:

$$\sin^2(\theta_W)^{CDF} = 0.2317 \pm 0.0075 \tag{13}$$

This leads, again assuming the Standard Model, to an upper limit on the top mass (see Figure 14) of:

$$M_{Top} < 220\ GeV\ at\ 95\%\ Confidence\ Level \tag{14}$$

Averaging the two determinations from UA2 and CDF, we find:

$$\sin^2(\theta_W)^{collider} = 0.2273 \pm 0.0059 \tag{15}$$

and a limit on the top mass that is naturally between the two individual limits:

$$M_{Top} < 230\ GeV\ at\ 95\%\ Confidence\ Level \tag{16}$$

4.2 The W Boson Width

The width of the W, Γ_W, measures the couplings of the W. One simple example of the power of the measurement is the dependence of Γ_W on the top mass. If $M_T << M_W$ the W decays into a $t\bar{b}$ and the W width is 33% larger than if the top

decay channel is closed to the W. One can thus search for the top quark completely independently of any specific decay mode of the top by measuring the W width. If the top quark decays in a non-standard fashion, such as to a charged Higgs scalar, the W width will still show the existence of the top if the top quark is light enough for the W to decay into it. The argument holds for other new couplings of the W, although most new effects would be expected to be at the percent level, smaller than the present sensitivity.

The measurement of the W width is indirect- it is a 'disappearance' experiment. It is a neat idea [23]. We believe we know how many W and Z bosons are created- this depends on the parton distribution functions and the standard model couplings of the quarks. We also know the partial widths for $W \rightarrow e\nu$ and $Z \rightarrow e^+e^-$, respectively. However the number of $W \rightarrow e\nu$ we observe also depends on the total width of the W- if there are other open channels open for the W to decay into, we will see fewer $W \rightarrow e\nu$ events.

In fact one measures the ratio of $W \rightarrow e\nu$ to $Z \rightarrow e^+e^-$ as the ratio of W to Z production is predicted highly accurately (many of the uncertainties in both the theoretical predictions and the experimental efficiencies cancel in the ratio). One consequently measures the ratio of the W and Z widths. The Z width is determined very precisely at LEP [2], allowing us to extract the W width.

UA1[24], UA2[25], and CDF[26] have all done similar analyses. (The CDF measurement does not yet include its muon analysis- this should be available shortly [27]). The results are:

$$\Gamma_W^{UA1} = 2.03 \pm 0.23\ GeV \tag{17}$$

$$\Gamma_W^{UA2} = 2.30 \pm 0.20\ GeV \tag{18}$$

$$\Gamma_W^{CDF} = 2.16 \pm 0.20\ GeV \tag{19}$$

Averaging these three, we get

$$\Gamma_W^{World} = 2.12 \pm 0.12\ GeV \tag{20}$$

I find it remarkable that one has a measurement of the W width at the 6% level.

The measured values are to be compared to the Standard Model prediction, assuming a W mass of 80.0 GeV, the top channel being closed, and a value of $\alpha_{strong} = 0.13$ of

$$\Gamma_W^{StandardModel} = 2.07\ GeV \tag{21}$$

The agreement of theory with experiment is very good. The dependence of the W width normalized to the width to $e\nu$ is shown in Figure 15.

We can extract a lower limit on the top mass from this measurement of the W width. Unlike the direct searches described in Section 5, this limit is independent of the decay mode of the top. It depends solely on the coupling of the W to $t\bar{b}$; if

the W decays in this mode it should show up in the total width of the W. The value of the width above implies a limit on the top mass of

$$M_{Top} > 53\ GeV\ at\ 90\%\ Confidence\ Level \tag{22}$$

and

$$M_{Top} > 49\ GeV\ at\ 95\%\ Confidence\ Level. \tag{23}$$

These limits are higher than the present limits from LEP.

4.3 New Limit on Heavy W Bosons

CDF has recently completed a search for heavy W bosons (W'), such as a right-handed W. One looks for the $e\nu$ decay, and constructs the transverse mass distribution just as in the W mass analysis described above. A heavy W would show up as a 'bump' at high transverse mass.

The transverse mass spectrum for events with one good electron with $E_T >$ 30 GeV and missing transverse energy> 30 GeV is shown in Figure 16. The points are the 1741 events that survive the selection from an exposure of 4.4 pb^{-1}; the histogram is a Monte Carlo calculation taking into account the width of the W and the detector resolution and acceptance. There are no events observed with transverse masses above 140 GeV. The spectrum is in excellent agreement with the expectation from the W alone, with no contribution from a W'.

To put a mass limit on a heavy W from the observations, one has to make assumptions about its couplings to $u\bar{d}$ and to $e\nu$, as the former contributes to the W' production, and the latter to the decay. CDF parameterizes the couplings to quarks with a parameter λ such that

$$\sigma(p\bar{p} \rightarrow W') = \lambda^2 \sigma_0$$

where σ_0 is the W' cross section with standard strength couplings to quarks. They also assume the standard model mixing angles.

The cross-section depends somewhat on the width of the W', $\Gamma_{W'}$. It is assumed [28] that the width increases linearly with the mass of the W', as one would expect if all other masses in the problem are negligible:

$$\Gamma_{W'} = (2.76\text{GeV})\ \frac{M_{W'}}{M_W}.$$

where 2.76 GeV is the lowest-order width of the W with 12 channels open.

Figure 17 shows the predicted cross-section with standard couplings, and the measured 95% C.L. limit, assuming a branching ratio to $e\nu$ of 1/12. The two curves cross at a value of $M'_W = 478\ GeV$, which is consequently the lower limit on the W' mass. Figure 18 shows the measured 95% C.L. limit versus W' mass parameterized in terms of the ratio of the coupling λ to the standard model value

for the W, and the ratio of the branching ratio to $e\nu$ to the standard model value of 1/12 (for a W' much heavier than the top). For $\lambda^2 B = 1$, the 'standard strength' coupling, the limit is the 478 GeV above.

Work is now proceding in CDF on extending the search to the decay mode $W' \rightarrow \mu\nu$. In addition, from a previous analysis of dielectron pairs, CDF has presented a preliminary limit for $Z' \rightarrow e^+e^-$ of $M_{Zprime} > 380\ GeV$ [29].

5 How Heavy is the Top Quark?

The top quark is one of the two remaining undiscovered 'fundamental' fermions of the Standard Model. It is now believed to be heavy enough that the only accelerator now running that can produce it is the hadron collider at Fermilab. In this section I describe the searches at CERN and Fermilab that have lead us to this conclusion. A detailed discussion of the CDF top search is given by James Bensinger in these same proceedings.

5.1 The experimental signature

In the Standard Model the top quark decays to a W boson and a b quark. The W then decays to one of the other isospin doublets, $e\nu$, $\mu\nu$, $\tau\nu$, $u\bar{d}$, $c\bar{s}$, and, if the top were light enough, $t\bar{b}$. The decays into the quark final states can take place into three colors, so, assuming a light top quark, there are 9 final states with quarks from the W and 3 final states with a charged lepton and neutrino. If the top is heavier than the W, as we now believe, then the decays to $t\bar{b}$ are kinematically forbidden and there are 6 final states where the W goes to quarks (the lepton modes are the same).

The production of the top also depends on its mass. If the top quark is lighter than the W, then one mechanism is the production of a W, with the subsequent W decay into $t\bar{b}$. At CERN, with its center-of-mass energy of $\sqrt{s} = 630\ GeV$, this would be the dominant production mechanism for a light (M_{top} about 60 GeV) top quark. The other mechanism, valid for top masses both larger and smaller than the W mass, is $t\bar{t}$ pair production by the strong interaction, dominantly through gluon- gluon scattering or $q\bar{q}$ annihilation. This mechanism is the dominant mechanism at Fermilab, where the higher energy makes for a larger gluon-gluon contribution (there are more gluons). One thus has a $t\bar{t}$ pair produced, with both the t and the $\bar{t}$ having substantial transverse momentum (typically a substantial fraction of the quark mass). Each then decays to a W and a b, and the W's then each decay. If the top is heavier than the W plus a b, the W bosons are real, and the $e - \nu$ mass is that of the W. If the top is lighter, the W's are virtual and the resultant lepton spectra from the W's are typical β decay spectra.

Figure 19 shows the statistical weights of the possible final states from the two W decays in the $t\bar{t}$ case, assuming the top is heavier than the W. The cleanest

signatures are those in which both W's decay into leptons. For the case where one decays into $\mu\nu$ and the other into $e\nu$, for example, the signature is one high p_T muon, one high p_T electron, and two neutrinos which are seen as large missing E_T. The b jets may or may not be visible, depending on the top mass. However, from Figure 19, one sees that only 2/81 $t\bar{t}$ events will have this signature.

Events in which one W goes to quarks and the other to a specific lepton pair (an $e\nu$ pair, for example) occur at a fraction of 12/81 of all decays. This signature results in a high p_T electron, missing Et, and at least two jets. It has the advantage of having a larger rate, but the disadvantage that there is substantial background from a continuum (i.e. not through the top) production of W plus 2 jets.

Events where both W's go to quarks occur at a branching ratio of 36/81. However the measured 4 jet background completely swamps the predicted signal.

5.2 Experimental Limits

The UA1 group has used an exposure of $4.7pb^{-1}$ from its 1988-1989 run to search for the top in two muon channels– μ plus jet, and $\mu\mu$. In the μ plus jet channel, they require that P_T^μ be greater than 12 GeV, and the rapidity of the muon be within ± 1.5 units. In the dimuon mode one muon is required to have P_T^μ greater than 8 GeV, and the other greater than 3 GeV. They then form a likelihood based on predicted distributions in four kinematic variables from top decay: isolation, P_T^μ, $\Delta\phi$ (between the muon and the jet, or between the two muons), and missing Et. The distributions in likelihood for the $\mu + jets$ data and for a 50 GeV top Monte Carlo sample with an exposure a factor of 10 larger than the data are shown in Figure 20. They define the signal region as likelihoods greater than 4. They find 2 events, and expect 2.8 ± 0.8 events from background. They quote a limit of $M_{top} > 60\ GeV$ at 95% $C.L.$ from their new limits combined with the results of their previous searches (see Figure 21).

The UA2 group [30] has looked for the top quark using the decay mode $t \rightarrow be\nu$ in a sample of 7.5 pb^{-1}. The signature is thus an electron, missing E_T, and one or more jets from either of the b quarks if the t was made by $W \rightarrow t\bar{b}$, or from the b or the other t (and its decay products) if the t came from $t\bar{t}$ pair production. For top quark masses near 60 GeV the former mechanism is about a factor of 7 larger than the latter, and the acceptance for the former is about half of the latter. The W decay to $t\bar{b}$ is thus the larger contributor to the expected signal. The UA2 collaboration selects events with a good electron with P_T greater than 12 GeV, and at least one jet with transverse energy greater than 10 GeV. In addition, they remove events in which the difference in azimuth between the electron and the highest energy jet is between 160 deg and 200 deg.

Figure 22 shows the UA2 transverse mass distribution for these events, where the transverse mass is $M_T^2 = 2E_T^e E_T^\nu (1 - cos(\Delta\phi))$, along with the predictions including and excluding top production. The UA2 measurement excludes a standard

model top quark if the mass is less than 69 GeV at 95% $C.L.$, as shown in Figure 23.

The CDF detector has the capability of detecting *both* muons and electrons (remember that UA1 does muons but not electrons in its present incarnation, and UA2 is a superb electron detector but doesn't have muon coverage). The initial limits from CDF came from a search in the electron + 2 or more jets mode, using the transverse mass distribution [31] ($M_T > 77$ *GeV at* 95% $C.L.$), and for a search in the electron-muon channel [32] ($M_T > 72$ *GeV at* 95% $C.L.$). New analyses have pushed up the limit significantly.

The transverse mass method used by UA2 and CDF no longer works for a top quark heavier than the W. In this case the transverse mass spectrum of the electron and neutrino does not depend on the top mass, as the W is real and the W decay is two-body. The new CDF limit comes entirely from di-lepton signatures.

The $e\mu$ signature asks for an electron and a muon, each with p_T greater than 15 GeV, with opposite charge. Top decays would be expected to give high momentum to both leptons. Figure 24a shows a scatterplot of the electron and muon momenta from simulation studies. Figure 24b shows the CDF data. There is one top candidate event in the top signal region. This event is shown in the $r-\phi$ view in the tracking chamber in Figure 25a; the 'Lego' plot of energy deposition in the $\eta-\phi$ plane is shown in Figure 25b. The electron has an E_T of 32 GeV; the muon has a P_T of 42.5 GeV. The two leptons are separated by an azimuthal angle of 137 degrees. A second muon of transverse momentum 10 GeV appears in the forward muon system, and there is a jet with E_T of 14 GeV. There is nothing wrong with this event that we can see.

The $e-\mu$ analysis can be applied to the e-e and $\mu-\mu$ channels as well, adding in another 2/81's of the decay matrix (Figure 19). For these channels there are new backgrounds, however, coming from lepton pairs from Z or virtual gamma decay. In addition to requiring E_T orP_T greater than 15 GeV, one requires missing Et ($\not\!\!E_T$) greater than 20 GeV, and the leptons to be non-collinear. Dileptons with invariant masses in the range between 75 and 105 GeV are removed to kill the Z background explicitly. Figure 26 shows the distribution of dielectron and dimuon events in the $\Delta\phi - \not\!\!E_T$ plane, as well as the expected distribution from Monte Carlo simulations of a 90 GeV top quark. There are no candidates in the data. For an 80 GeV top quark one would expect a total of 7.5 events (4.6 $e\mu$, 1.4 ee, and 1.5$\mu\mu$). One such event ($e\mu$) is observed. The limit from these channels is $M_T > 84$ *GeV* (95% C.L.).

In addition, CDF has searched for low P_T muons in the electron+jets and the muon+jets channels. The low P_T muon would come from the semileptonic decay mode of a b quark (70%) or c quark (30%) in the decay chain of the top. The main backgrounds are hadronic 'punchthrough' (non-interacting hadrons mimicking a muon), and decay-in-flight. These are discriminated against by eliminating events where the muon is close ($\Delta R < 0.6$) to either of the two highest E_T jets. No top

candidates are found.

The predicted cross-sections and the measured upper limits from each of these signatures of top production are shown in Figure 27. The band represents the range of theoretical predictions of the top production cross-section. The mass limits are derived from where the upper limit on top production intersects the lower band of the prediction. The result of combining all the dilepton mode searches extends the CDF top quark mass limit to $M_T > 89\ GeV$ at 95% C.L. (The limit is preliminary).

This now places the top mass well above the W mass (80 GeV), and most likely above the Z mass (91 GeV). We used to think that the boson masses represented a mass scale much larger than the quark and lepton mass scale. It is no longer true. Perhaps there is something fundamental going on here [33]- why is the top so heavy? (and why are the others so light?). In many ways it has turned out to be more interesting than a discovery of a 35 GeV top would have been.

6 B Mesons and Charm Spectroscopy

There are many interesting questions that can be studied in the B and C systems. For B's, for example, there are the B_d and B_s lifetimes, $B^0 - \bar{B}^0$ mixing, rare B decays, precision measurements of the Kobayashi-Maskawa matrix elements, and, eventually, the study of CP violation in B decay. There are a large number of heavy quarks made in a collider; both UA1 and CDF have measured that about 10% of all jets have a charmed quark carrying at least 10% of the jet momentum [34]. B quarks are also copious- the total cross-section for B production is expected to be 45 microbarns at $\sqrt{s} = 1.8\ TeV$.

B quark physics at hadron colliders is just beginning. The UA1 group members were bold pioneers in the field, but it is only with the advent of the new much larger data samples and new high resolution studies that many of the rest of us have realized the potential. The experimenting is much more straightforward than most of us had thought, and there are exciting prospects of much higher luminosities (factors of 10-1000) and much more sophisticated detectors, particularly in the areas of triggering, where there are factors of 10-100 to be gained, high resolution vertex detectors to resolve the secondary decays, photon detection, and particle identification.

6.1 The S States– ψ, ψ', *and* Υ Production

We remind the reader that the ψ is the 1S state of a c and a $\bar{c}$ quark, and the ψ' is the 2S state. The Υ is the analogous 1S state for the $b\bar{b}$ system. UA1 has collected a large sample of $\psi \rightarrow \mu^+\mu^-$ decays [35]. The ψ can be produced directly, can feed down from ψ' and χ production, or can be created as the decay products of b quarks. We believe that the observed ψs are dominantly from either B decay or from χ decay. Figure 28 shows the dimuon mass spectrum in the ψ region. The

Monte Carlo curve includes both the detector resolution and a small amount of ψ'. The fit gives 1393 ± 31 ψ events, and a ψ mass of 3.101 ± 0.005 GeV. The number of ψ' events is 99 ± 17, (7.1% of the ψ) with a mass of 3.69 GeV. The observed width for the ψ, which is completely dominated by the detector resolution, is $\sigma(\psi) = 151 \pm 4$ MeV. By comparing the density of tracks near the ψ to what they expect from χ decay and from B decay the UA1 group concludes that the fraction of ψs from χ decay is

$$f_\chi = 0.76 \pm 0.02 \pm 0.12,$$

i.e., that most of the ψs are from χ decay (see below).

UA1 also sees a clear signal for the ψ' in the decay mode

$$\psi' \rightarrow \psi\pi^+\pi^-$$

The distribution of the mass of the $\psi\pi\pi$ system minus the mass of the ψ is shown in Figure 29.

CDF has also has a dimuon spectrum that includes these peaks. Figure 30 shows the uncorrected dimuon mass spectrum, with both muons required to have $P_T > 4$ GeV. Notice the ψ and ψ' peaks, as well as the enhancement in the Υ region.

Figure 31 shows the ψ region enlarged. One sees the radiative tail on the ψ. The fitted mass is $M_\psi = 3.0962 \pm 0.0007$ GeV, in good agreement with the world value of 3.097 GeV. The observed width of the peak, which derives entirely from the detector resolution, is $\sigma = 24.6$ MeV. The P_T spectrum of the ψs is shown in Figure 32. There are about 1700 ψ events in this sample.

Figure 33 shows the ψ' region of the dimuon spectrum. There are 72 ± 17 ψ' events in the peak (about 4% of the ψ). The ψ' is also observed in the $\psi' \rightarrow \psi\pi^+\pi^-$ decay mode: In Figure 34 the invariant mass of the $\psi\pi\pi$ system is shown, where all tracks within a cone of radius 1.0 about the ψ in $\eta - \phi$ space have been taken in pairs, assuming they are pions. A clear ψ' peak rises above the combinatoric background.

The Υ region as observed by the CDF detector is shown in detail in Figure 35. In the fit shown the widths are assumed to be the same, as they are dominated by resolution. The 1S, 2S, and 3S states are nicely resolved.

6.2 The P States– χ_s Production

CDF has directly observed χ decays into the ψ. One looks for a gamma ray nearby the ψ in the calorimeter. Figure 36 shows the mass difference between the $\psi - \gamma$ system and the ψ. A nice peak is seen at 430 ± 12 MeV. The resolution is not sufficient to resolve the three different angular momentum states (J = 0,1,2) of the χ.

6.3 The B meson production cross section

B quarks decay semileptonically into a charm quark plus lepton pair. Figure 37 shows the P_T spectrum of muons in the UA1 μ + jet sample. The solid line is the Monte Carlo prediction including the fraction from $b\bar{b}$ ($33 \pm 5\%$) and π and K decay in flight (30%). The fraction of B's in the sample is determined from the property of B decays that the muon will in general have a larger transverse momentum with respect to the rest of the B decay products (the jet from the c quark) than it would in the fragmentation of lighter quarks. This is shown in Figure 38, where the spectrum of muons is plotted versus this momentum. The Monte Carlo is then used to go back from the measured muon cross-section to the b quark cross- section versus P_T. Figure 39 shows the new preliminary results on the b cross-section; the cross-section for the inclusive production of a b quark above a minimum P_T is plotted versus that threshold (i.e. it's an integral cross-section). The QCD predictions shown are in good agreement with the data. The circles are determinations from dimuon data, with the open circle being a new preliminary point from the 1989 data. For a $P_T^{min}(B)$ of 14 GeV, the measured integral cross-section is 0.16 ± 0.054 microbarns.

CDF has also looked for B mesons decaying into final states either with a ψ or with a single lepton. Figure 40 shows the inclusive electron spectrum from CDF. The upper set of data points are for all electrons. The lower are with identified W and Z boson decays subtracted. The upper curve is the prediction from b and c quark decays from Isajet, normalized to the data. The lower curve, which is much steeper than the data, is the Isajet prediction from charm alone. The data are consistent with being mostly from B decays- i.e, there is a rather pure source of B events at a high rate. If one reconstructs pairs of tracks near the electron as a pion and a kaon, and makes the invariant mass for all such pairs, one sees the D^0 (Figure 41). This is presumably from the decay chain $b \rightarrow ce\nu$. A cross section measurement is in progress.

6.4 Rare B decays- $B \rightarrow \mu^+\mu^-$

Knowing the cross-section for B production, UA1 can then search for rare B decays into final states and set limits on the B branching ratios. They have searched for the flavor-changing neutral current decay $B \rightarrow \mu^+\mu^-$. They require two muons each with $P_T > 3\ GeV$, and further require the dimuon pair to have $P_T > 7\ GeV$. The pair is required to have the invariant mass of the B to within their resolution, $5.1 < M_{\mu\mu} < 5.5\ GeV$ (Figure 42). Six events are observed, with a quoted estimated background of 5.0± 1.0. A limit then is placed on the branching ratio:

$$BR\,(B^0_{d,s} \rightarrow \mu^+\mu^-) \;<\; 1.0 \times 10^{-5} \;\; (90\%\ C.L.)$$

This is a factor of 5 better than previous measurements.

A similar search for $B^0 \rightarrow \mu^+\mu^- + X$ results in the limit:

$$BR\,(B^0_{d,s} \rightarrow \mu^+\mu^- + X) \;<\; 6.0 \times 10^{-5} \;\; (90\%\ C.L.),$$

and UA1 has also a new limit for the exclusive decay mode of the B:

$$BR\,(B^0_{d,s} \rightarrow K^{0*}\mu^+\mu^-) \;<\; 2.6 \times 10^{-5} \;\; (90\%\; C.L.).$$

CDF has also set a limit on the rare decay of the B_d by normalizing to the rate of ψ' production:

$$BR\,(B^0_d \rightarrow \mu^+\mu^-) \;<\; 3.2 \times 10^{-6} \;\; (90\%\; C.L.).$$

This is an order of magnitude better than new limits from the e^+e^- machines [36], demonstrating the power of having a very large production cross section.

6.5 Exclusive B decays– $B \rightarrow \psi K$

Most recently, CDF has exploited the resolution of its magnetic spectrometer to measure rare exclusive decay modes of the B. They take all tracks with P_T greater than 2.5 GeV one-at-a-time near the ψ and form the invariant mass, assuming one track is a charged K. One then looks to see if there is a signal for the process

$$B^\pm \rightarrow \psi K^\pm$$

This process has been seen at Argus [37] and Cleo [38], and has a measured branching ratio [36] of $8.0 \pm 2.8 \times 10^{-4}$. Figure 43 shows the invariant mass spectrum, with a fit to the background plus a peak. The peak has 16 ± 6 events. This is approximately equal to the present world sample. It should be emphasized that the trigger was not optimized for this mode in the last run, and these nice results are somewhat serendipitous: with care and some luck CDF should be able to accumulate on the order of 100 times as many ψ's (and therefore $B \rightarrow \psi$'s) next run.

7 Summary and Prospects for the Future

A great deal about the Standard Model has been learned in the past year from hadron colliders. Perhaps the most important result is that, although we haven't discovered it yet, it seems that the top quark is truly heavy, with a mass greater than the W and Z boson masses. This may be an important clue in the search for answers to the big questions, e.g., where does mass come from, why quarks and leptons, why three generations?

With the data from the next run the CDF and D0 groups hope to extend the reach for the top quark substantially, and with the run after that to search all the way to the upper bound if the top hasn't yet been found. To be specific, the top cross section [39] drops a factor of 10 as the top mass increases from the present limit of 89 GeV to about 138 GeV. CDF expects a factor of 10 more data next run (the peak luminosity is expected to be a factor of 5-10 higher, and both the integrated

efficiency and the ratio of average to peak luminosity should be appreciably higher). Another factor of 2 in data, also possible in this next run, raises the reach by almost 20 GeV beyond the 138 GeV, to about 157 GeV. In fact, the detection efficiency is also rising with top mass, as the b jets are getting stiffer, and the top is getting more central (a small effect). Figure 44 shows typical efficiencies for the decay modes listed in Figure 19, for a CDF-like detector and a 90 GeV top. The efficiencies are small, and can be improved. The new CDF silicon vertex detector will also allow new strategies. The existence of D0 is another potential factor of at least 2 in sensitivity. In addition, it is possible that the Tevatron energy will be raised from $\sqrt{s}$ of 1.8 TeV to 2.0 TeV, increasing the top cross section by 30%. Finally, the run beyond the next one should push the reach out to the 200 GeV of the upper limit on the top mass.

Another important result is the precision measurement of the W mass from UA2 and from CDF. This constrains both the top quark mass from above, and also the existence of any other generations heavier than the Z. The precision is remarkable, and the measurement uncertainties, both statistical and systematic, are so far limited by the statistics of the data samples. Both UA2 and CDF will have bigger data samples, and it will also be interesting to see how well D0 does. We can hope to lower the uncertainty on the W mass by at least a factor of 3 in the next several years from its present value of 310 MeV.

QCD tests now reach out to scales on the order of 1 TeV with no sign of compositeness for the partons. Detailed QCD higher order predictions agree well with the measurements for a wide variety of tests. The prospects for exploration exist: a factor of 10 in data will extend the reach in jet-jet invariant mass by 190 GeV, for example.

The search for a heavy charged vector boson such as a right-handed W has found no such object decaying to $e\nu$ with standard coupling up to a mass of 478 GeV (95% $C.L.$). The search in the $\mu\nu$ decay mode will add to the sensitivity. (I will bet that such things exist). The search for $Z \rightarrow e^+e^-$ puts a limit on new Z bosons, again assuming standard couplings, of 380 GeV.

Finally, UA1 and CDF have shown that one can do B physics that, at least for some topics such as exclusive decay modes and searches for rare decays, is quite competitive with the best one can do at present at e^+e^- colliders. For example, CDF has 16 events of the exclusive decays $B \rightarrow \psi K^{\pm}$. With improved triggering and more luminosity it should be possible to accumulate up to $\times 100$ more events next run. As one learns how to exploit the large B cross-section at hadron colliders with silicon vertex detectors and smarter triggers these machines become candidates for the next B factory. I believe that it is possible that the shortest route to studies of CP violation in the B system may be by improving experiments at upgraded existing hadron colliders rather than building new B factory accelerators.

There have been many other results that I have had to ignore due to lack of time. It is a rich environment for the experimentalist.

I would like to thank Paris Sphicas, Michel DellaNegra, and colleagues for providing the latest results from UA1, and Luigi Dilella and Joe Incandela for the same for UA2. I was helped a great deal by Avi Yagil with χ and Υ plots, by Milciades Contreras from his excellent talk on top limits at Duke, and by Claudio Campagnari with both the W width and top limits. I would like to thank all of my colleagues on CDF. Finally, I would like to thank the organizers for an excellent conference.

References

1. F. Abe et al. (CDF collaboration), Phys.Rev.Lett. 63, (1989), 720
2. For a summary of the latest LEP results, see F. Dydak, XXth International Rochester Conference, Singapore, 1990.
3. G.S. Abrams et al. (Mark II Collaboration), Phys. Rev. Lett. 63, (1989), 724. Also see F. Dydak, op cit.
4. Proposal for an Upgraded CDF Detector, the CDF Collaboration, submitted to Fermilab October, 1990. Please note the 'if'.
5. C. Albajar et al., (UA1 Collaboration) Z. Phys. C4 (1989) 15
6. J. Alitti et al. (UA2 Collaboration), CERN EP/90-2, to appear in Z. Phys. C.
7. F. Abe et al. (CDF collaboration), Nucl. Instrum. Methods Phys. Res., Sect. A 271, 387 (1988) and references therein.
8. H.J. Frisch in APS Conference Proceedings of the Annual Meeting of the DPF, Brookhaven Natl. Lab Upton N.Y., Oct. 8, 1976.
9. See, for example, the talk of Karlheinz Meyer in the 8th Topical Workshop on Proton-Antiproton Collider Physics, 1-5 Sept. 1989, Castiglione della Pescaia, Italy, G. Bellettini and A. Scribano, ed. This is the definition used in the UA2 multijet analyses, for example. For single jet spectra clusters are merged, and for spectroscopy, as in the W mass, a cone algorithm somewhat similar to the CDF algorithm is used.
10. D. Duke and J.F. Owens, Phys. Rev D30, 49 (1984) E. Eichten, I. Hinchliffe, K.Lane, and C. Quigg, Rev. Mod. Phys. 56, 579 (1984).
11. E. Eichten, K. Lane, and M. Peskin, Phys. Rev. Lett. 50, 811 (1983).
12. Z. Kunszt and W.J. Stirling, Phys. Lett. 171B, 307 (1986).
13. Ian Hinchliffe, private communication.
14. This variable is called $X3$ in the CDF notation- the two original partons in the incoming beams are called 1 and 2, and the three outgoing jets are called 3, 4, and 5 in decreasing order in E_T.
15. S.L. Glashow, Nucl. Phys. 22, 579 (1961); S. Weinberg Phys. Rev. Lett. 19, 1264 (1967), A. Salam, p. 367, Almqvist and Wiksell, Sweden, 1968.
16. M. Veltmann,Nucl. Phys. B123, 89 (1977), M. Chanowitz, M. Furman, and I. Hinchliffe, Phys. Lett. 78B, 285 (1978), Nucl. Phys. B153,402 (1979)
17. U. Amaldi et al., Phys. Rev. D36, 1385 (1987); G. Costa et al, Nucl. Phys. B297, 244 (1988), P. Langacker, Phys. Rev. Lett. 63, 1920 (1989), J. Ellis and G.

Fogli, Phys. Lett B231, 189 (1989),W. Marciano, Nucl. Phys. B (Proc. Suppl.11,5 (1989).
18. M. Chanowitz, Heavy Flavor Physics Symposium, Bejing, Aug. 1988, LBL preprint LBL-26547, Feb. 1989
19. I use the convention that $c = 1$ both in the text and for the units of energy, momentum, and mass. This convention is unambiguous.An enormous amount of time is (mis)spent getting the c's and c^2's right (look in the literature for the units of Γ_Z, for example.)
20. G.Altarelli, R.K. Ellis, M. Greco, G. Martinelli, Nucl.Phys. B246, 12(1984); S.D. Ellis, R. Kleiss, W.J. Stirling, Phys. Lett. B154, 435(1985); P.B. Arnold, R.K. Ellis, M.H. Reno, Phys. Rev. D40, 613 (1989).
21. J. Alitti et al (UA2 collaboration), Phys. Lett B241,150 (1990).
22. F. Abe et al., Fermilab Preprint PUB-90/161-E, to be published in Phys. ReV.Lett.; ibid. Fermilab Preprint PUB-90/162-E, submitted to Phys. ReV.D,
23. N. Cabibbo,Third Topical Workshop on Proton-Antiproton Collider Physics, Rome, 12 Jan, 1983, pp. ; F. Halzen and M. Mursula, Phys. Rev. Lett. 51, 857 (1983).
24. P. Sphicas, private communication.
25. J. Alitti et al. (UA2 Collaboration), CERN EP/90-20, to appear in Z. Phys. C.
26. F. Abe et al, submitted to Phys. Rev. D. This number has changed slightly from the published number, F. Abe et al, Phys. Rev. Lett. 64, 152 (1990), only because the Z width from LEP has come down slightly.
27. R. L. Swartz Jr., private communication.
28. If the W' couples to the W or Z, the width can grow faster, up to the 5th power of the Wprime mass. See G. Altarelli, B. Mele, M. Ruiz-Altaba, CERN-TH5523/89, and D. Gerdes et al, CDF Note 1218, May 1990.
29. M. Gold (CDF collaboration), High P_T W and Z production and Drell- Yan, 1990 Aspen Winter Conference, Jan., 1990
30. T Akesson et al., Z. Phys. C46, 179 (1990)
31. F. Abe et al., Phys. Rev. Lett. 64, 142 (1990)
32. F. Abe et al., Phys. Rev. Lett. 64, 147 (1990)
33. Y. Nambu, BCS Mechanism, Quasi-Supersymmetry, and Fermion Mass Matrix, Talk presented at the Kasimirz Conference, EFI88-39 (July 1988), EFI-88-62(Aug. 1988); EFI-89-08; V. Miransky, M. Tanabashi, and K. Yamawaki, Mod. Phys. Lett. A4, 1043 (1989); Phys. Lett. B221, 117 (1989); W. Bardeen, C. Hill, and M. Lindner, Phys. ReV. D41, 1647 (1990); W. Marciano, Phys. Rev. D41, 219 (1990). See also C. Hill, Invited Talk presented at DPF '90, Houston Texas, Jan. 5, 1990, Fermilab-CONF-90/57-T for references and a summary.
34. M. Ikeda et al (the UA1 collaboration), in Proceedings of the Ninth Topical Workshop on Proton-Antiproton Physics, Castiglione, Italy, September 1989 (to be published); F. Abe et al., (the CDF collaboration) Phys.Rev.Lett. 64,348 (1990); G. Redlinger, Ph.D. thesis, Univ. of Chicago, 1990 (unpublished).

35. I would like to thank P. Sphicas for the latest UA1 plots that are shown here, as well as for help.
36. Particle Data Group, Physics Letters B239, 1990.
37. H. Albrecht et al. (Argus collaboration), Phys. Lett. B199, 451 (1987)
38. C. Bebek et al.(Cleo collaboration), Phys. Rev. D36, 1289 (1987)
39. P. Nason, S. Dawson, and R.K. Ellis, Nucl. Phys. B303, 607 (1988)

Figure Captions

Figure 1. a) The UA1 apparatus in plan view. For the most recent run the electromagnetic calorimeters were removed.
b) The UA2 apparatus in plan view.
c) The CDF apparatus in elevation view. Only one half is shown– the apparatus is front-back symmetric.
Figure 2. The UA2 dijet mass spectrum.
Figure 3. The UA2 dijet W mass bump, with the continuum subtracted.
Figure 4. The CDF dijet mass spectrum. The solid curve is a QCD prediction with the DO2 parton distribution. The data have not yet been corrected for detector resolution.The average systematic uncertainty from the energy scale and other effects is shown in the lower left. Also shown is a band representing a range of typical theoretical predictions obtained by varying the Q^2 scale from twice P_T^2 to half P_T^2, and varying the choice of parton distribution funcitions among ELHQ1, EHLQ2, DO1, and DO2.
Figure 5. The CDF dijet mass spectrum- these are the same data as in Figure 4, but what is plotted is (data-theory)/theory, on a linear scale.
Figure 6. The CDF dijet mass spectrum. Four theoretical spectra are also shown: the QCD prediction, with and without the contribution from a contact term.
Figure 7. A CDF 'typical' 3-jet event
a) the 'Lego' plot of calorimeter energyin $\eta - \phi$ space,
b)the r-ϕ plot from the tracking chamber showing clearly the jet structure of the two jets that are in the central region.
Figure 8. Distributions from the UA2 4-jet studies. The notation is that the highest E_T jet is jet 1, the second highest jet 2, etc. Ω_{14} is thus the angle between the highest and lowest energy jets.
a) The distribution in the 4-jet invariant mass. The histogram is the prediction of an order α_S^4 calculation by Kunszt and Stirling.
b) The distribution in sphericity, again compared to the QCD prediction.
c) The distributions in the angles between the 4 jets.
Figure 9. The CDF 3-jet distributions:
a) The distribution of events in the variable X3, where X3 is the fraction of the 3-jet mass carried by the leading (highest E_T) jet.The solid line is the Papageno program QCD prediction; the dashed line is phase space.
b) The similar distribution in X4, where X4 is the fraction of the 3-jet mass carried by the next highest E_T jet. Again the QCD prediction is the solid line; it agrees well with the data. The dashed line again represents the prediction from phase space only (no matrix elements).
Figure 10. The UA2 W mass measurement distributions. In each case the line is the best fit Monte Carlo curve:
a) The electron transverse momentum.

b) The neutrino transverse momentum.
c) The transverse mass.
Figure 11. The transverse mass distributions from the CDF W mass measurement .
a) The transverse mass for electron events
b) The transverse mass for muon events
Figure 12. The CDF W mass measurement lepton transverse momentum distributions. In each case the solid line is the best fit. The region of fit is indicated by dashed vertical lines.
a) The electron P_T spectrum.
b) The muon P_T spectrum.
c) The electron neutrino P_T spectrum.
d) The muon neutrino P_T spectrum.
Figure 13. The UA2 W mass measurement and the Standard Model predictions (from ref. 21). The solid lines show the relationship of the W,Z, and top masses for a value of the Higgs mass of 100 GeV. The dotted line corresponds to a Higgs mass of 10 GeV, and the dashed line to 1000 GeV.
Figure 14. The CDF value of $\sin\theta_W$ versus the top quark mass. The solid horizontal line gives the central value–the dashed lines are one sigma errors. The vertical dashed line indicates the CDF lower limit on the top mass by direct searches.
Figure 15. The dependence of the W width on the top quark mass, and the CDF value for the W width.
Figure 16. The transverse mass spectrum from the CDF collaboration search for a heavy W. One sees the tail of the usual W. The histogram is the Monte Carlo simulation of the expected distribution.
Figure 17. The 95% *C.L.* limit on the cross-section for the production of a heavy W as a function of the W' mass. The dotted line is the expected cross-section; the solid line is the experimental upper limit, assuming standard couplings.
Figure 18. The limit on the product of the coupling to quarks times the branching ratio to $e\nu$ for a W', as a function of the W' mass.
Figure 19. A table of the weights of the final states from the two W bosons in $t\bar{t}$ decays. The top is assumed to be heavier than the W so that the $t\bar{b}$ decay channel is closed to the W. Small effects due to masses of the final states have been ignored. As each W can decay in 9 different ways (3 lepton doublets + 2 quark doublets $\times$ 3 colors) there are 81 different final states. We assume one cannot distinguish any of the different $q\bar{q}$ states from another.
Figure 20. The distribution in likelihood from the UA1 top quark search. The signal region is taken as likelihoods greater than 4.
Figure 21. The cross-section limit on top production from UA1.
Figure 22. The transverse mass distribution as seen by UA2. The dotted curve shows the expected signal for a top mass of 65 GeV, and the solid curve is the best fit with no top production.

Figure 23. The cross-section limit on top production from UA2.
Figure 24. a) The expected distribution in the $E_T^e - P_T^\mu$ plane for a 70 GeV mass top quark from simulation studies. The exposure is $80pb^{-1}$, about 20 times the actual data. b) The CDF data from $4.7pb^{-1}$. The events at low values of E_T^e and P_T^μ are from B decays. There is one top candidate (arrow).
Figure 25 a.) The $r - \phi$ view of the one top candidate event. b.) The $\eta - \phi$ view of the one top candidate event.
Figure 26. The distribution of dilepton events in the $\Delta\phi$-missing E_T plane. a.) The dielectron data. b.) The dimuon data. c. The expected distribution for a large sample (unnormalized) of Monte Carlo decays of a 90 GeV top quark.
Figure 27. The combined dilepton limits on the top quark from the CDF collaboration. The band represents theoretical predictions of the top production cross-section. The mass limits are derived from where the upper limit on top production intersects the lower band of the prediction.
Figure 28. The dimuon mass spectrum in the ψ region from the UA1 collaboration. The histogram is for opposite sign muons; the crosshatched histogram is for same sign. The line is the Monte Carlo including the detector resolution.
Figure 29. The distribution of the mass of the $\psi\pi\pi$ system minus the mass of the ψ from UA1. The peak is the ψ'.
Figure 30. The uncorrected dimuon mass spectrum from CDF. Both muons are required to have $P_T > 4\ GeV$. The same sign background is shown as a dotted line. The peaks are the ψ and Υ systems; the shape of the continuum is governed by the trigger thresholds.
Figure 31. The ψ region of the CDF dimuon mass spectrum. Again, the same sign background is shown as a dotted line.
Figure 32. The P_T spectrum of the ψ sample. The lower end of the spectrum is cut off by trigger thresholds in the present sample. It is partly by lowering these thresholds that many more $\psi's$ can be obtained.
Figure 33. The ψ' region of the CDF dimuon spectrum. The same sign background is shown as a dotted line.
Figure 34. The invariant mass of the $\psi\pi\pi$ system, where all tracks within a cone of radius 1.0 about the ψ in $\eta - \phi$ space have been taken in pairs, and it is assumed that they are pions. The peak is the ψ', as in Figure 33.
Figure 35. The Υ region of the CDF dimuon mass spectrum. The line is a fit to three Gaussians of equal width and a background.
Figure 36. The mass difference between the $\psi - \gamma$ system and the ψ. The peak is from the χ states.
Figure 37. The P_T spectrum of muons in the UA1 μ + jet sample. The solid line is the Monte Carlo prediction including the fraction from $b\bar{b}$ ($33 \pm 5\%$) and π and K decay in flight (30%).
Figure 38. The points are the UA1 distribution of events versus the P_T of the muon relative to the jet. B decays in general will have larger P_T than charm or

lighter quark decays, as shown by the Monte Carlo curves. From these curves the B fraction is determined to be $33 \pm 5\%$.

Figure 39. The cross-section for the inclusive production of a b quark above a minimum P_T^{min} versus P_T^{min} for the rapidity interval $|\eta| < 1.5$. The QCD predictions are α^3 predictions from Ellis et al. The circles are determinations from dimuon data, with the open circle being a new preliminary point from the 1989 data.

Figure 40. The inclusive electron spectrum from CDF. The upper set of data points is for all electrons. The lower points have identified W and Z boson decays subtracted. The upper curve is the prediction from b and c quark decays from Isajet, normalized to the data. The lower curve, which is much steeper than the data, is the Isajet prediction from charm alone.

Figure 41. The invariant mass distribution from pairs of tracks near the ψ, taken as $K\pi$ in pairs. The bump is the D^0.

Figure 42. a) The dimuon invariant mass spectrum from the UA1 search for $B^0 \to \mu^+\mu^-$. b) An enlarged view of the B mass region.

Figure 43. The invariant mass spectrum, with a fit to the background plus a peak, for the process

$$B^{\pm} \to \psi K^{\pm}.$$

Figure 44. The efficiencies (ϵ) and the product of efficiency times branching ratio ($\epsilon \times B$) for the decay modes of the two (real) W bosons from heavy $t\bar{t}$ pairs, for a CDF-like detector. The requirement of a soft muon in the e-jets or μ-jets channel costs one an additional factor of 15 or so.

Table Captions

I. A summary of the UA2 fits to the transverse mass and momentum distributions from W decays. The uncertainties are the statistical uncertainties from the fit. (From Reference 21.)

II. A summary of the corrections and systematic uncertainties from the UA2 transverse mass fits. All values are in MeV. (From Reference 21.)

III. A summary of the corrections and systematic uncertainties from the CDF transverse mass fits. All values are in MeV. (From Reference 22.)

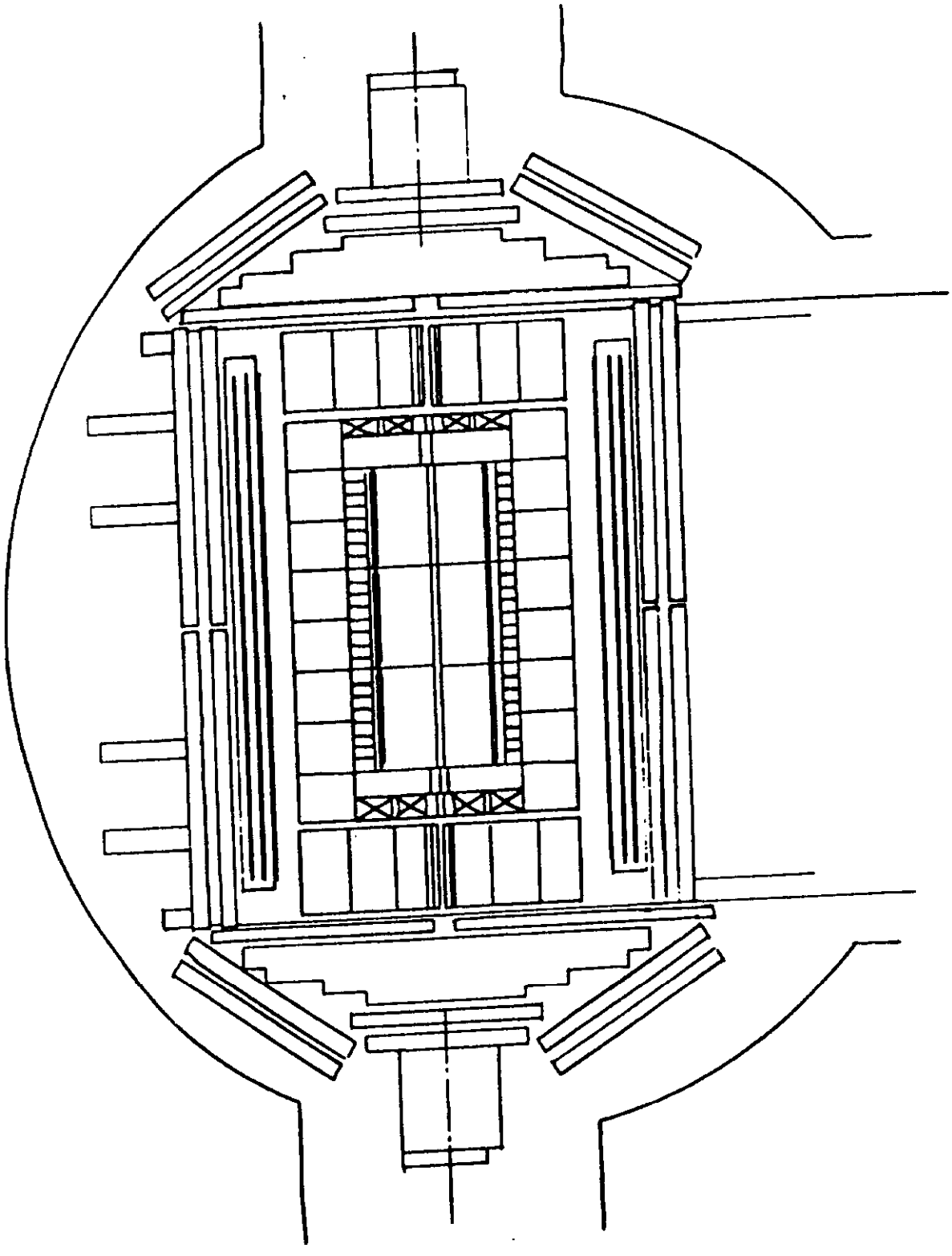

Figure 1a

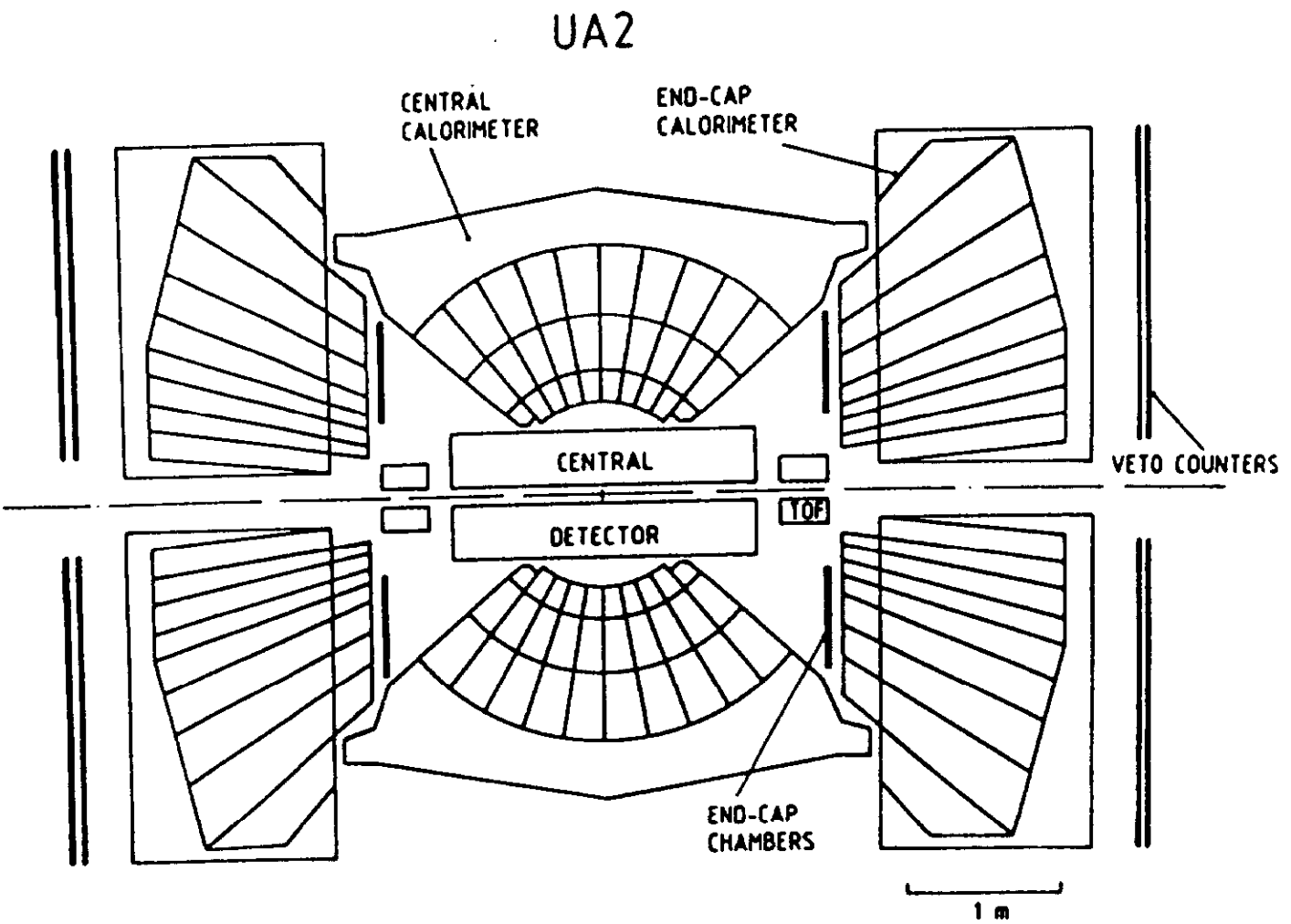
UA2
CENTRAL CALORIMETER
END-CAP CALORIMETER
CENTRAL DETECTOR
TOF
VETO COUNTERS
END-CAP CHAMBERS
1 m

Figure 1b

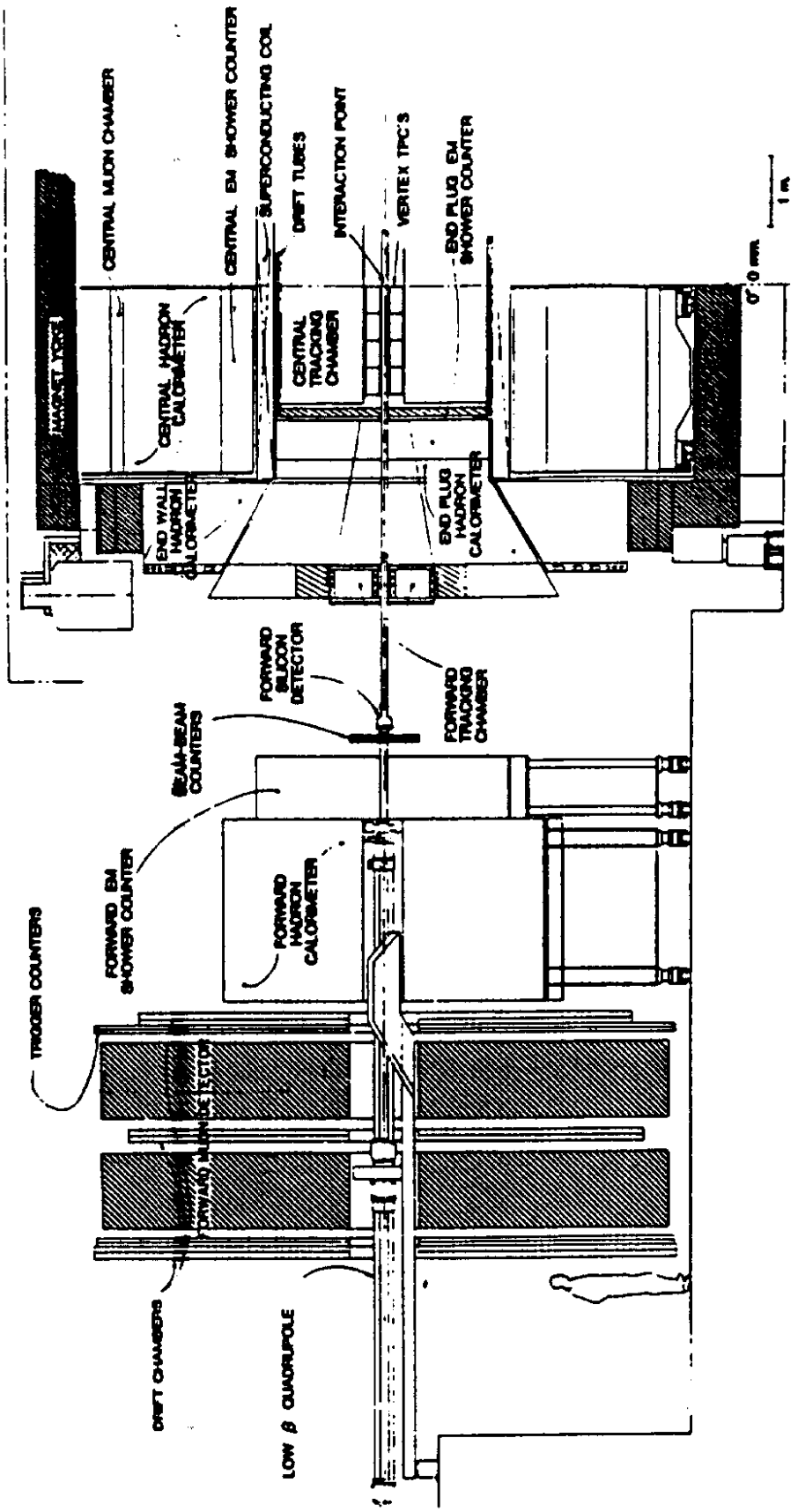
CENTRAL MUON CHAMBER
CENTRAL EM SHOWER COUNTER
SUPERCONDUCTING COIL
DRIFT TUBES
INTERACTION POINT
VERTEX TPC'S
END PLUG EM SHOWER COUNTER
CENTRAL HADRON CALORIMETER
CENTRAL TRACKING CHAMBER
END WALL HADRON CALORIMETER
END PLUG HADRON CALORIMETER
FORWARD SILICON DETECTOR
FORWARD TRACKING CHAMBER
BEAM-BEAM COUNTERS
FORWARD EM SHOWER COUNTER
FORWARD HADRON CALORIMETER
TRIGGER COUNTERS
DRIFT CHAMBERS
LOW β QUADRUPOLE
0° 10 mm
1 m

Figure 1c

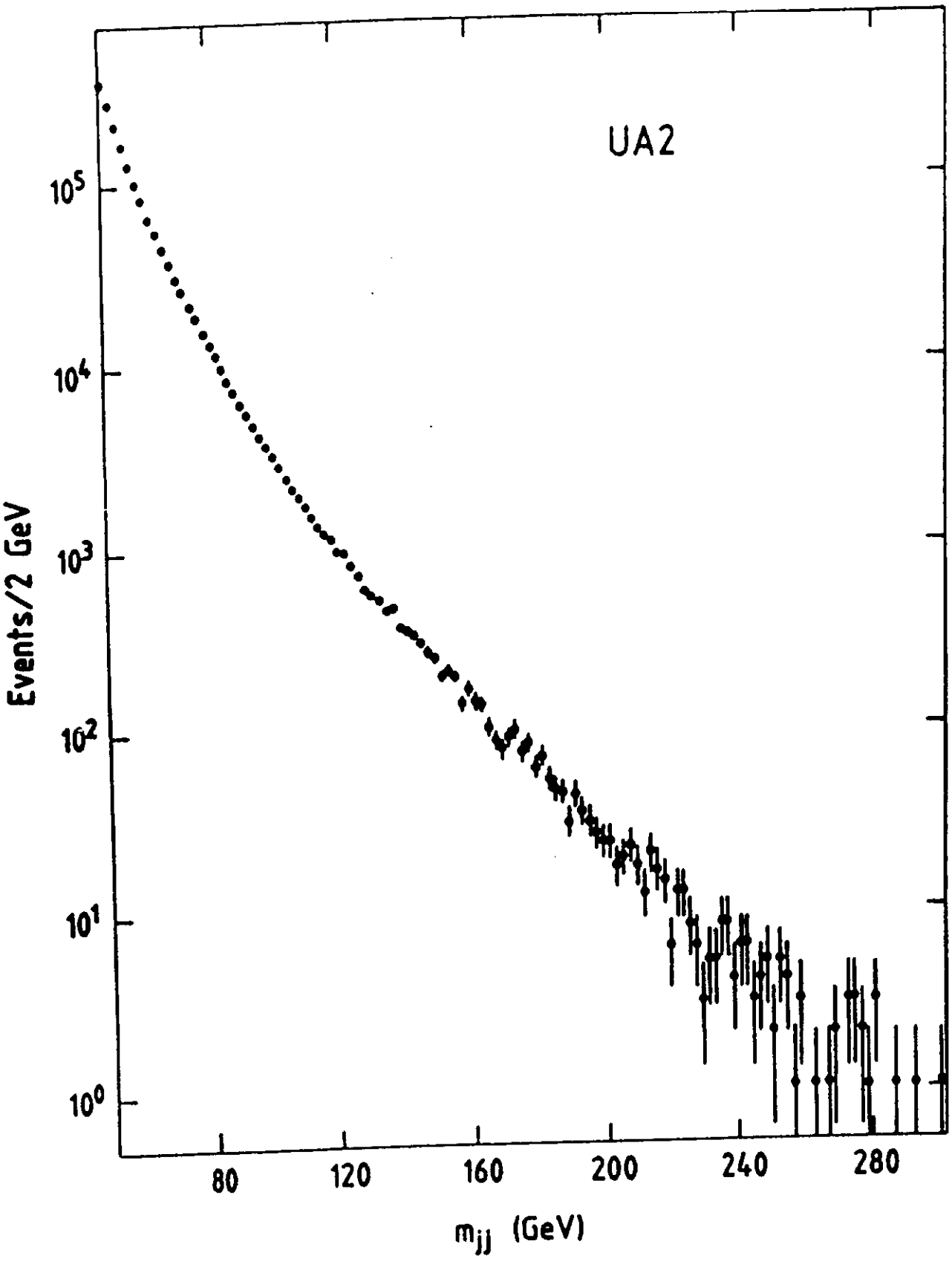
UA2
Events/2 GeV
10^5
10^4
10^3
10^2
10^1
10^0
80
120
160
200
240
280
m_{jj} (GeV)

Figure 2

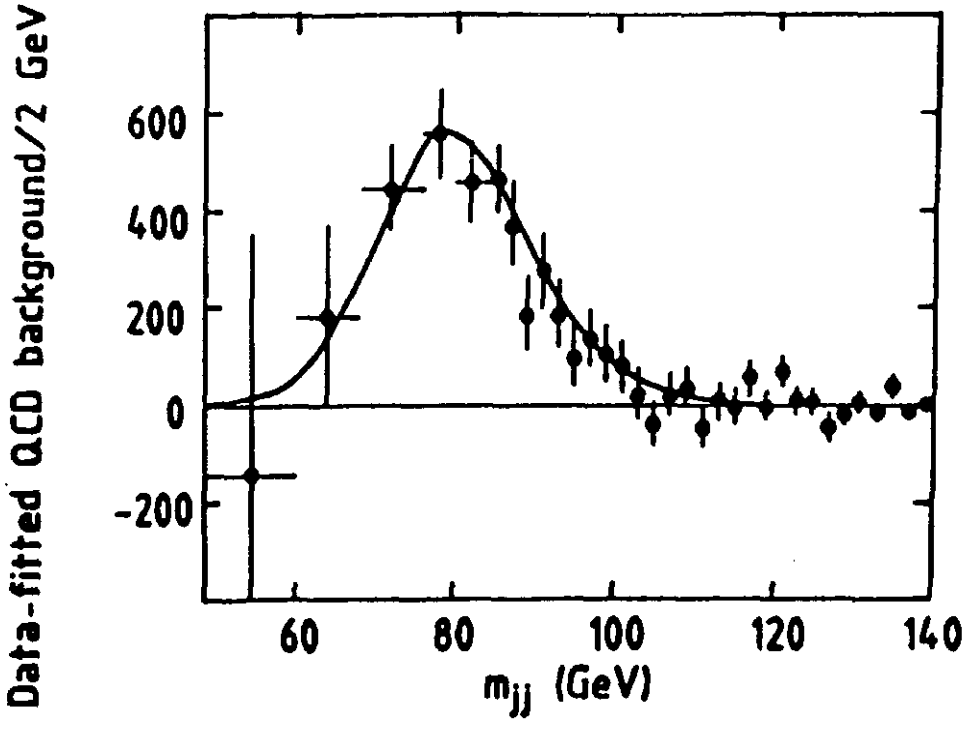
Data-fitted QCD background/2 GeV
600
400
200
0
-200
60
80
100
120
140
m_{jj} (GeV)

Figure 3

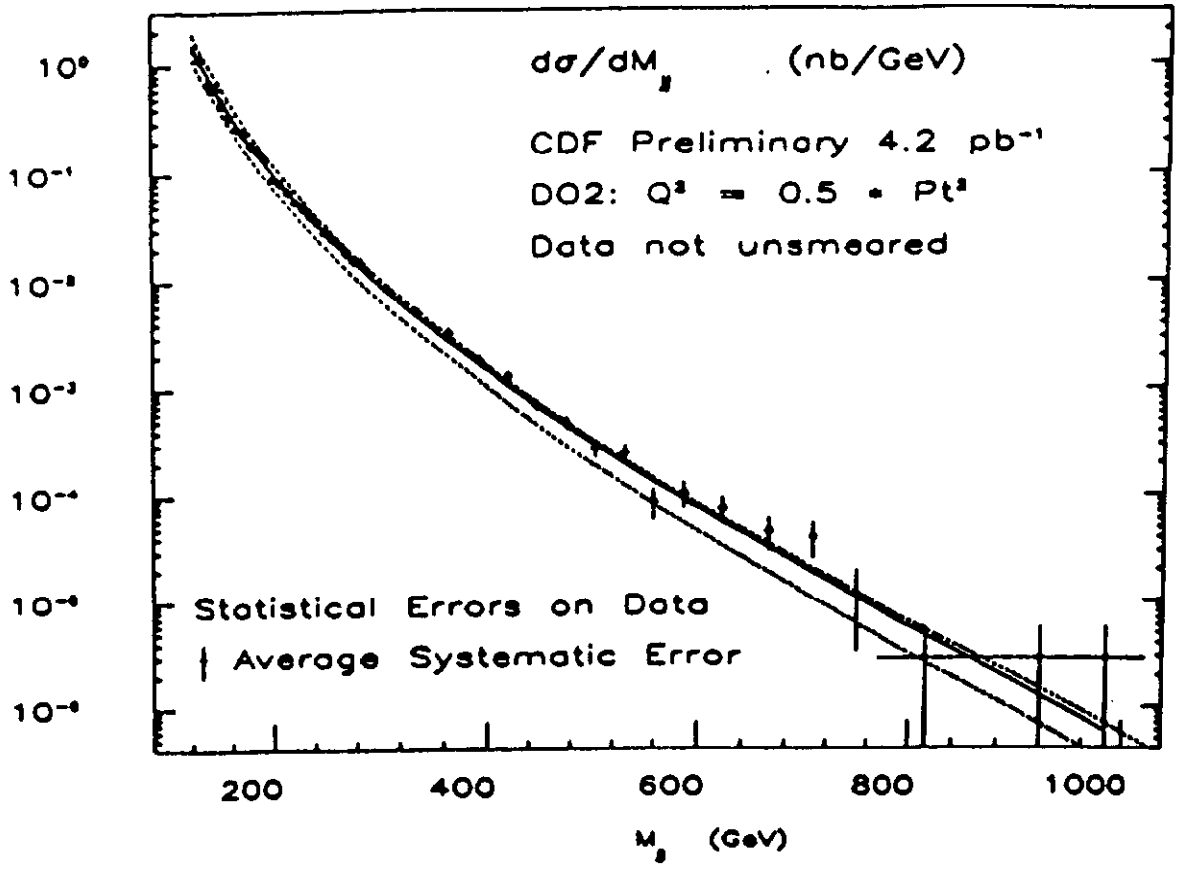
dσ/dM_jj (nb/GeV)
CDF Preliminary 4.2 pb⁻¹
DO2: Q² = 0.5 * Pt²
Data not unsmeared
Statistical Errors on Data
Average Systematic Error
10⁰
10⁻¹
10⁻²
10⁻³
10⁻⁴
10⁻⁵
10⁻⁶
200
400
600
800
1000
M_jj (GeV)

Figure 4

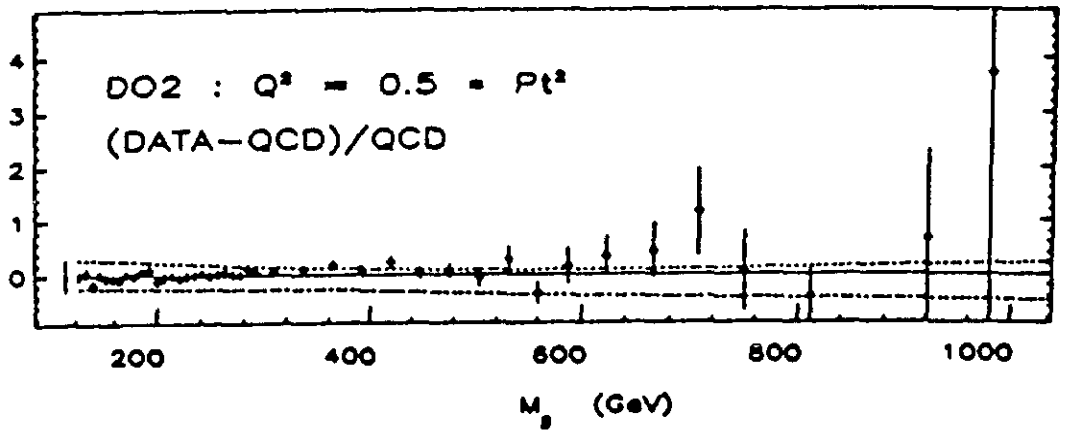

Figure 5

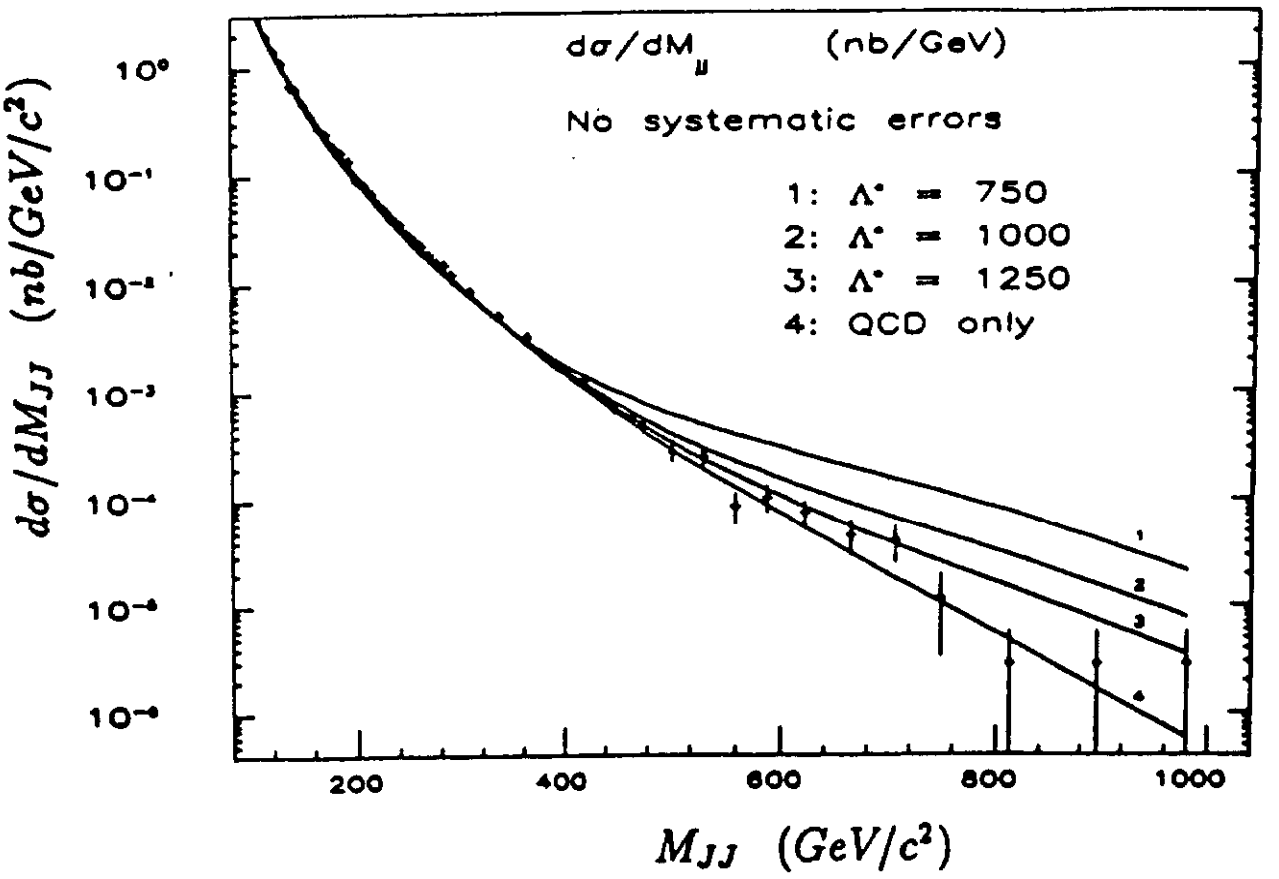
dσ/dM_JJ (nb/GeV)
No systematic errors
1: Λ* = 750
2: Λ* = 1000
3: Λ* = 1250
4: QCD only
dσ/dM_JJ (nb/GeV/c²)
M_JJ (GeV/c²)
10⁰
10⁻¹
10⁻²
10⁻³
10⁻⁴
10⁻⁵
10⁻⁶
200
400
600
800
1000

Figure 6

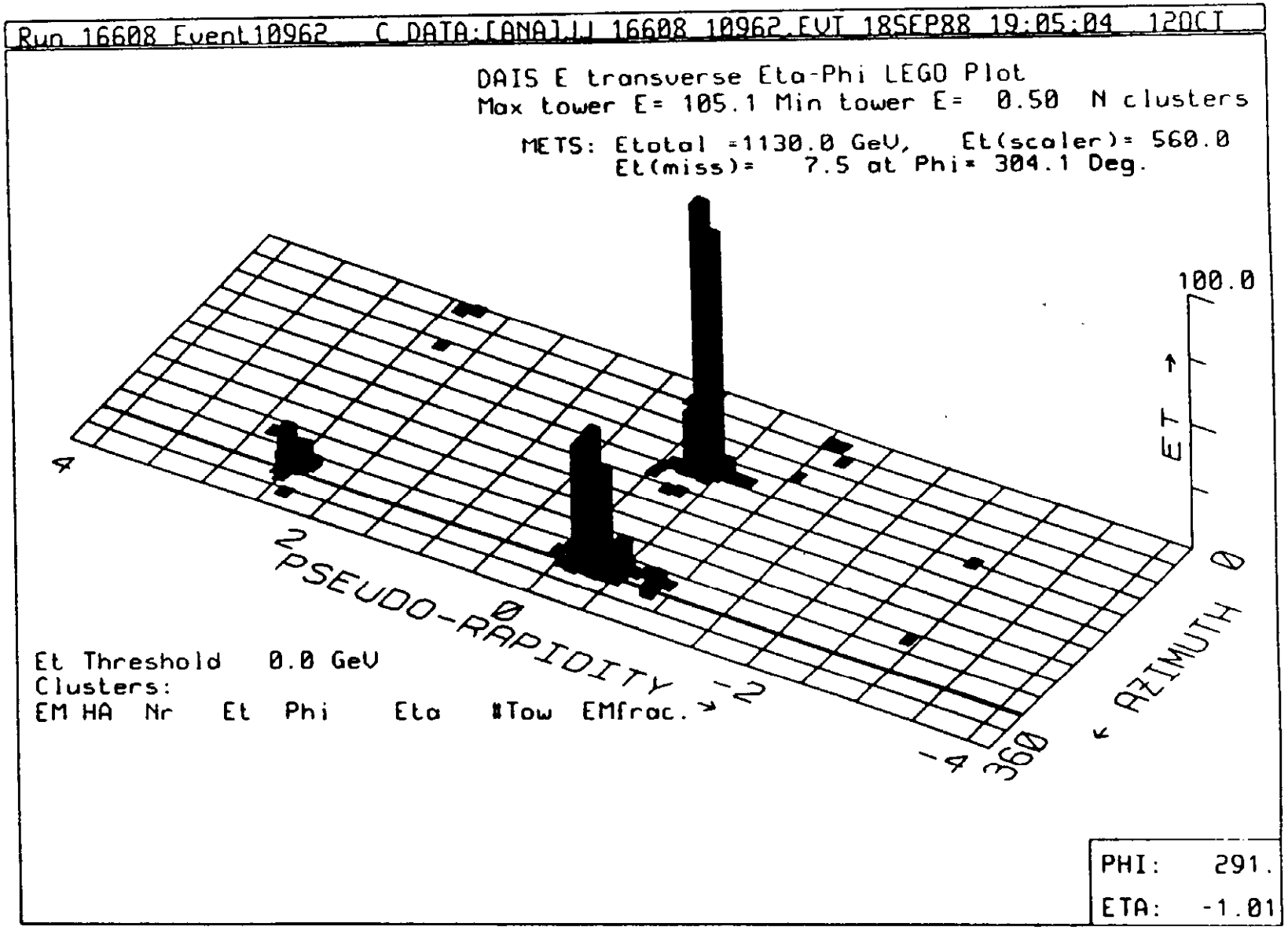
Run 16608 Event 10962 C_DATA:[ANA]JJ_16608_10962.EVT 18SEP88 19:05:04 120CT
DAIS E transverse Eta-Phi LEGO Plot
Max tower E= 105.1 Min tower E= 0.50 N clusters
METS: Etotal =1130.0 GeV, Et(scaler)= 560.0
Et(miss)= 7.5 at Phi= 304.1 Deg.
100.0
ET
4
2
0
-2
-4
PSEUDO-RAPIDITY
0
360
AZIMUTH
Et Threshold 0.0 GeV
Clusters:
EM HA Nr Et Phi Eta #Tow EMfrac.
PHI: 291.
ETA: -1.01

Figure 7a

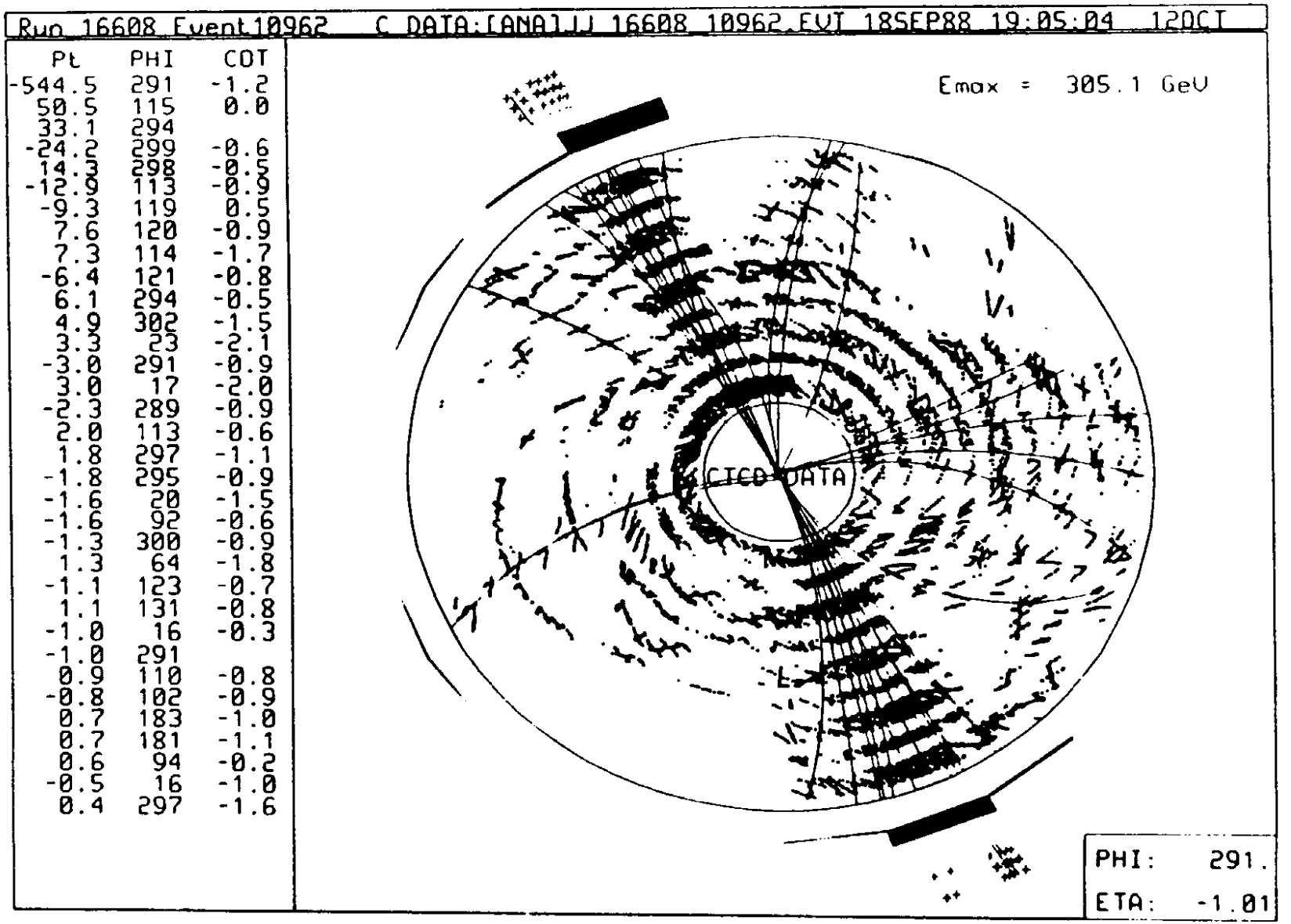
Run 16608 Event 10962 C DATA:[ANA]JJ_16608_10962.EVT 18SEP88 19:05:04 12OCT
Pt PHI COT
-544.5 291 -1.2
50.5 115 0.0
33.1 294
-24.2 299 -0.6
14.3 298 -0.5
-12.9 113 -0.9
-9.3 119 0.5
7.6 120 -0.9
7.3 114 -1.7
-6.4 121 -0.8
6.1 294 -0.5
4.9 302 -1.5
3.3 23 -2.1
-3.0 291 -0.9
3.0 17 -2.0
-2.3 289 -0.9
2.0 113 -0.6
1.8 297 -1.1
-1.8 295 -0.9
-1.6 20 -1.5
-1.6 92 -0.6
-1.3 300 -0.9
1.3 64 -1.8
-1.1 123 -0.7
1.1 131 -0.8
-1.0 16 -0.3
-1.0 291
0.9 110 -0.8
-0.8 102 -0.9
0.7 183 -1.0
0.7 181 -1.1
0.6 94 -0.2
-0.5 16 -1.0
0.4 297 -1.6
Emax = 305.1 GeV
CICO DATA
PHI: 291.
ETA: -1.01

Figure 7b

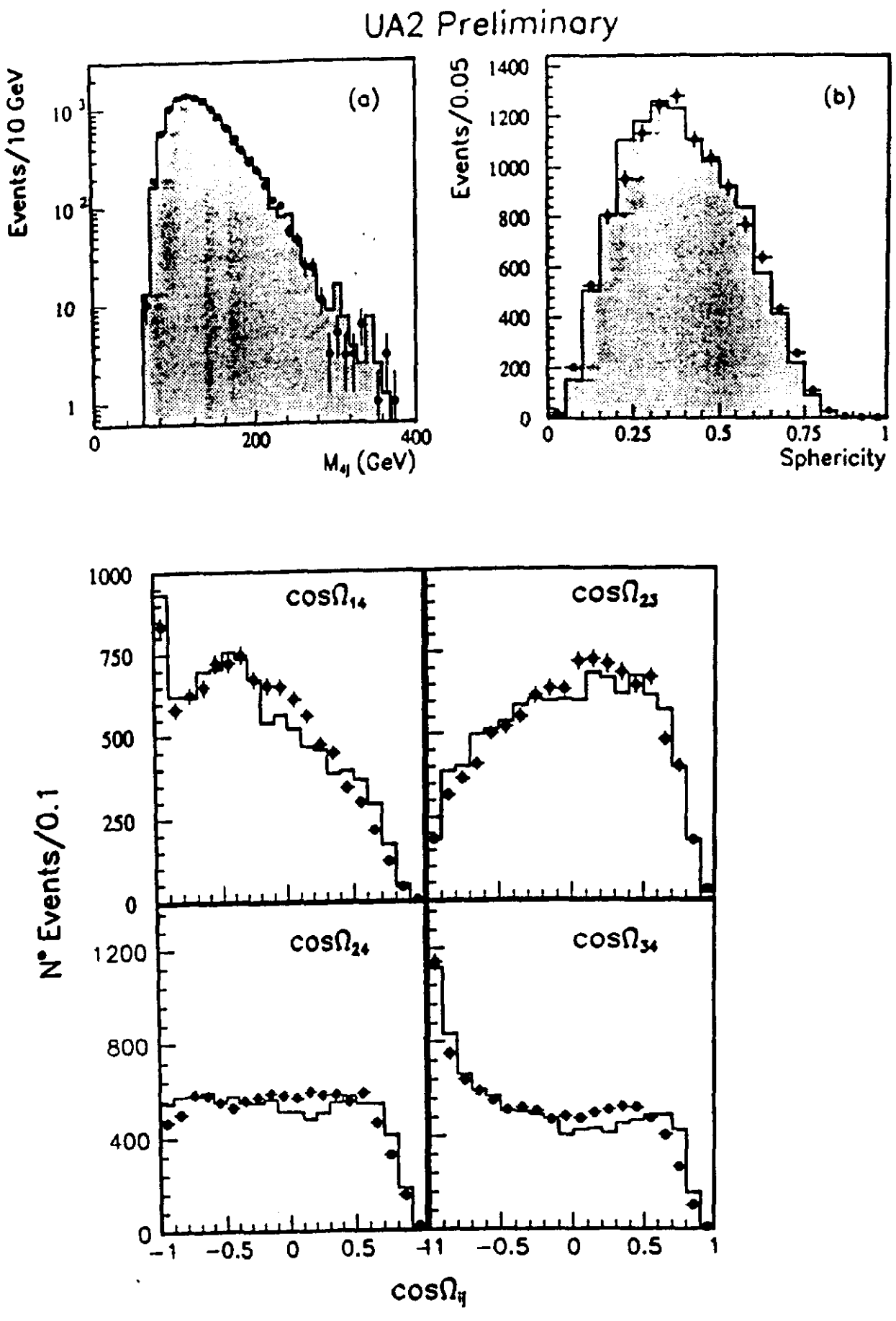
UA2 Preliminary
Events/10 GeV
(a)
M_{4j} (GeV)
Events/0.05
(b)
Sphericity
N° Events/0.1
$\cos\Omega_{14}$
$\cos\Omega_{23}$
$\cos\Omega_{24}$
$\cos\Omega_{34}$
$\cos\Omega_{ij}$

Figure 8

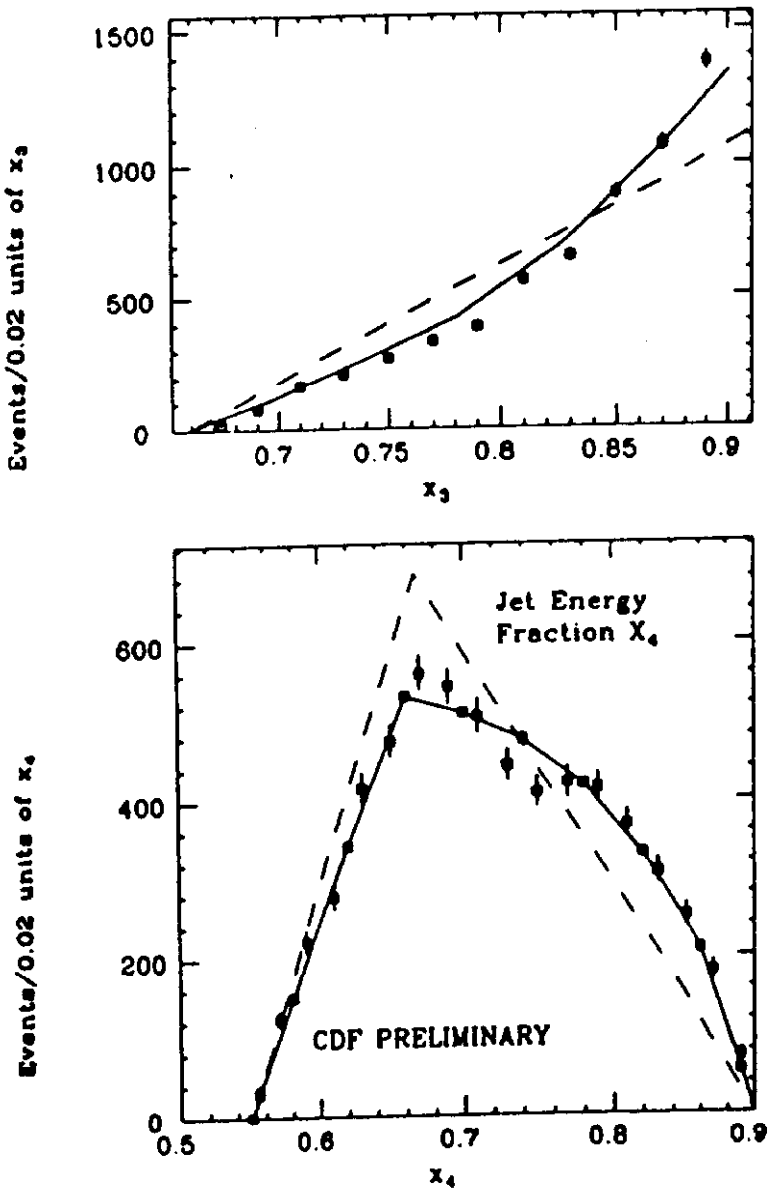
1500
1000
500
0
0.7
0.75
0.8
0.85
0.9
x_3
Events/0.02 units of x_3
600
400
200
0
0.5
0.6
0.7
0.8
0.9
x_4
Events/0.02 units of x_4
Jet Energy
Fraction X_4
CDF PRELIMINARY

Figure 9

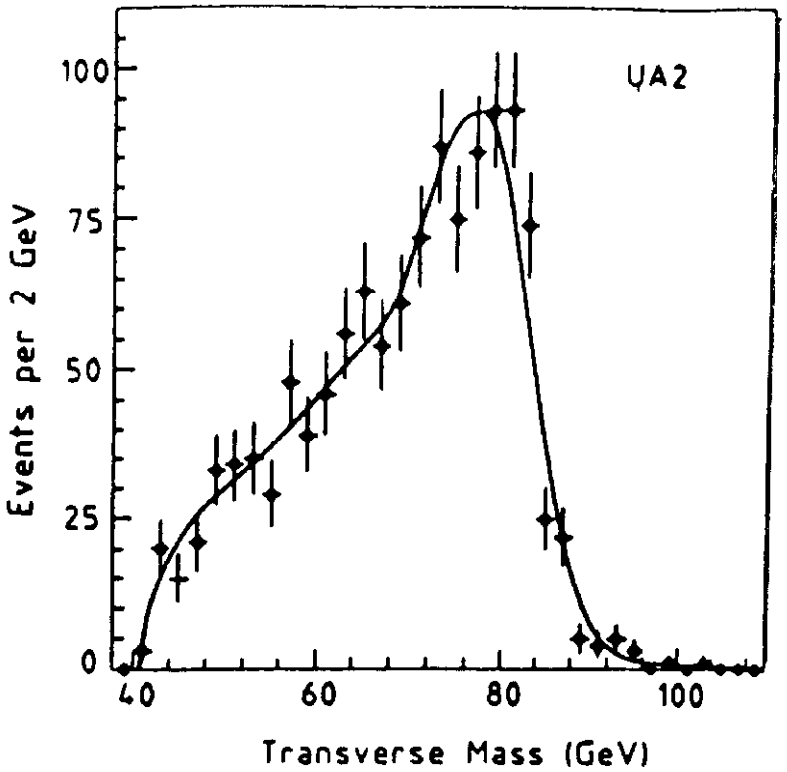
UA2
Events per 2 GeV
100
75
50
25
0
40
60
80
100
Transverse Mass (GeV)

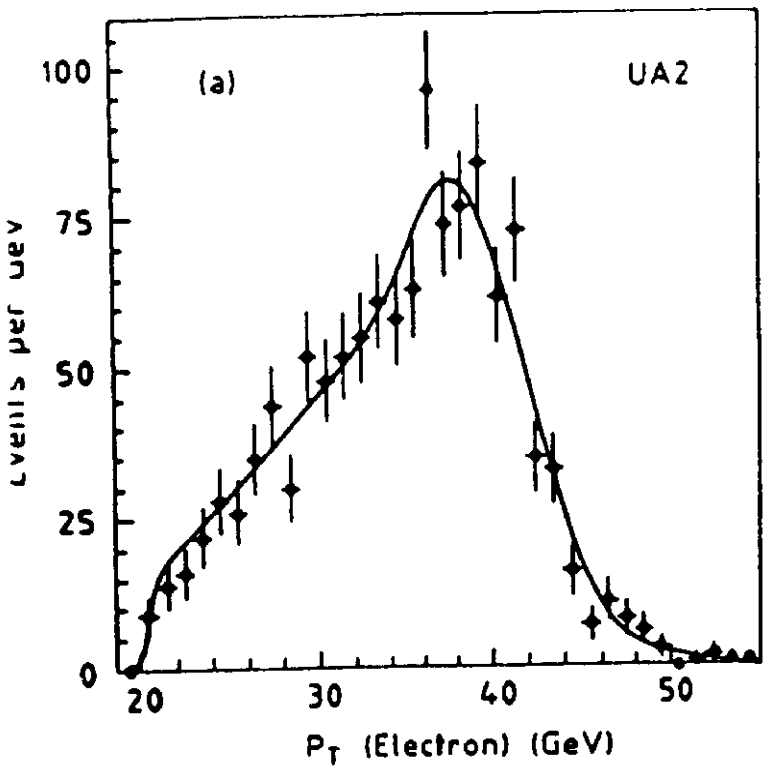
(a)
UA2
100
75
50
25
0
20
30
40
50
P_T (Electron) (GeV)

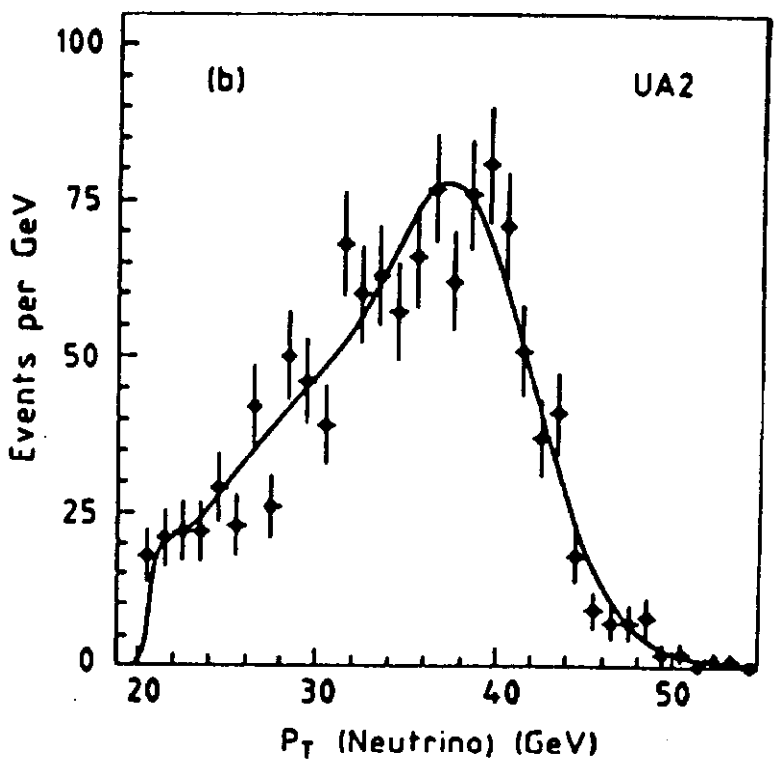
(b)
UA2
Events per GeV
100
75
50
25
0
20
30
40
50
P_T (Neutrino) (GeV)

Figure 10

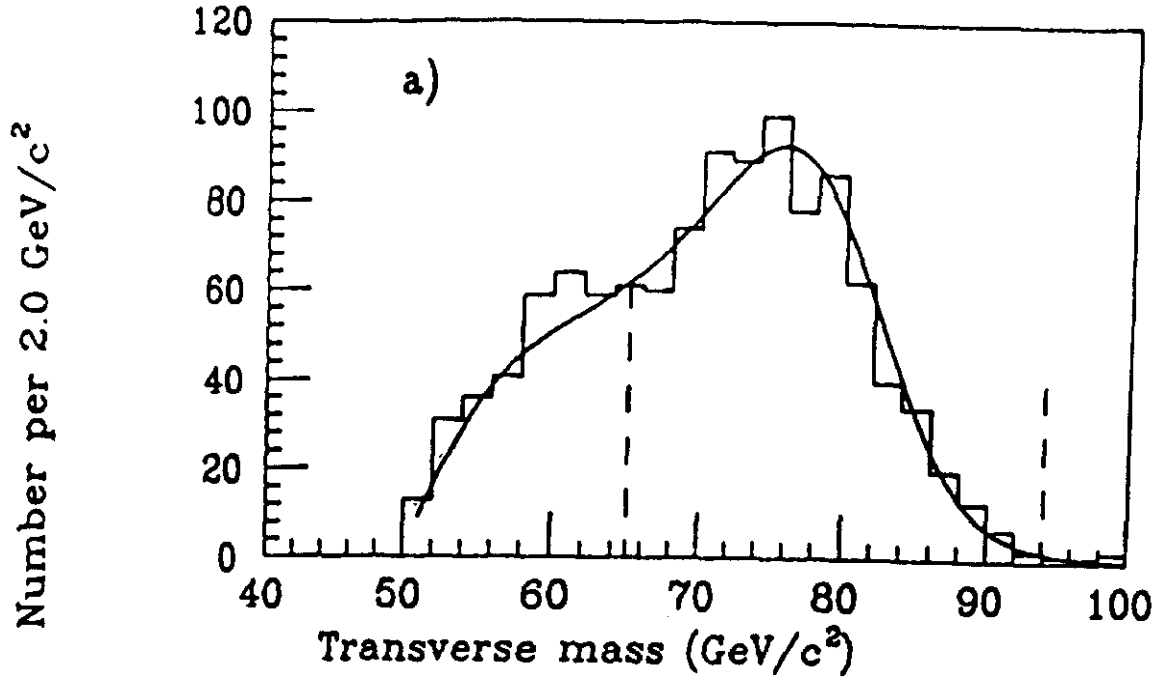
a)
Number per 2.0 GeV/c²
Transverse mass (GeV/c²)
0
20
40
60
80
100
120
40
50
60
70
80
90
100

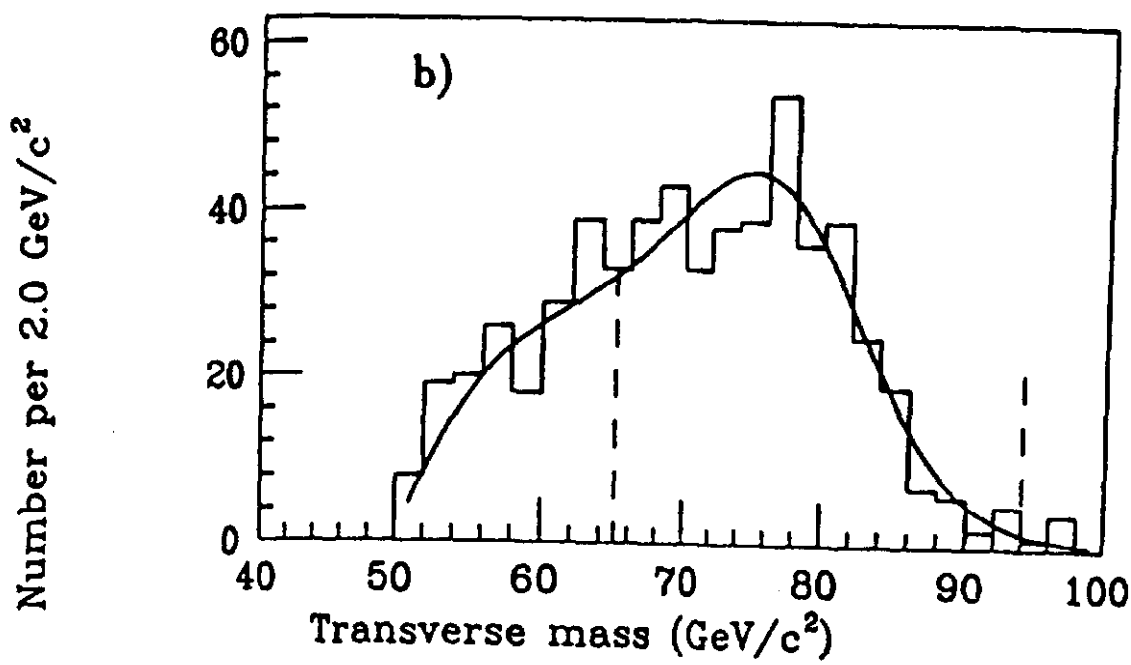
b)
Number per 2.0 GeV/c²
Transverse mass (GeV/c²)
0
20
40
60
40
50
60
70
80
90
100

Figure 11

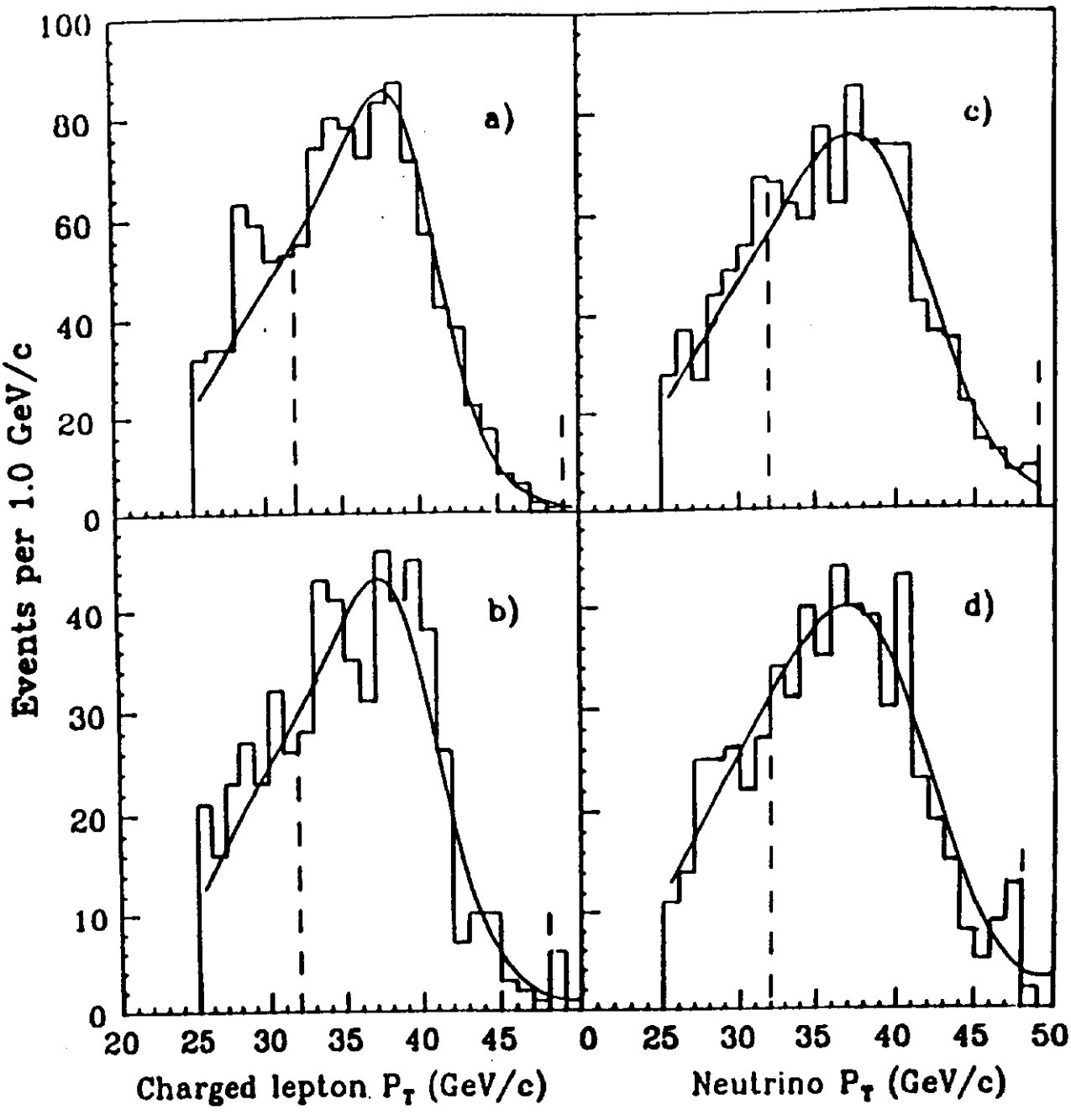
a)
b)
c)
d)
Events per 1.0 GeV/c
Charged lepton P_T (GeV/c)
Neutrino P_T (GeV/c)

Figure 12

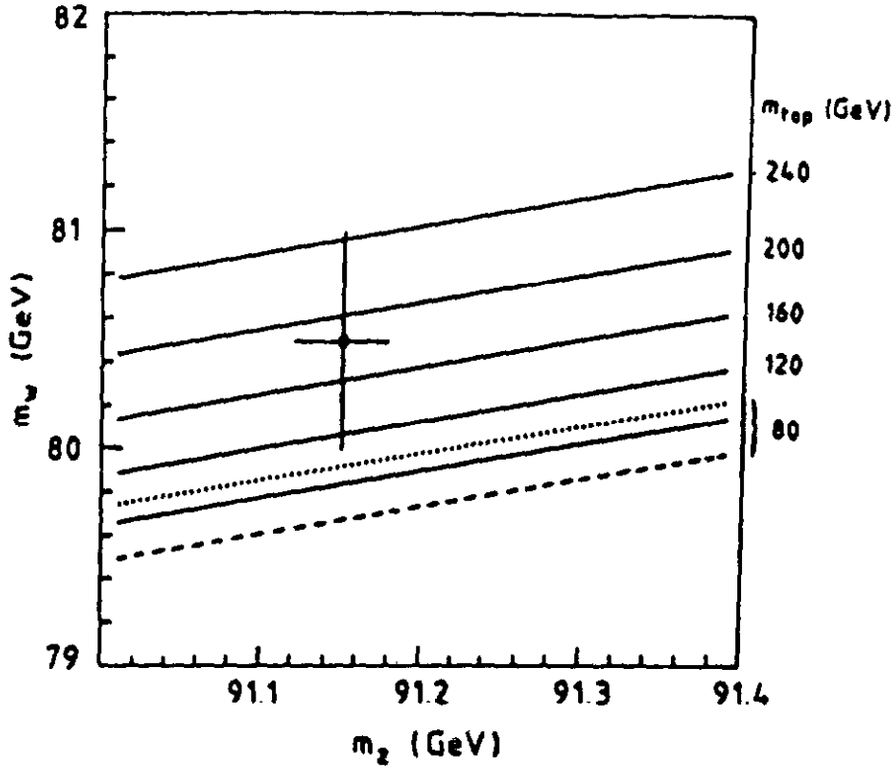
82
81
80
79
m_W (GeV)
91.1
91.2
91.3
91.4
m_Z (GeV)
m_{top} (GeV)
240
200
160
120
80

Figure 13

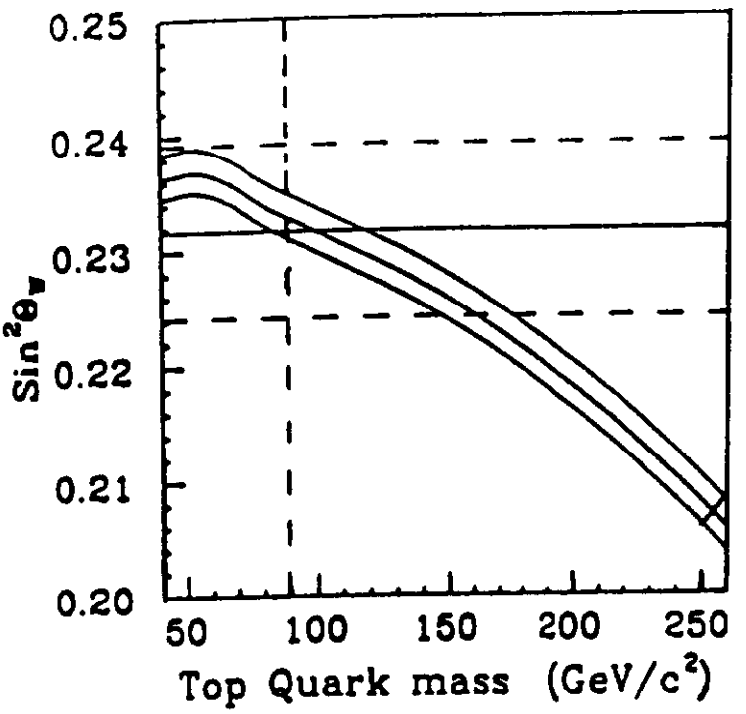
0.25
0.24
0.23
0.22
0.21
0.20
$\sin^2\theta_W$
50
100
150
200
250
Top Quark mass (GeV/c^2)

Figure 14

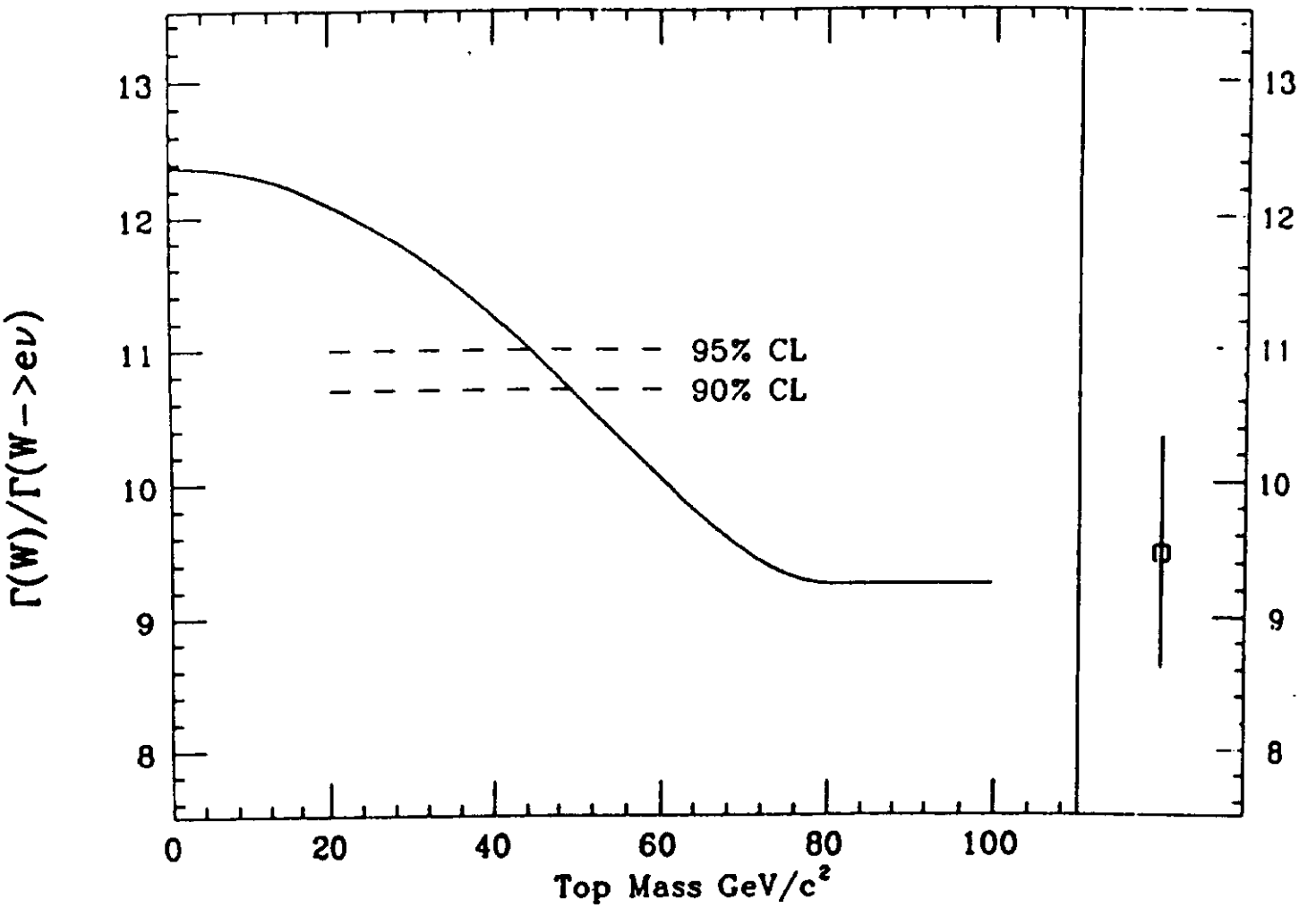

Figure 15

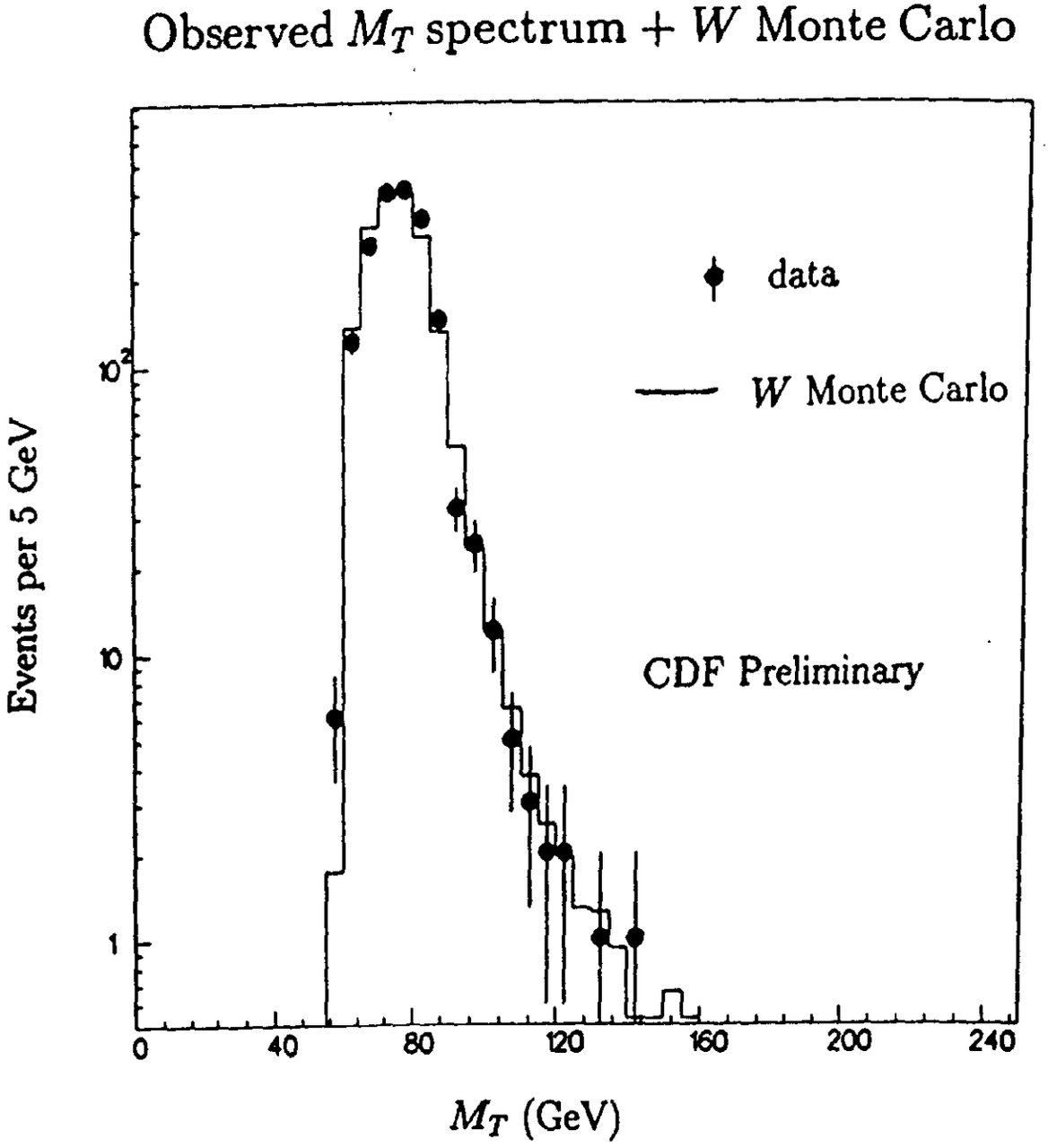
Observed M_T spectrum + W Monte Carlo
data
W Monte Carlo
CDF Preliminary
Events per 5 GeV
10^2
10
1
0
40
80
120
160
200
240
M_T (GeV)

Figure 16

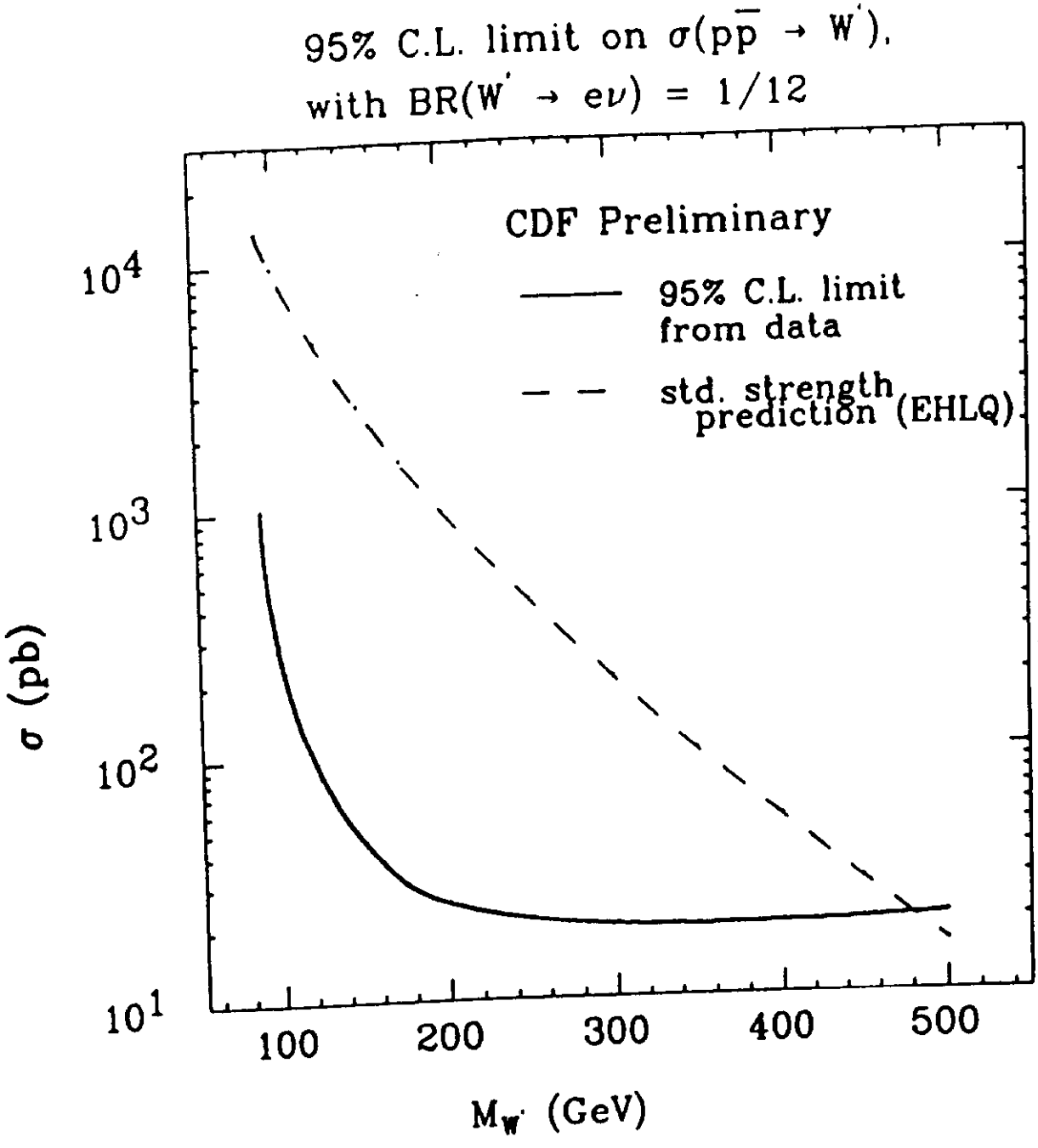
95% C.L. limit on σ(pp̄ → W'),
with BR(W' → eν) = 1/12
CDF Preliminary
95% C.L. limit from data
std. strength prediction (EHLQ)
σ (pb)
10^4
10^3
10^2
10^1
100
200
300
400
500
M_W' (GeV)

Figure 17

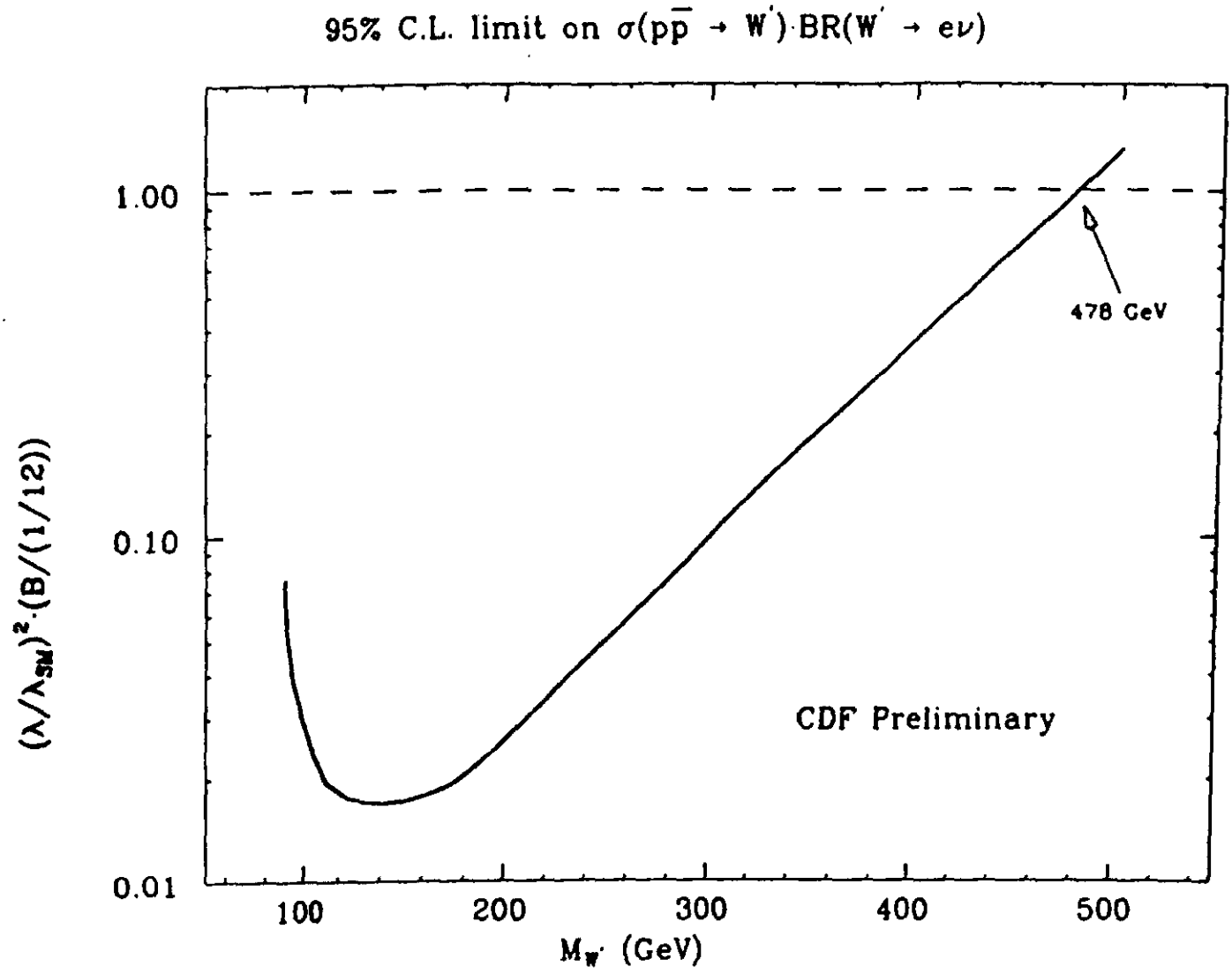
95% C.L. limit on $\sigma(p\bar{p} \rightarrow W') \cdot BR(W' \rightarrow e\nu)$
1.00
0.10
0.01
$(\lambda/\lambda_{SM})^2 \cdot (B/(1/12))$
478 GeV
CDF Preliminary
100
200
300
400
500
$M_{W'}$ (GeV)

Figure 18

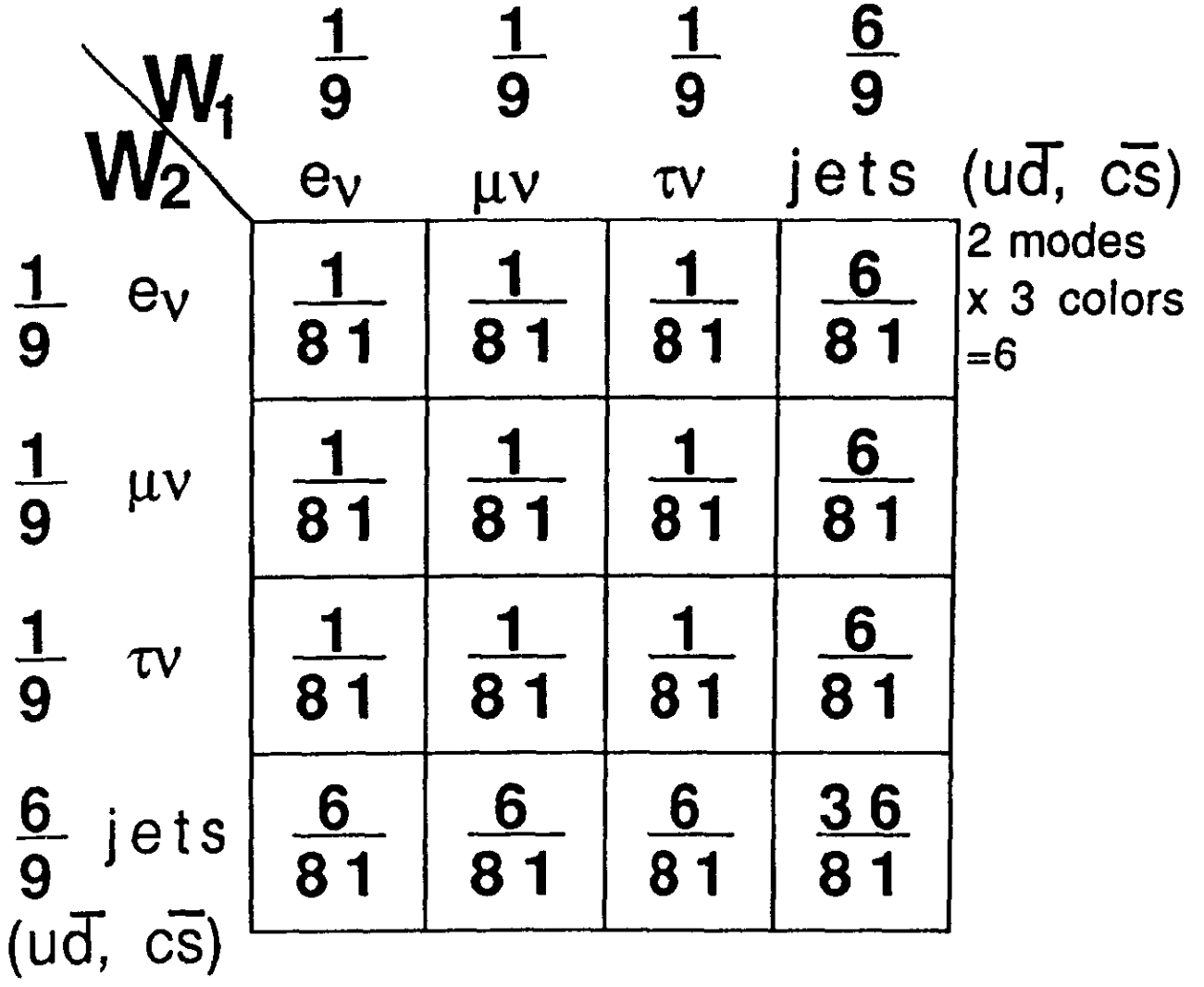
W1
W2
1/9 1/9 1/9 6/9
eν μν τν jets (ud̄, c s̄)
1/9 eν
1/9 μν
1/9 τν
6/9 jets (ud̄, c s̄)
1/81 1/81 1/81 6/81
1/81 1/81 1/81 6/81
1/81 1/81 1/81 6/81
6/81 6/81 6/81 36/81
2 modes
x 3 colors
=6

Figure 19

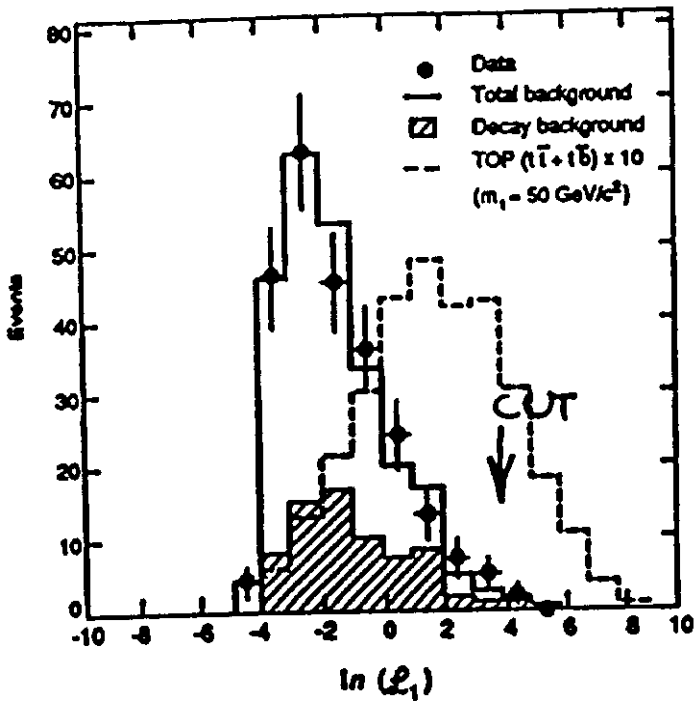
Data
Total background
Decay background
TOP ($t\bar{t}+t\bar{b}$) x 10
(m_t = 50 GeV/c^2)
CUT
Events
$\ln(\mathcal{L}_1)$

Figure 20

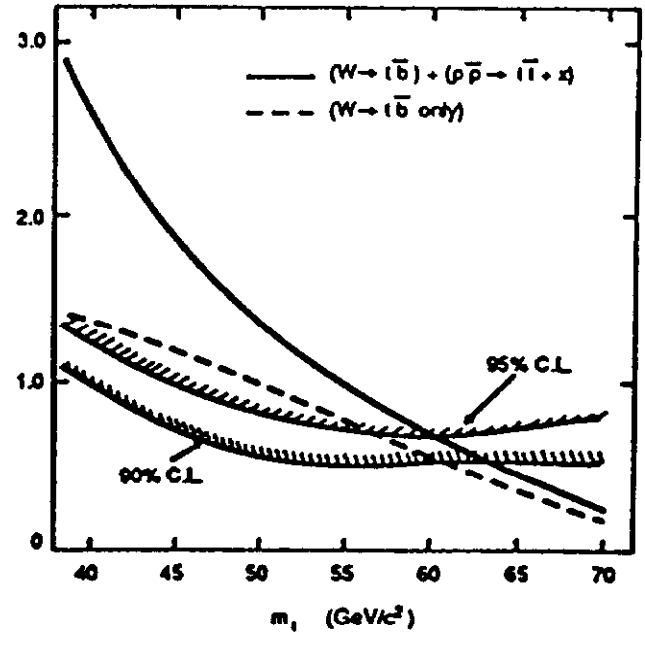

Figure 21

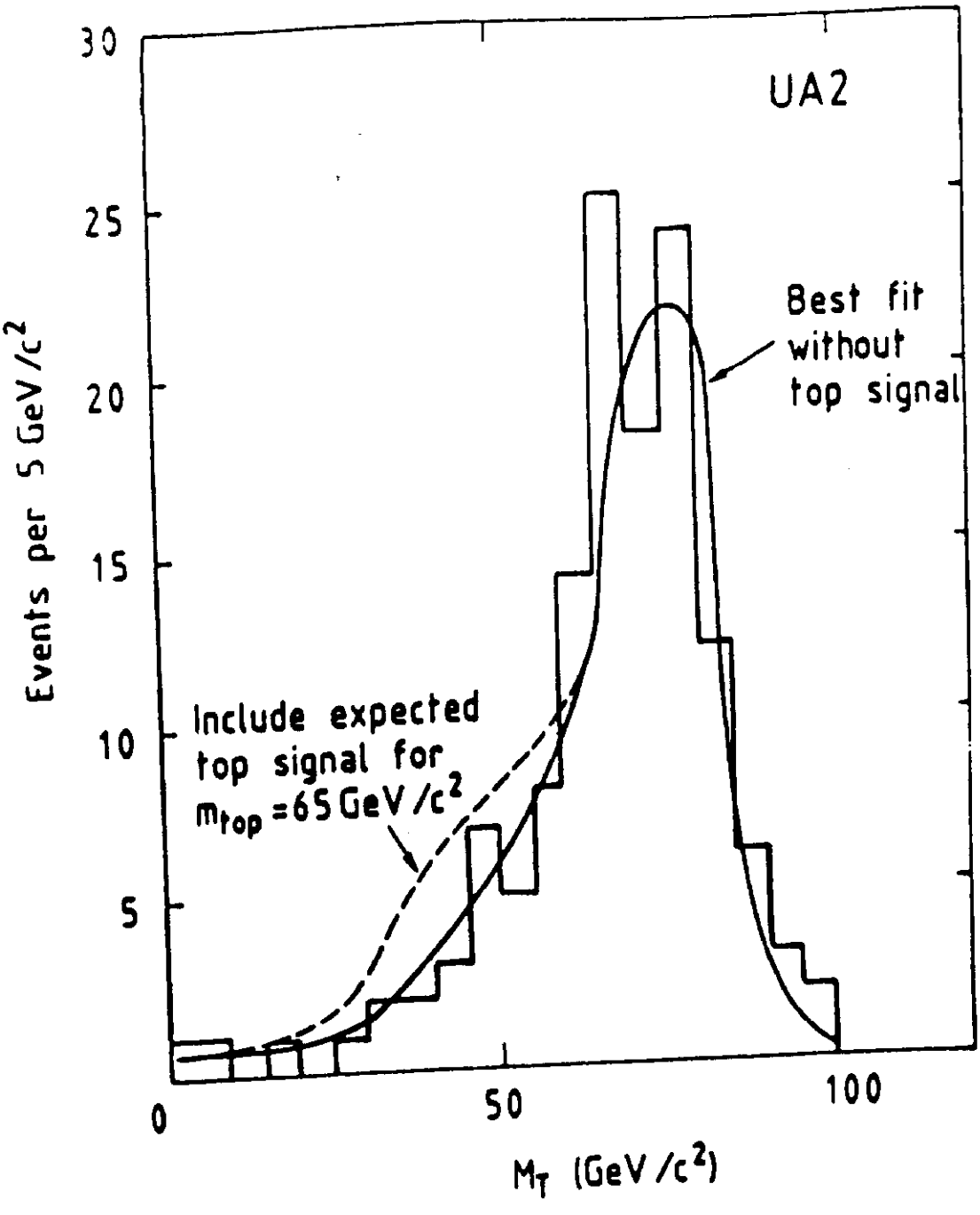
UA2
Best fit
without
top signal
Include expected
top signal for
$m_{top} = 65\,GeV/c^2$
Events per 5 GeV/c^2
M_T (GeV/c^2)
0
50
100
5
10
15
20
25
30

Figure 22

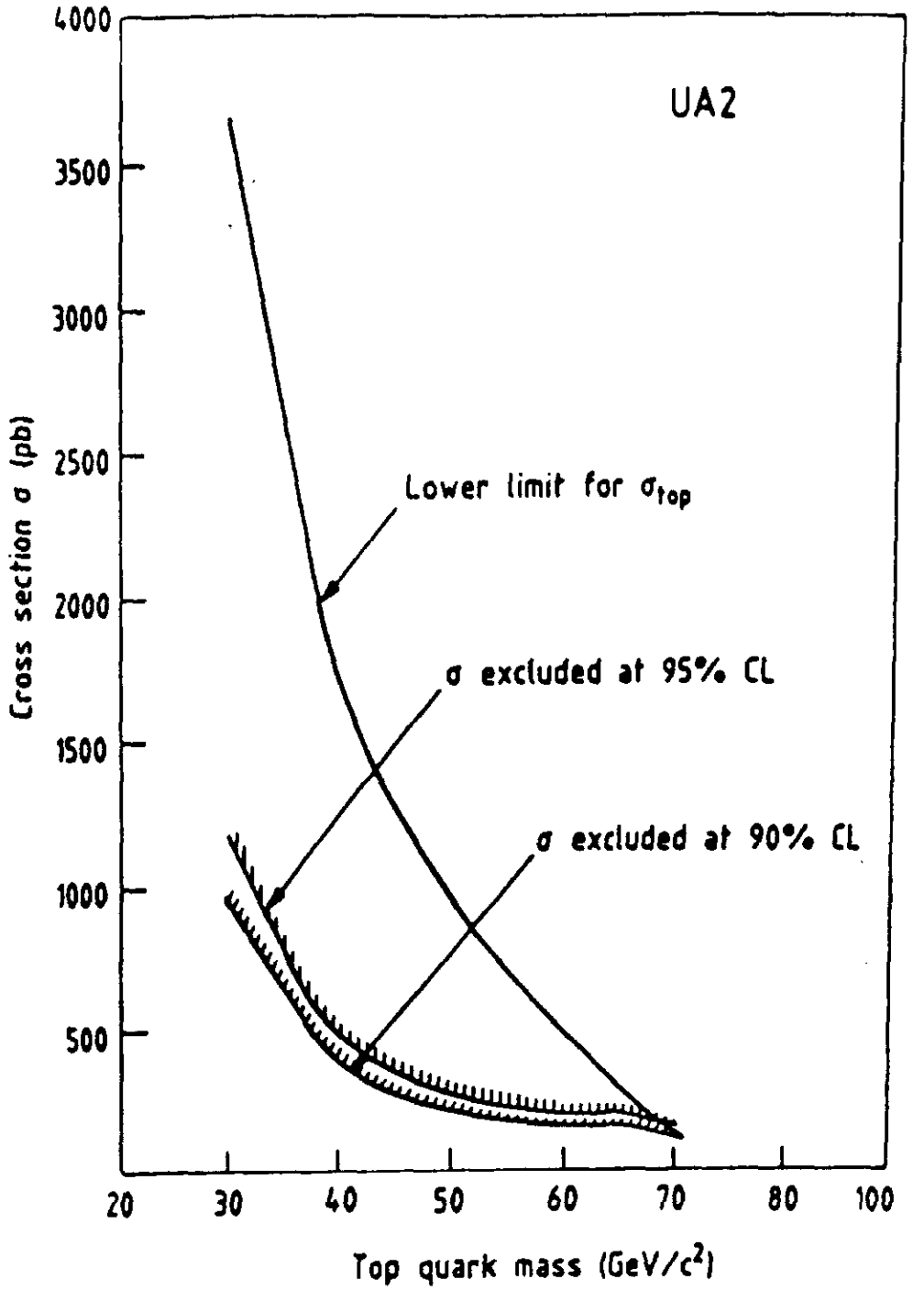
UA2
Lower limit for σ_{top}
σ excluded at 95% CL
σ excluded at 90% CL
Cross section σ (pb)
4000
3500
3000
2500
2000
1500
1000
500
20
30
40
50
60
70
80
100
Top quark mass (GeV/c²)

Figure 23

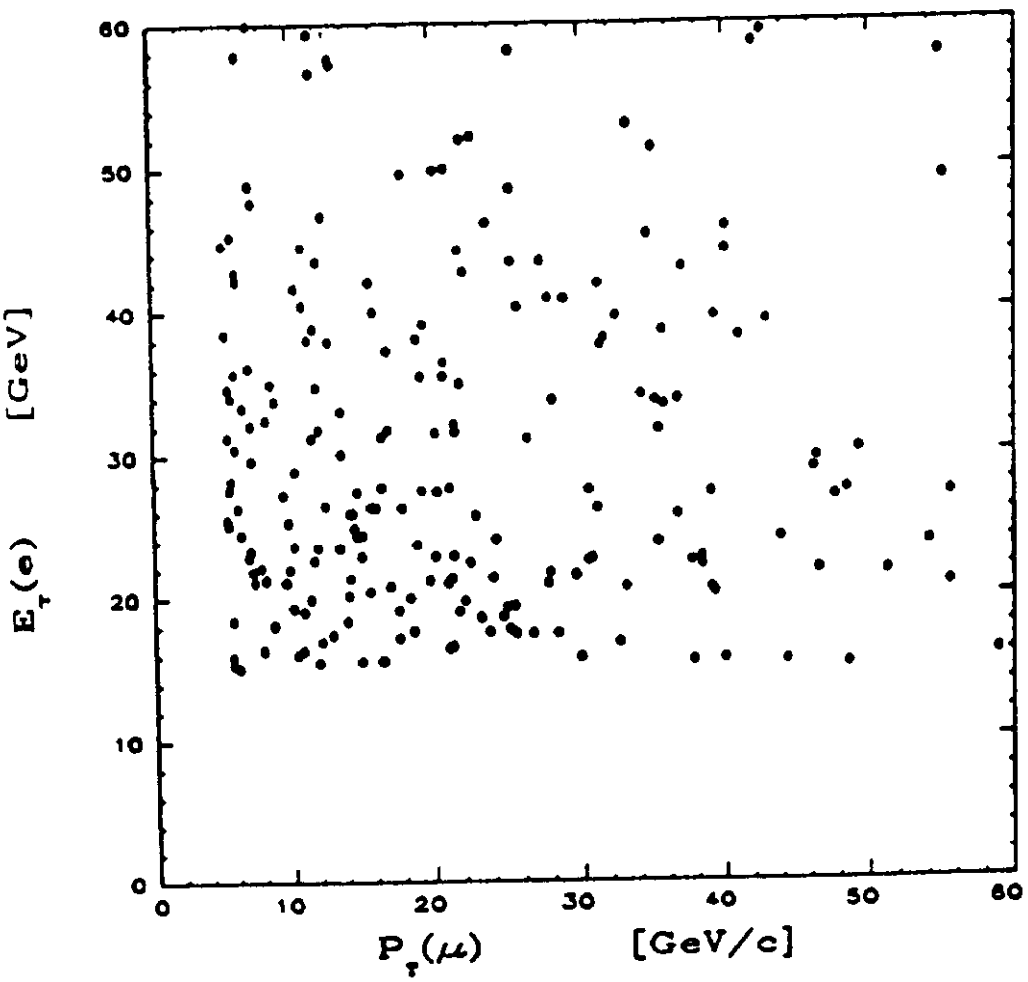

Figure 24a

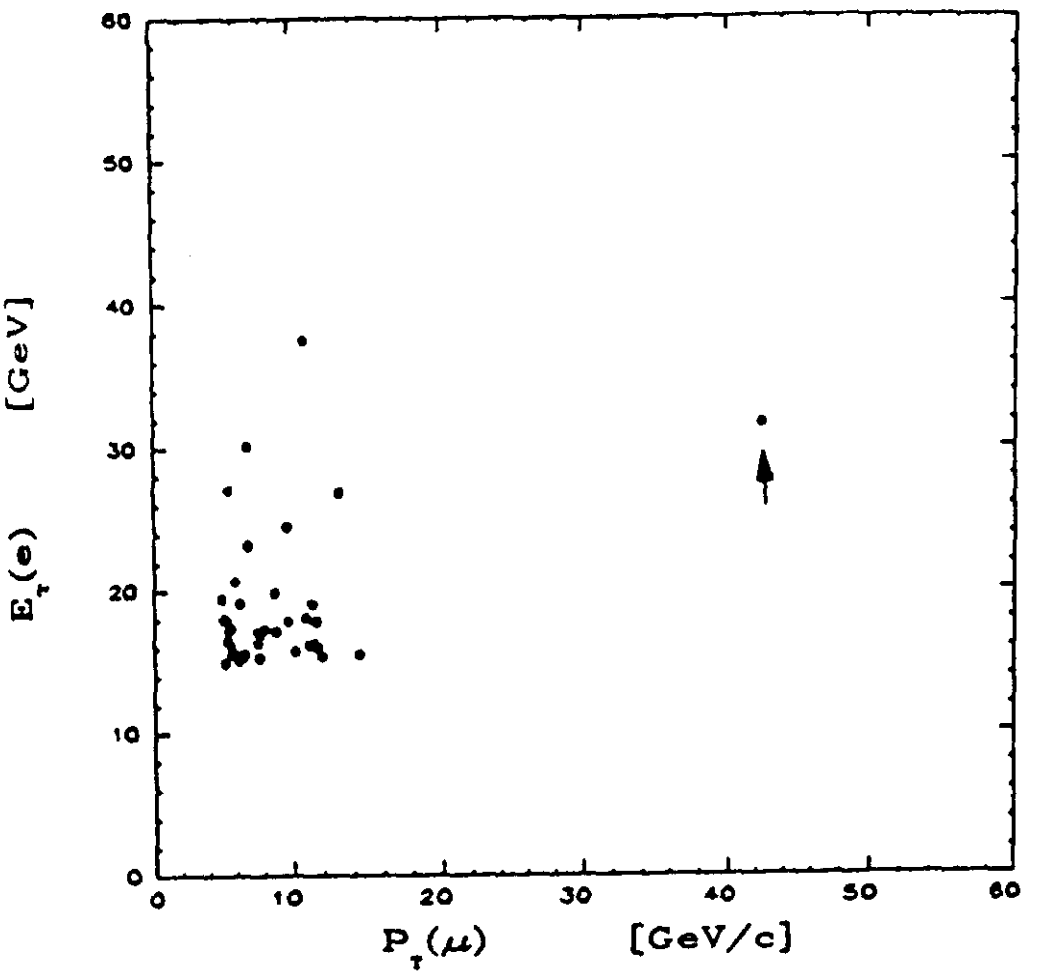

Figure 24b

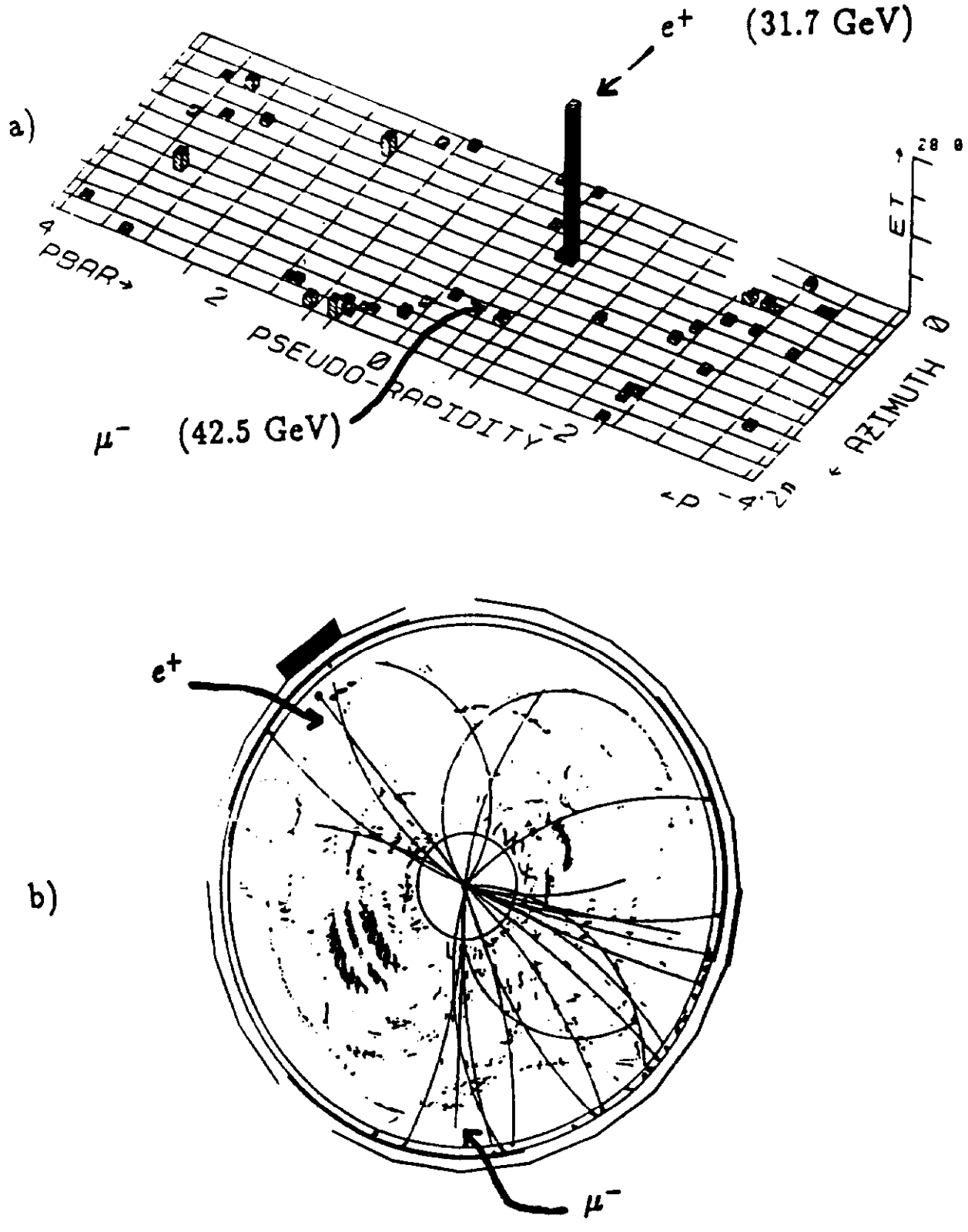

Figure 25

CDF Preliminary

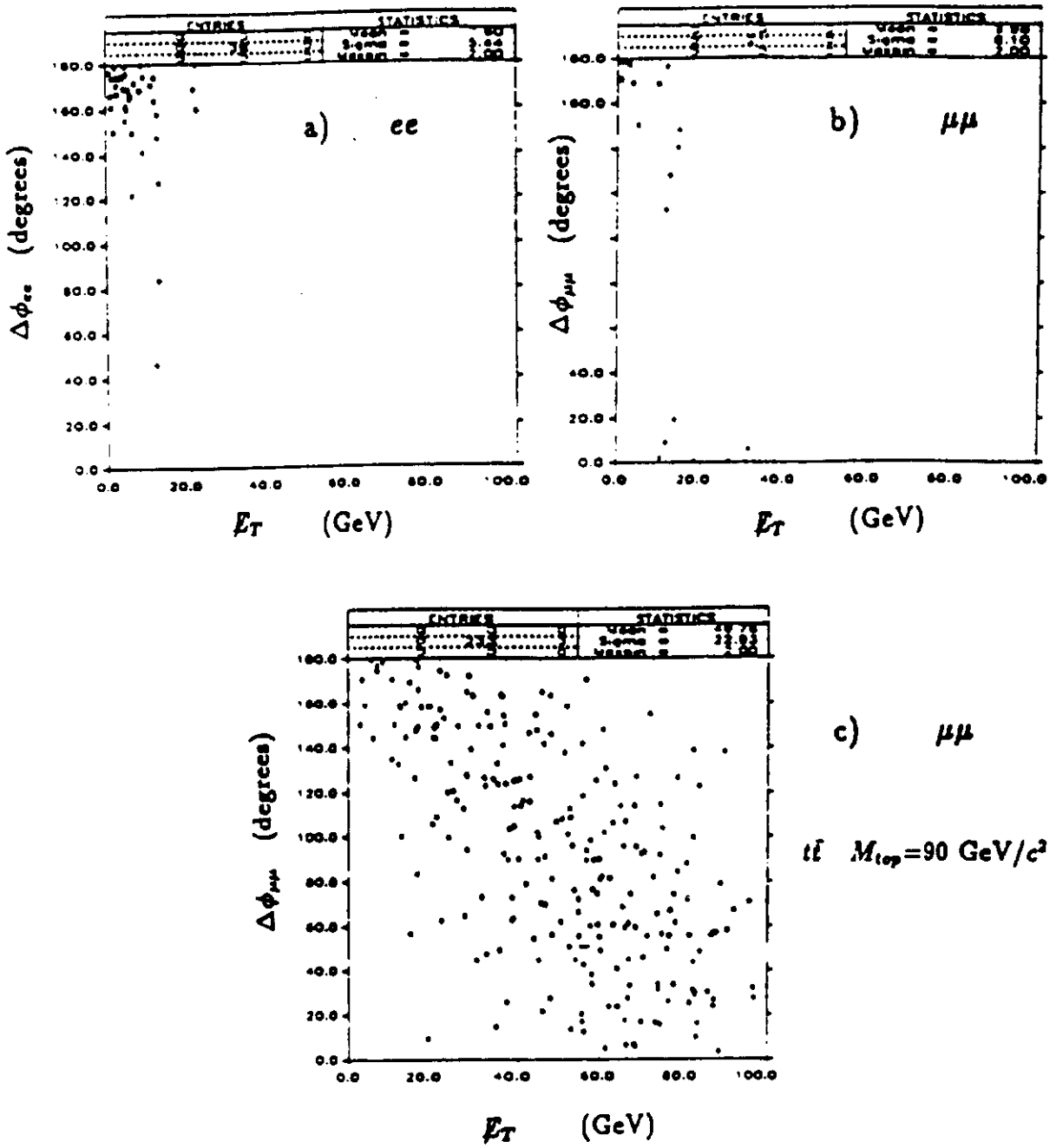

Figure 26

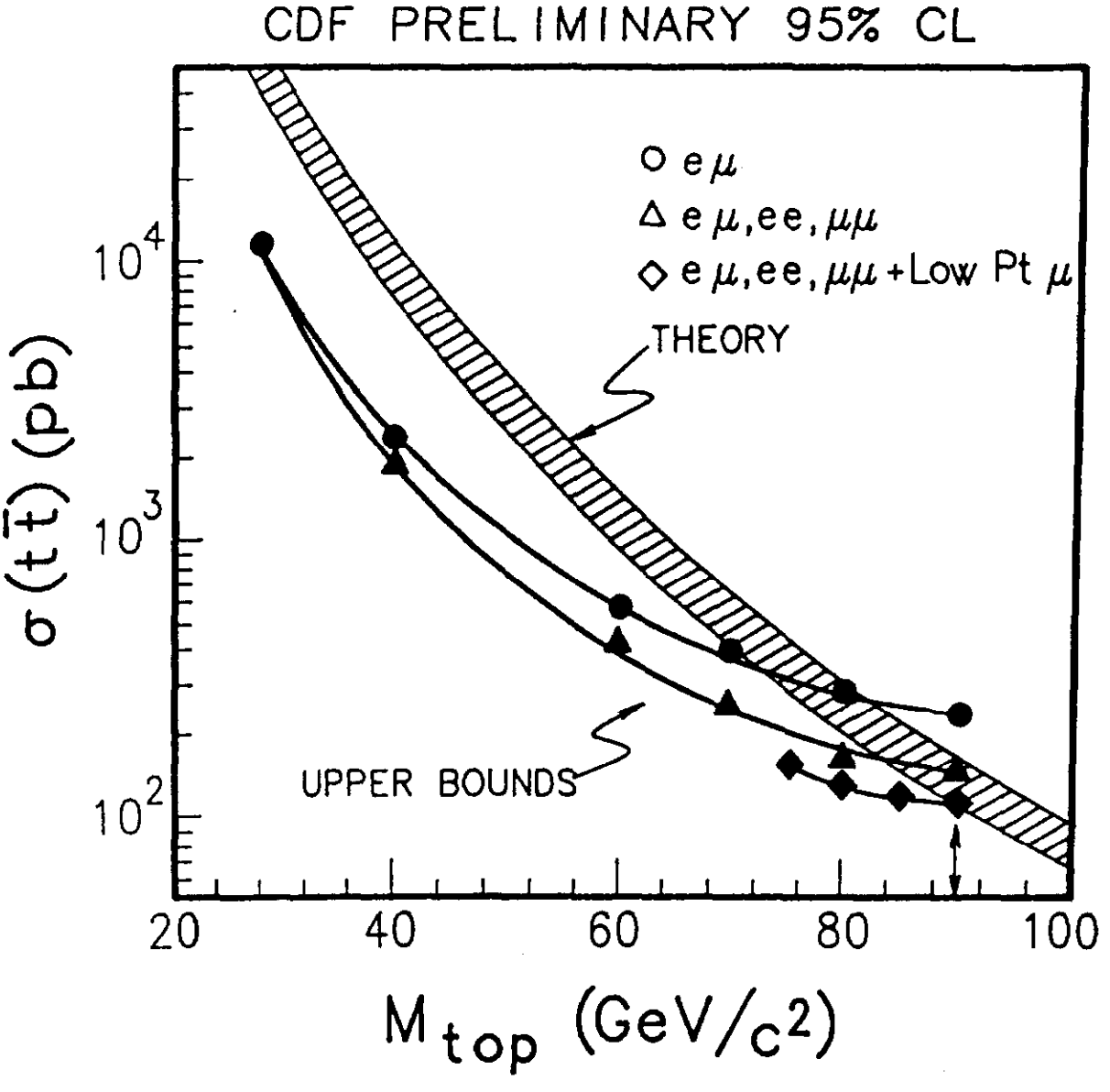
CDF PRELIMINARY 95% CL
e μ
e μ, ee, μμ
e μ, ee, μμ + Low Pt μ
THEORY
UPPER BOUNDS
σ (tt̄) (pb)
10^4
10^3
10^2
20
40
60
80
100
M top (GeV/c^2)

Figure 27

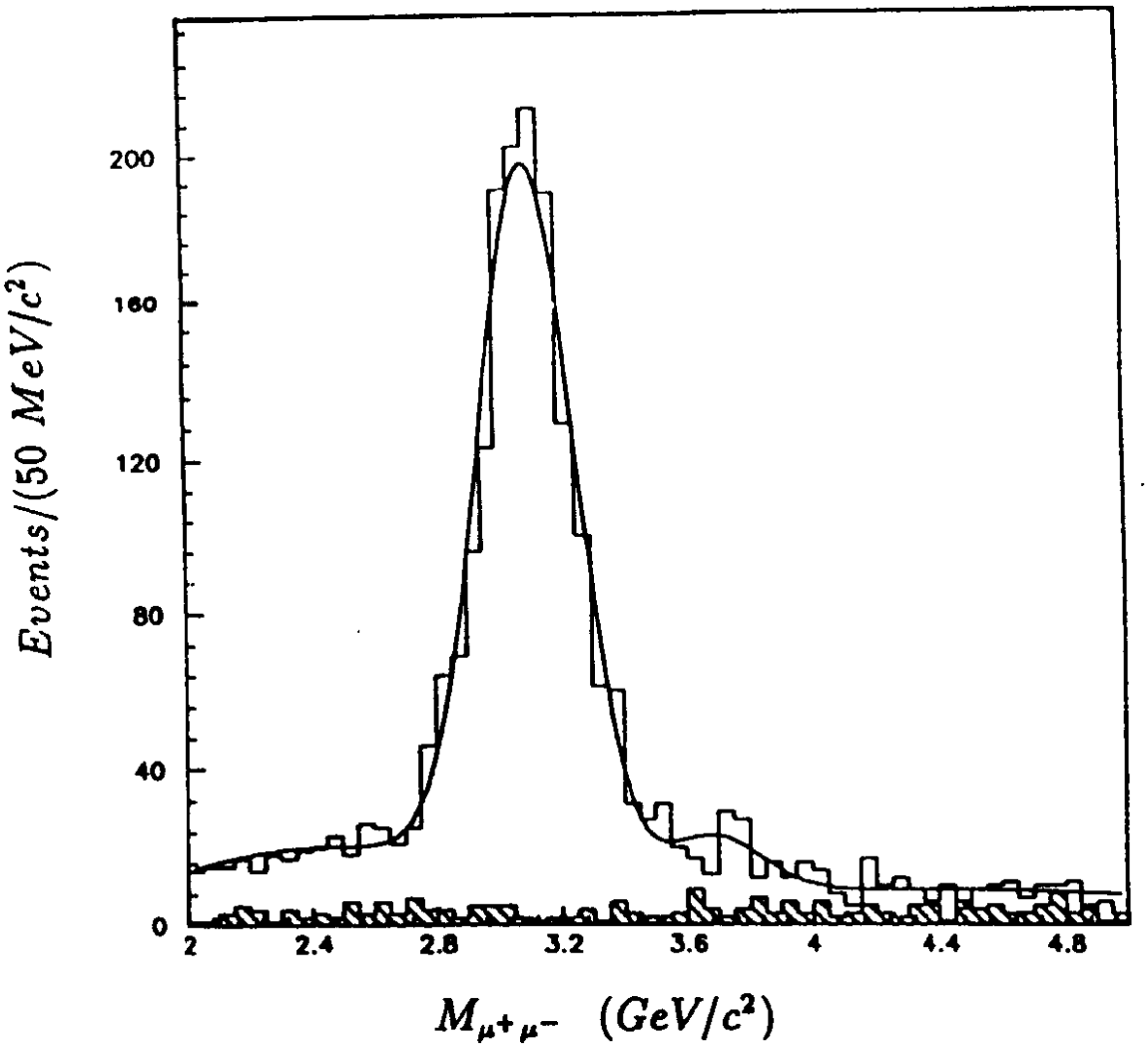

Figure 28

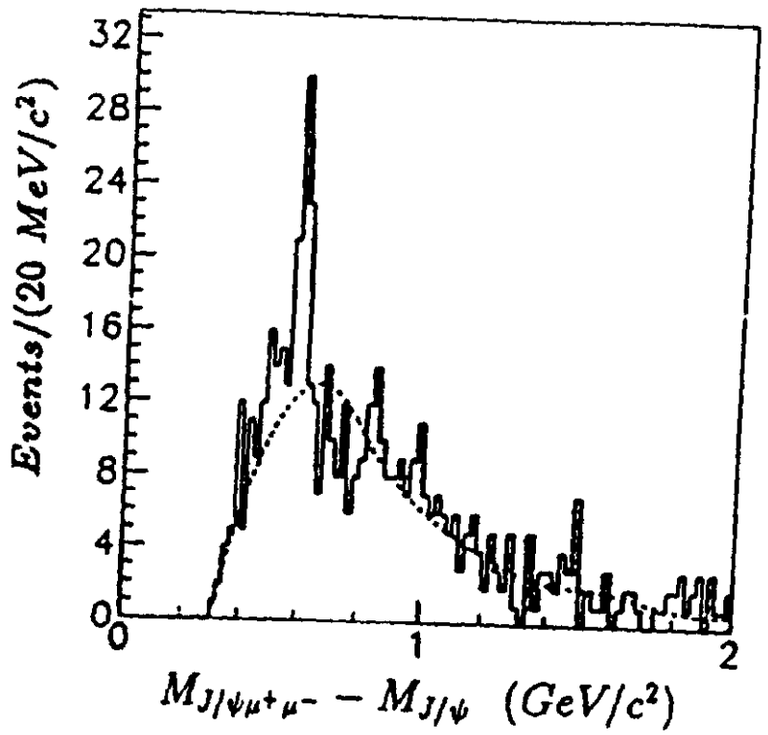

Figure 29

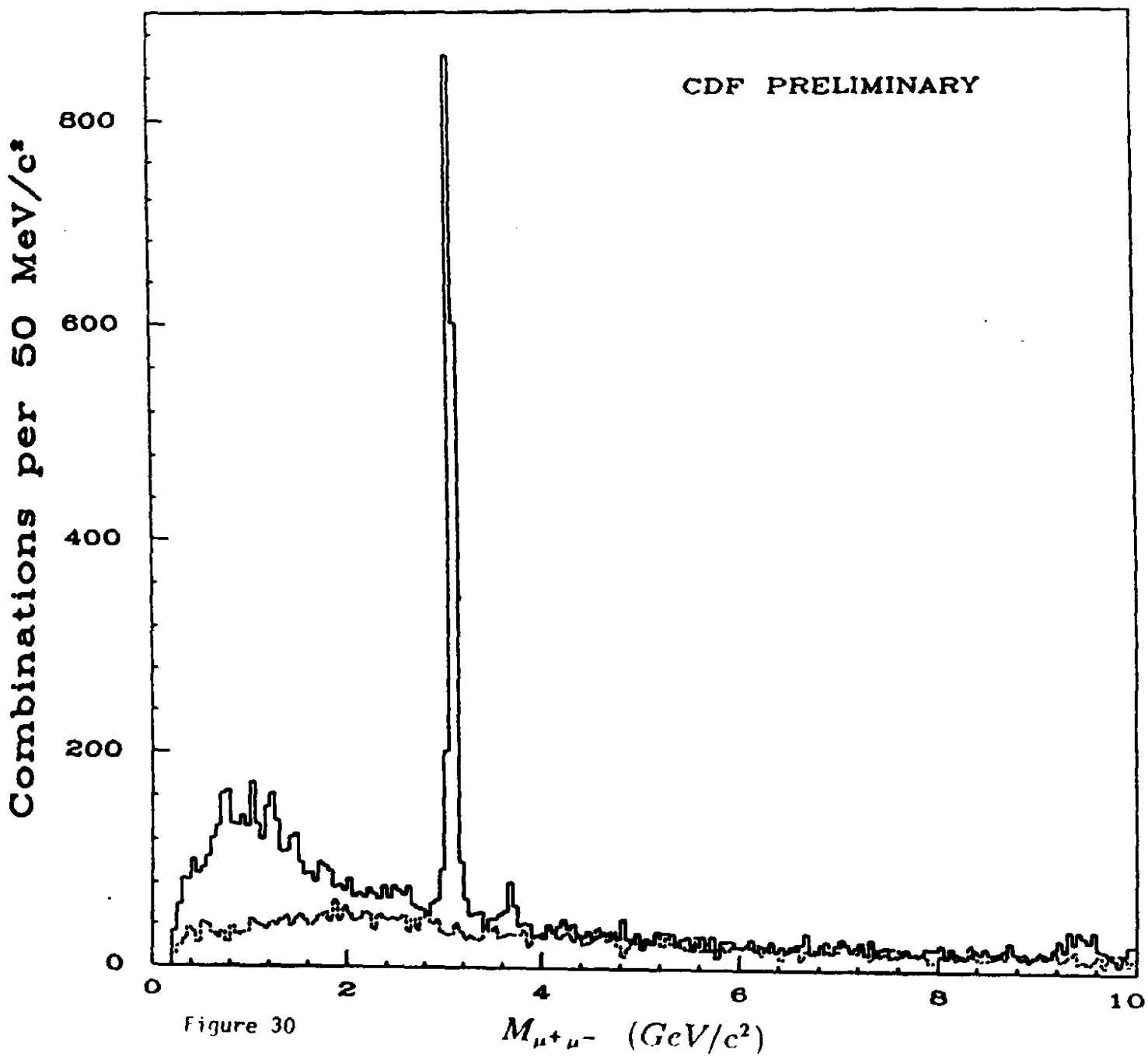
CDF PRELIMINARY
Combinations per 50 MeV/c²
800
600
400
200
0
0
2
4
6
8
10
$M_{\mu^+\mu^-}$ (GeV/c^2)

Figure 30

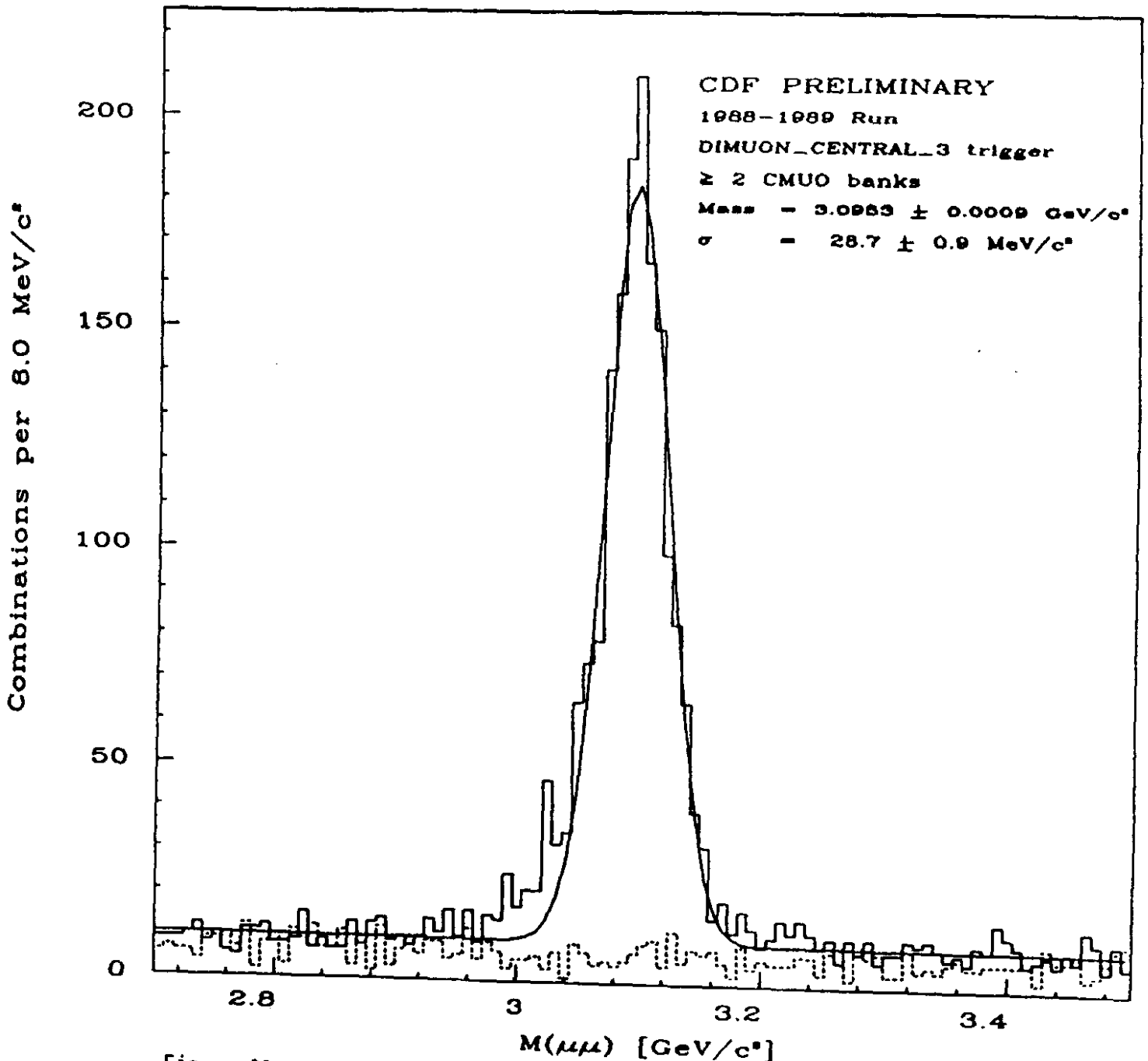
CDF PRELIMINARY
1988-1989 Run
DIMUON_CENTRAL_3 trigger
≥ 2 CMUO banks
Mass = 3.0953 ± 0.0009 GeV/c²
σ = 28.7 ± 0.9 MeV/c²
Combinations per 8.0 MeV/c²
200
150
100
50
0
2.8
3
3.2
3.4
M(μμ) [GeV/c²]

Figure 31

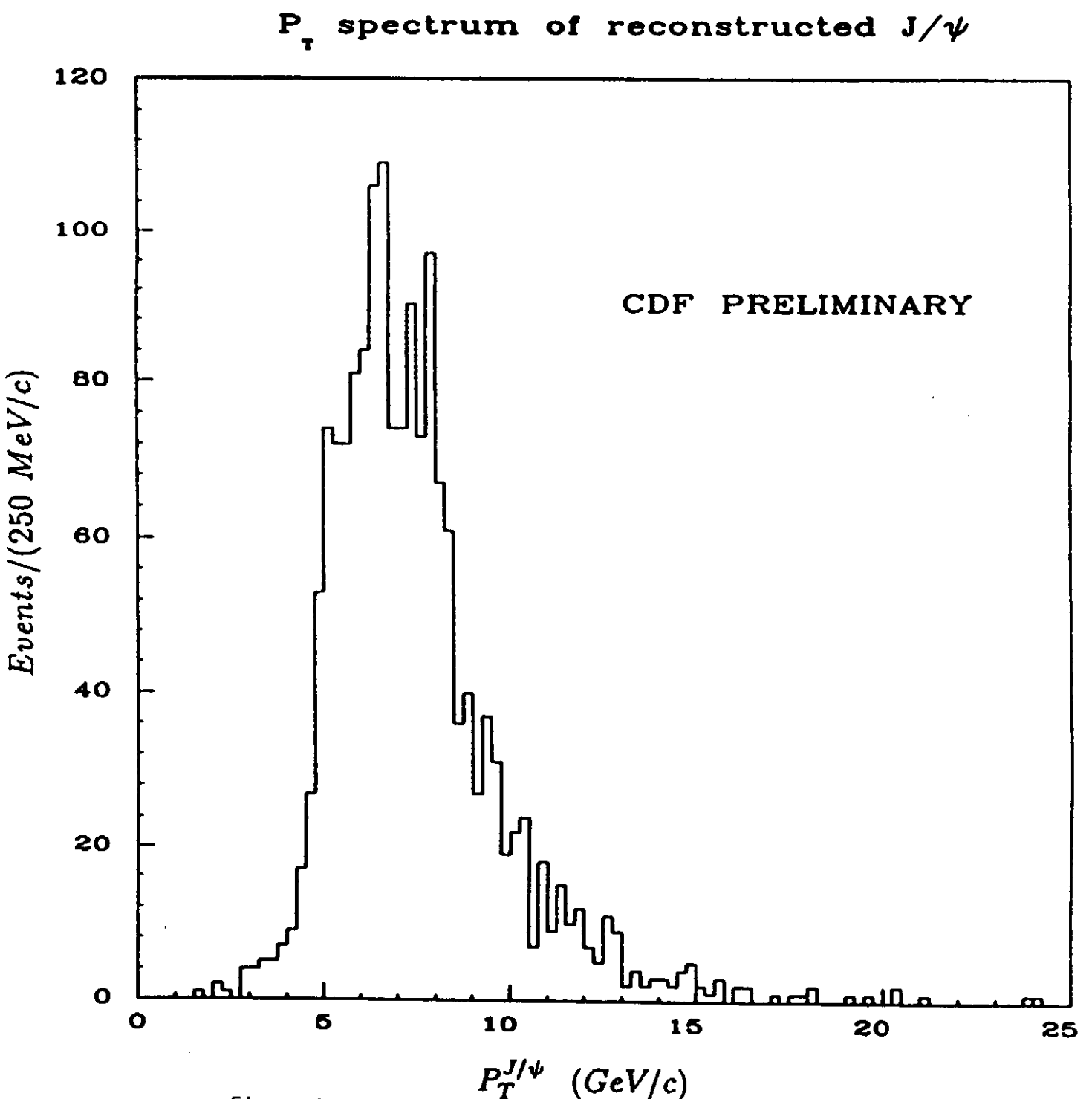
P_T spectrum of reconstructed J/ψ
CDF PRELIMINARY
Events/(250 MeV/c)
0
20
40
60
80
100
120
0
5
10
15
20
25
P_T^{J/ψ} (GeV/c)

Figure 32

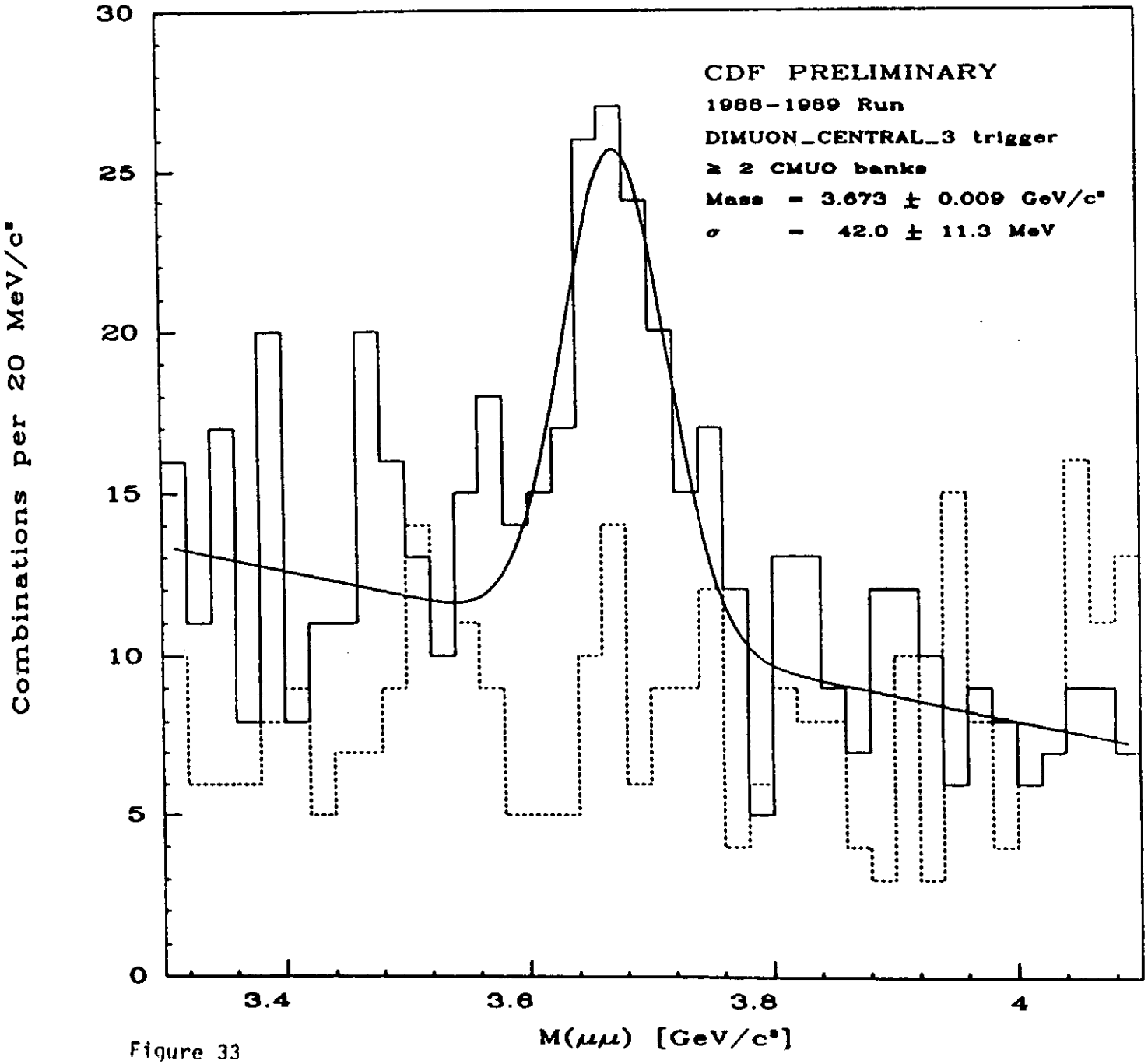
CDF PRELIMINARY
1988-1989 Run
DIMUON_CENTRAL_3 trigger
≥ 2 CMUO banks
Mass = 3.673 ± 0.009 GeV/c²
σ = 42.0 ± 11.3 MeV
Combinations per 20 MeV/c²
M(μμ) [GeV/c²]
0
5
10
15
20
25
30
3.4
3.6
3.8
4

Figure 33

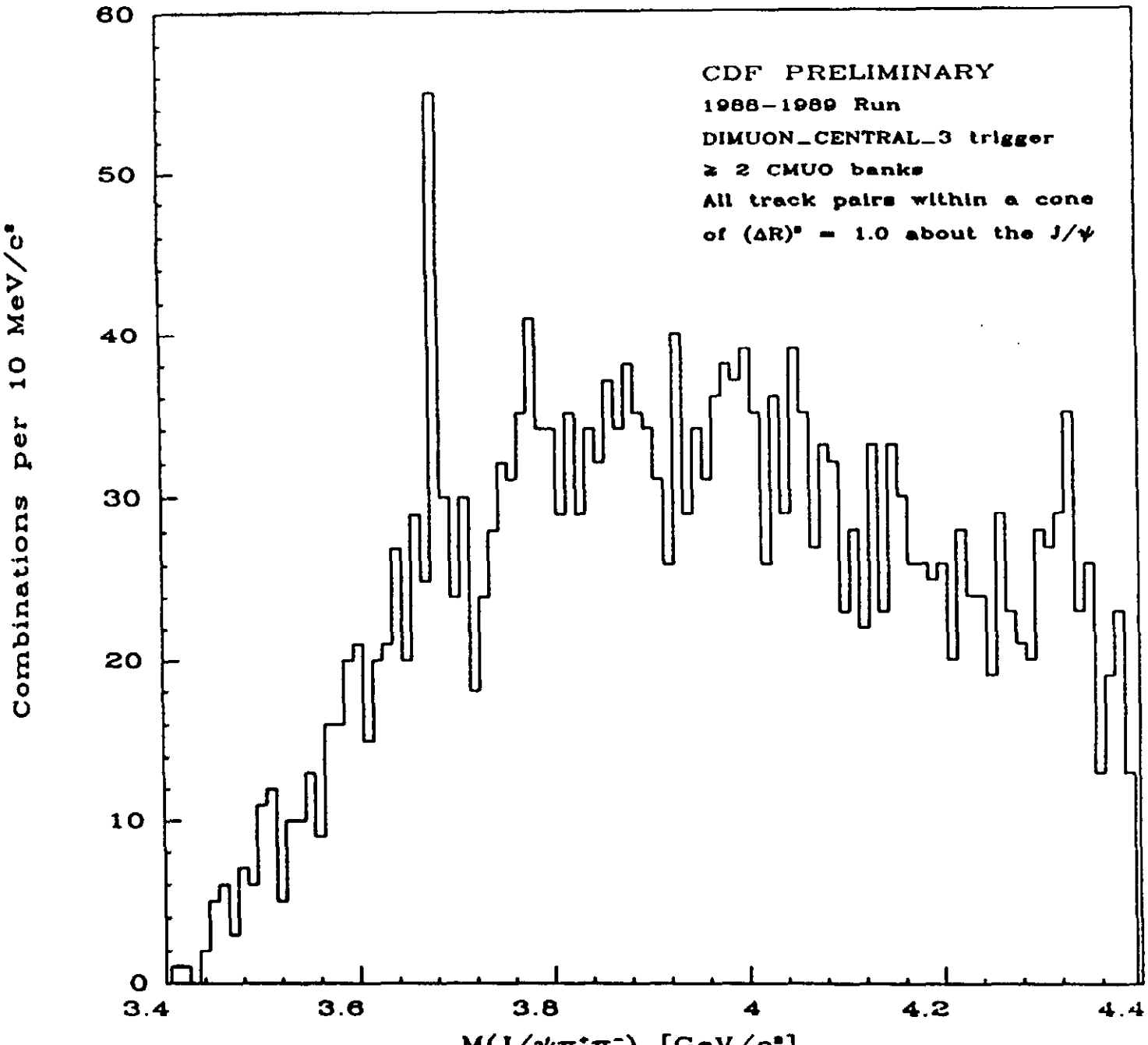
CDF PRELIMINARY
1988–1989 Run
DIMUON_CENTRAL_3 trigger
≥ 2 CMUO banks
All track pairs within a cone
of (ΔR)² = 1.0 about the J/ψ
Combinations per 10 MeV/c²
M(J/ψπ⁺π⁻) [GeV/c²]
0
10
20
30
40
50
60
3.4
3.6
3.8
4
4.2
4.4

Figure 34

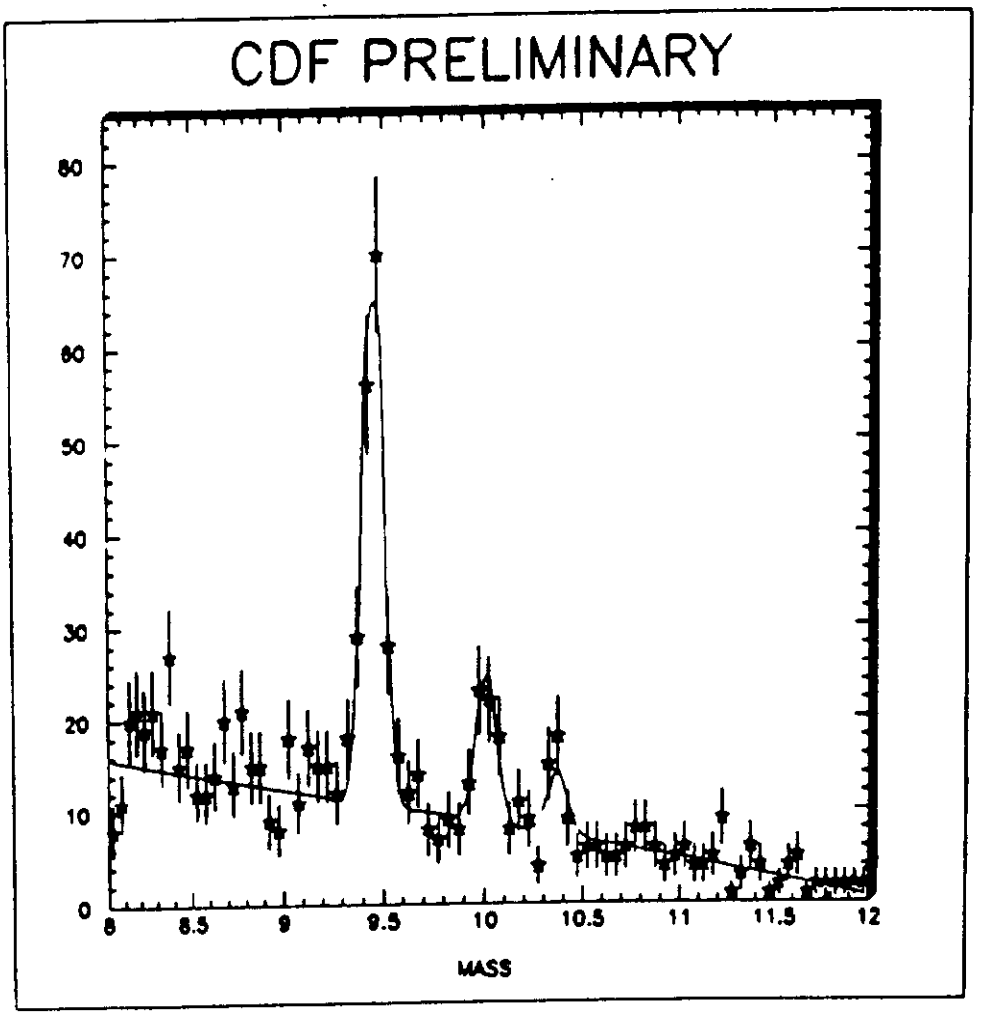
CDF PRELIMINARY
80
70
60
50
40
30
20
10
0
8
8.5
9
9.5
10
10.5
11
11.5
12
MASS

Figure 35

430 ± 12 MeV mean of fit

width = 5.4 MeV

≠ = ψ sidebands

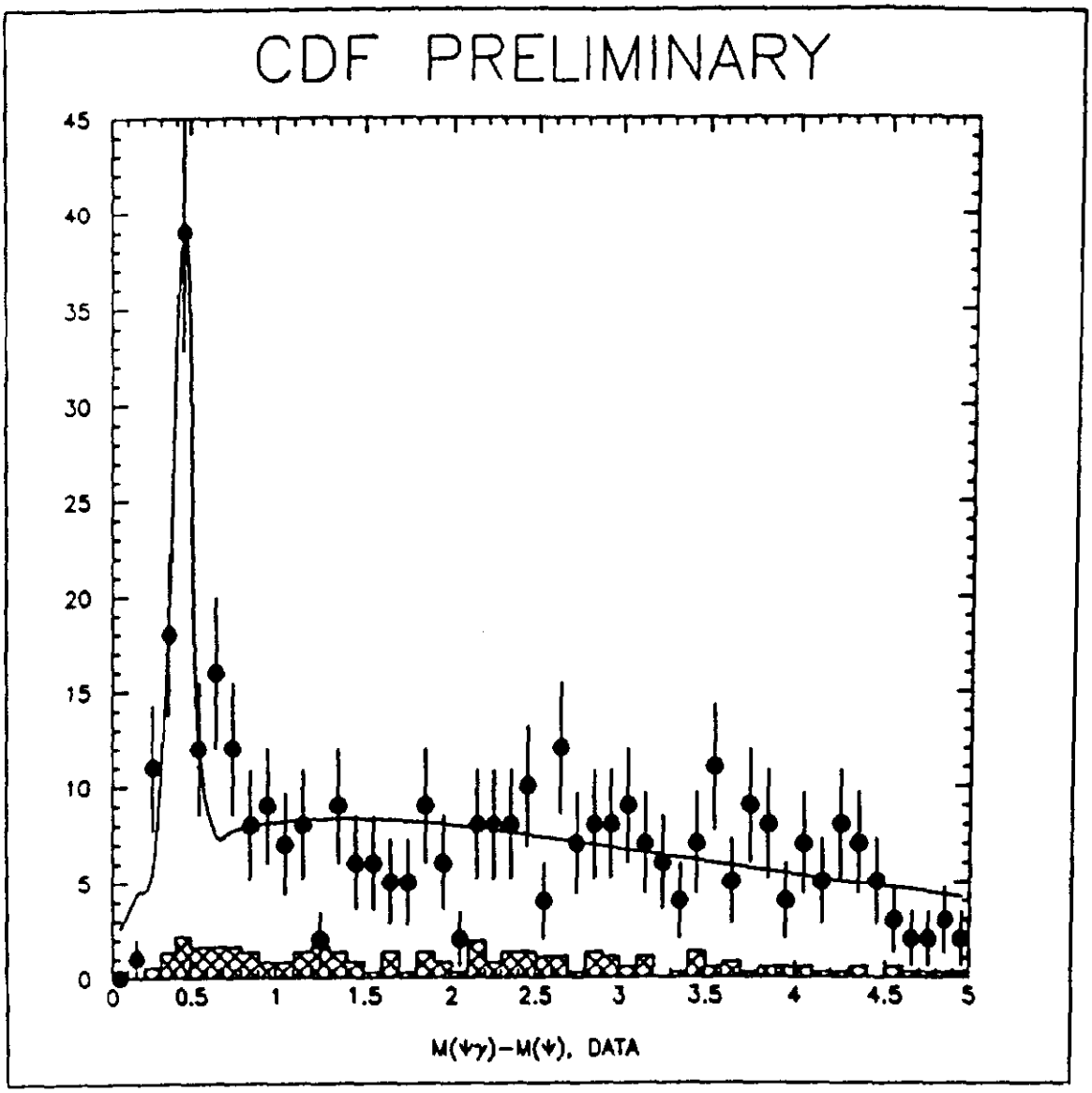

N / 100 MeV

Figure 36

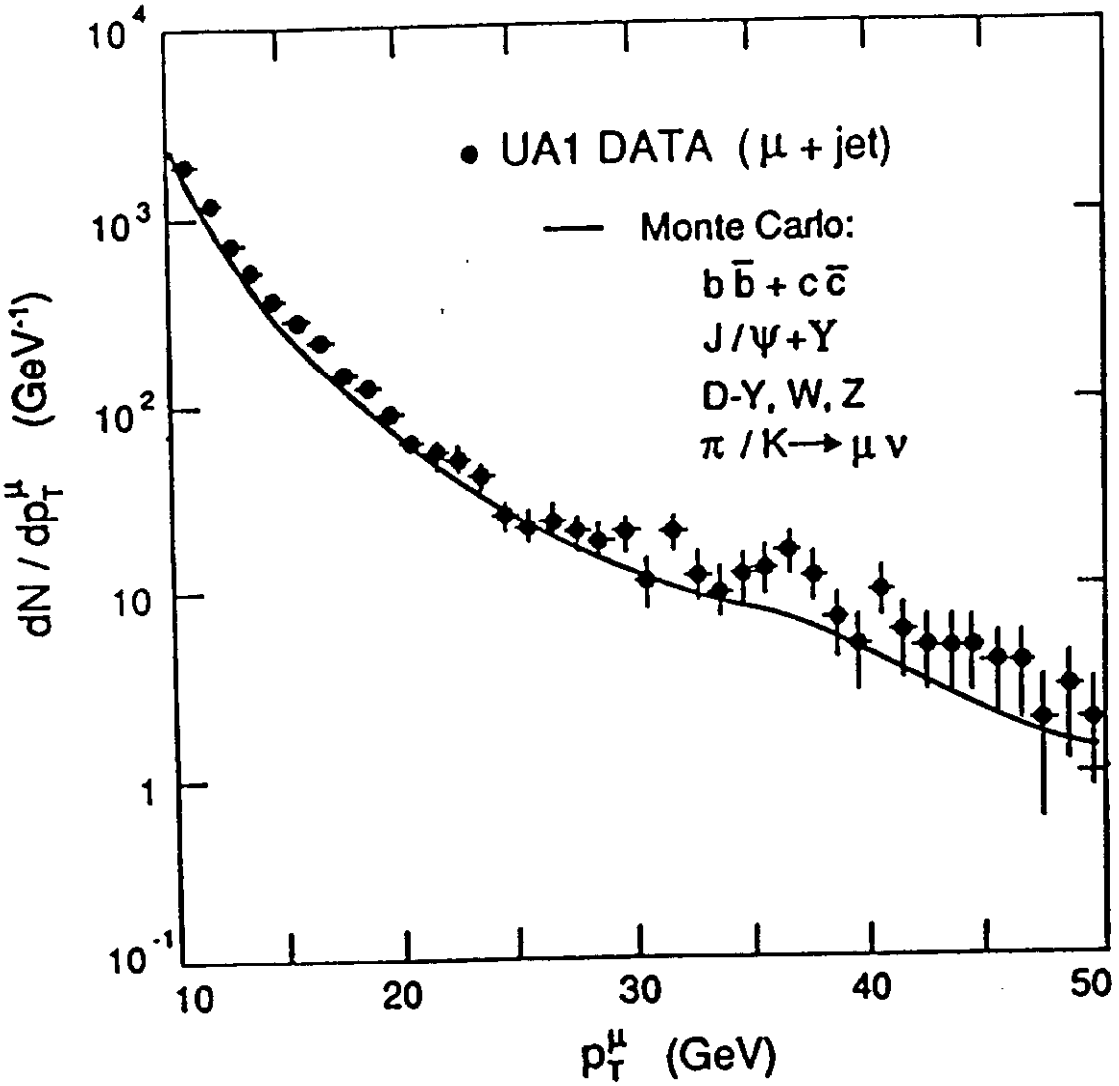
• UA1 DATA (μ + jet)
— Monte Carlo:
b b̄ + c c̄
J/ψ+Υ
D-Y, W, Z
π / K → μ ν
dN / dp_T^μ (GeV^-1)
p_T^μ (GeV)
10^4
10^3
10^2
10
1
10^-1
10
20
30
40
50

Figure 37

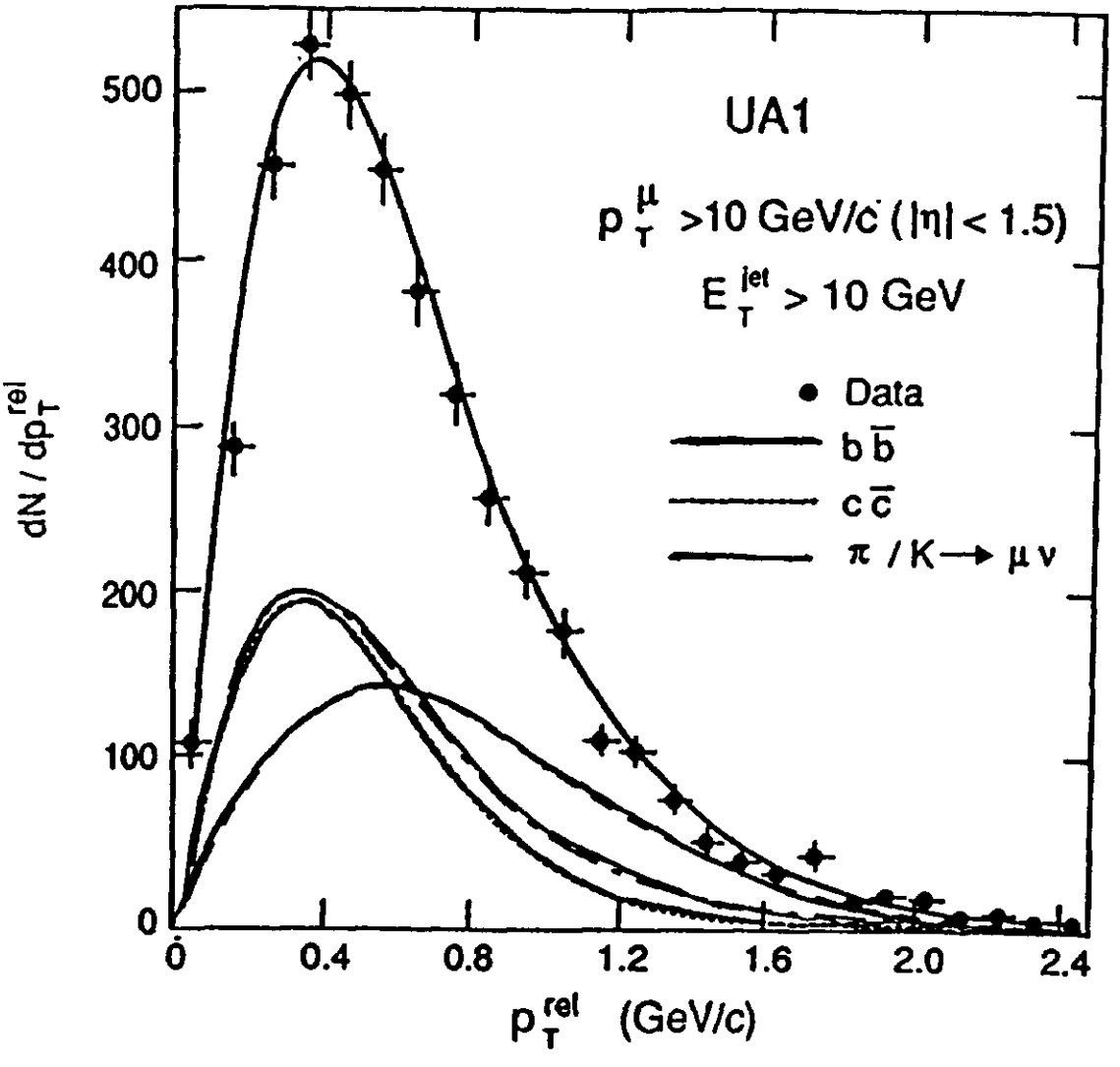
UA1
p_T^μ >10 GeV/c (|η| < 1.5)
E_T^{jet} > 10 GeV
Data
b b̄
c c̄
π / K → μ ν
dN / dp_T^{rel}
p_T^{rel} (GeV/c)
0
100
200
300
400
500
0.4
0.8
1.2
1.6
2.0
2.4

Figure 38

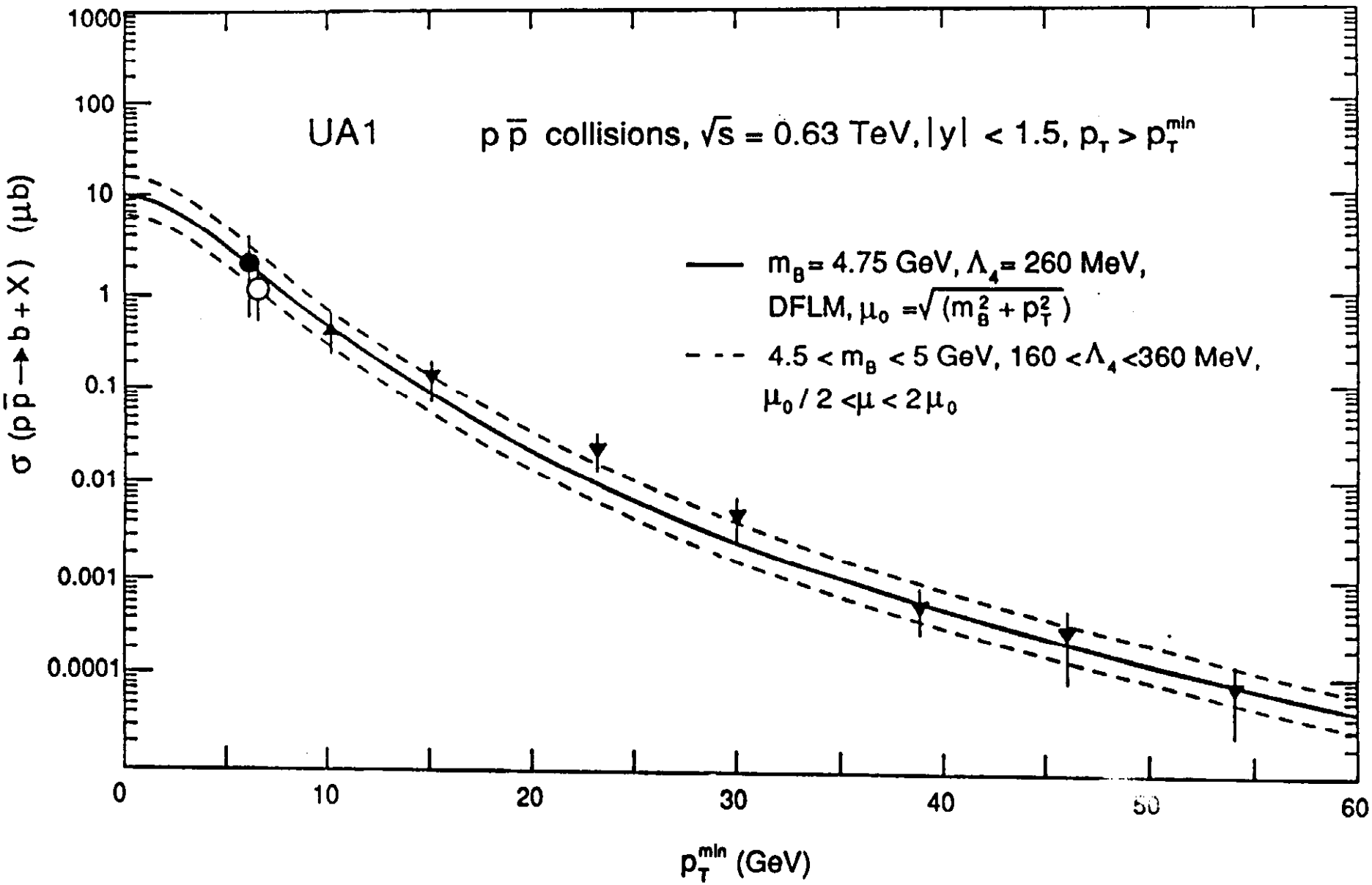
UA1
p p̄ collisions, √s = 0.63 TeV, |y| < 1.5, p_T > p_T^min
m_B = 4.75 GeV, Λ_4 = 260 MeV,
DFLM, μ_0 = √(m_B^2 + p_T^2)
4.5 < m_B < 5 GeV, 160 < Λ_4 < 360 MeV,
μ_0 / 2 < μ < 2 μ_0
σ (p p̄ → b + X) (μb)
p_T^min (GeV)
1000
100
10
1
0.1
0.01
0.001
0.0001
0
10
20
30
40
50
60

Figure 39

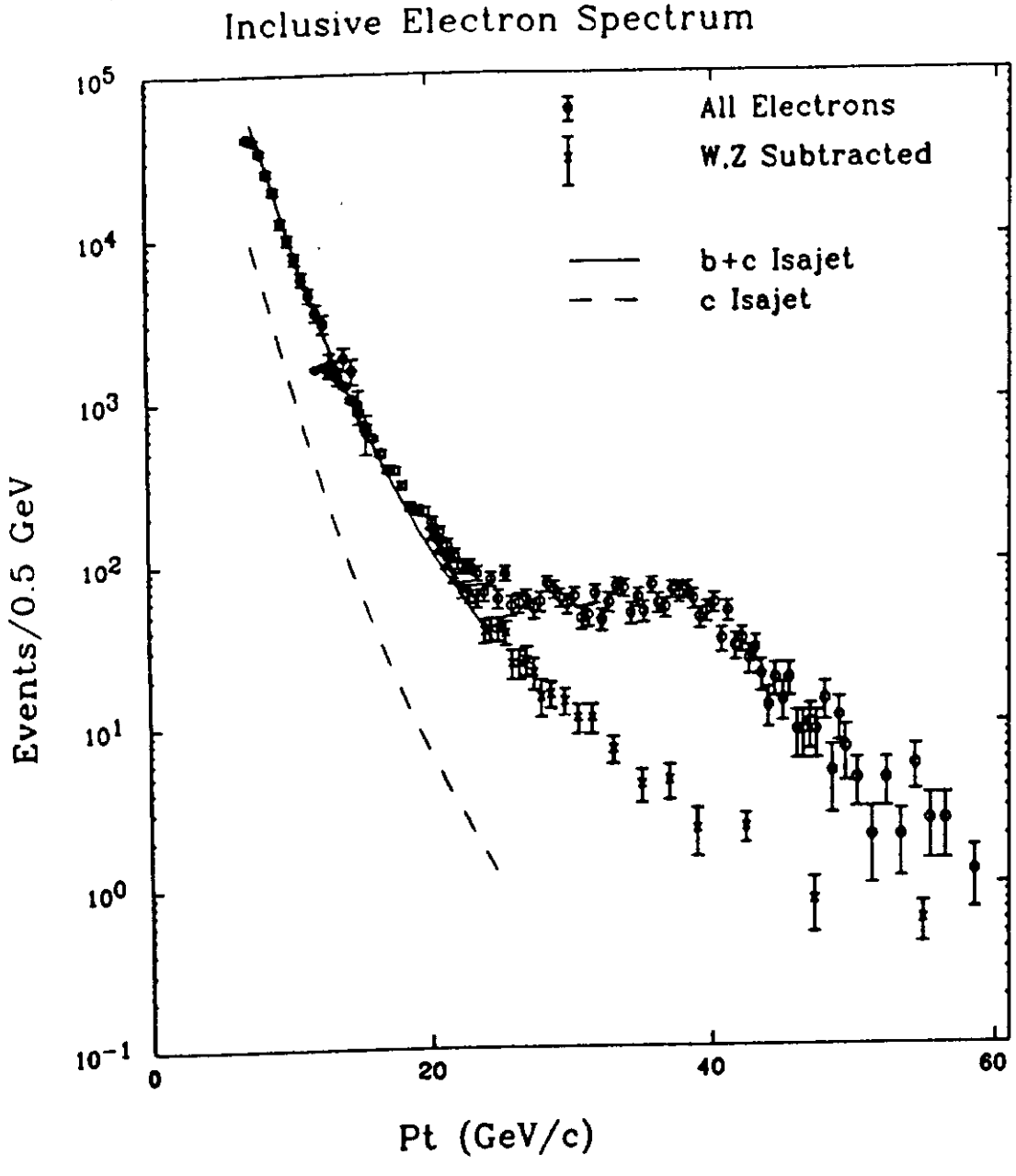
Inclusive Electron Spectrum
All Electrons
W,Z Subtracted
b+c Isajet
c Isajet
Events/0.5 GeV
Pt (GeV/c)
10^5
10^4
10^3
10^2
10^1
10^0
10^{-1}
0
20
40
60

Figure 40

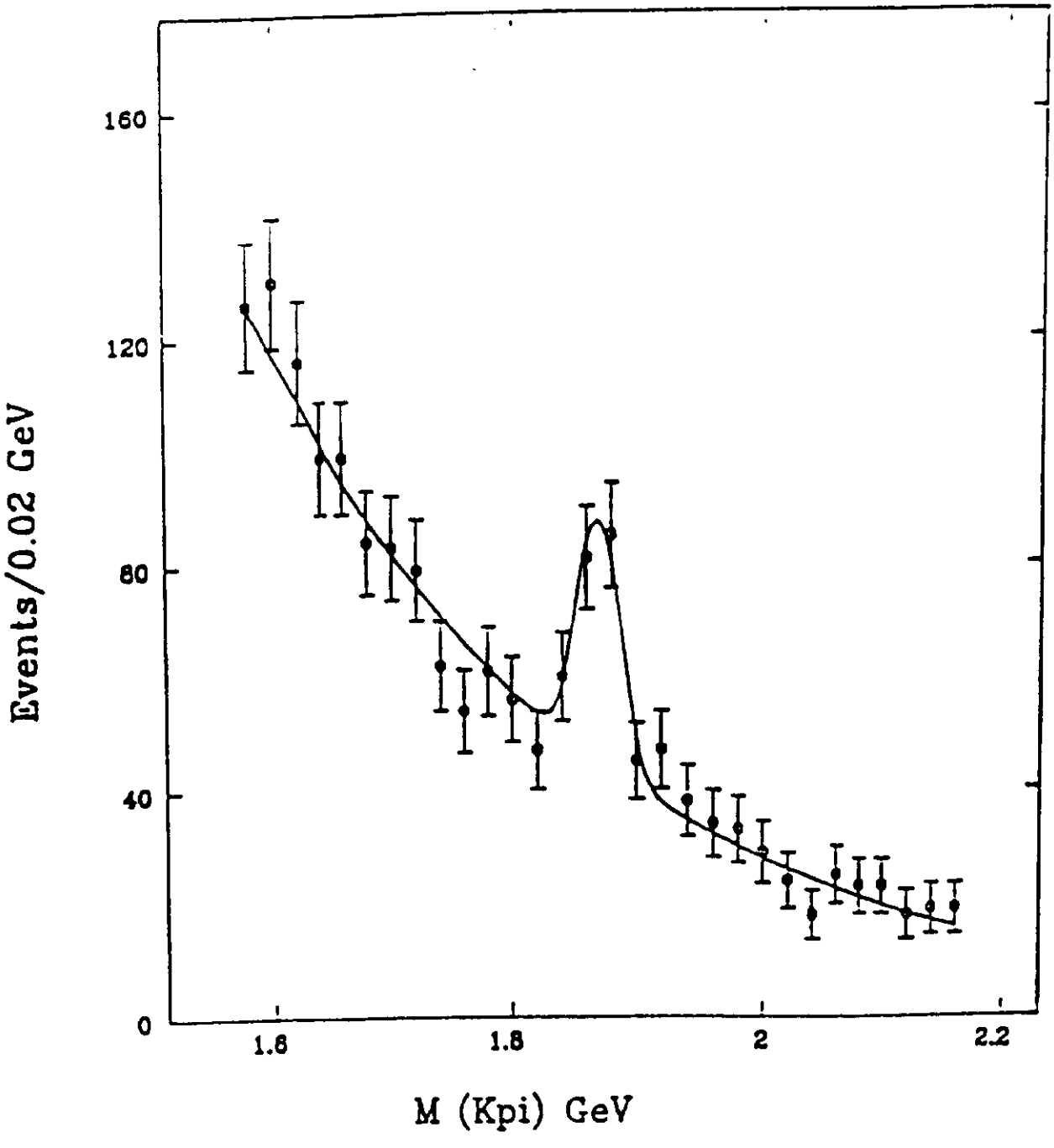

Figure 41

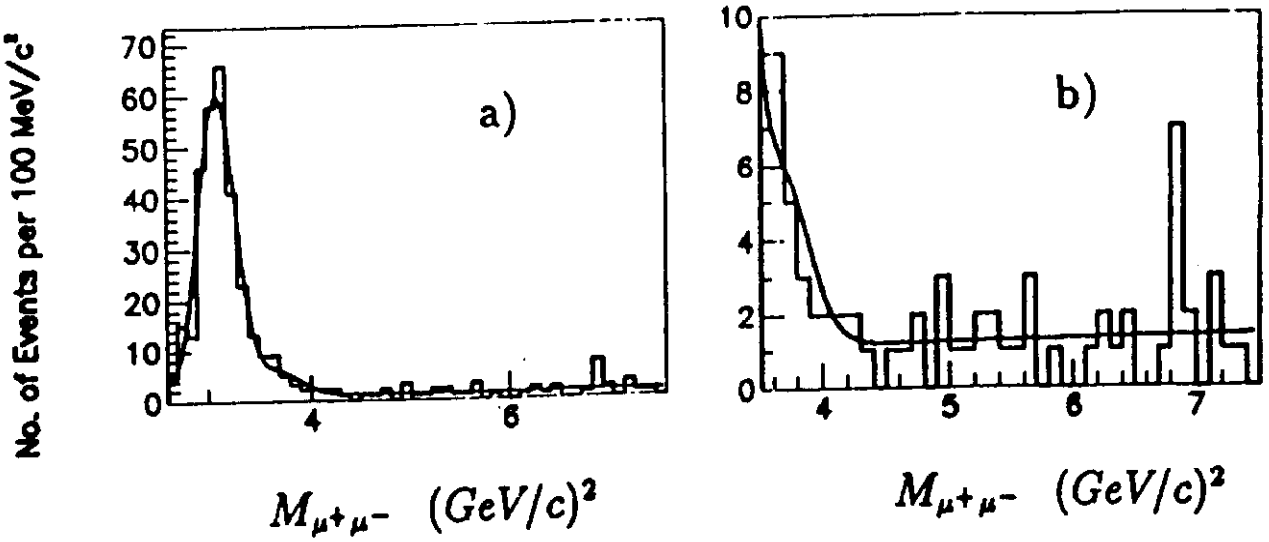

Figure 42

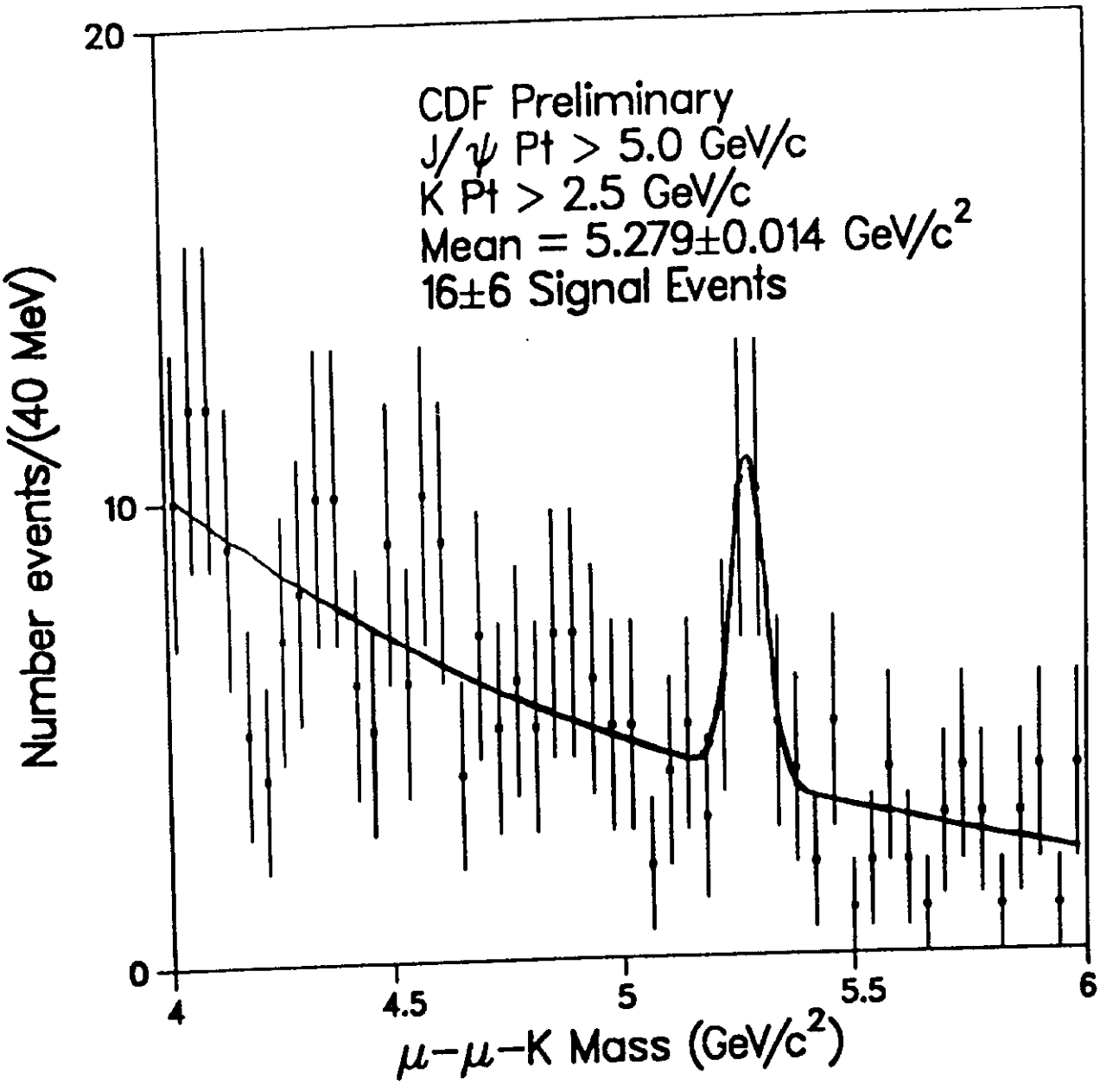
CDF Preliminary
J/ψ Pt > 5.0 GeV/c
K Pt > 2.5 GeV/c
Mean = 5.279±0.014 GeV/c²
16±6 Signal Events
Number events/(40 MeV)
20
10
0
4
4.5
5
5.5
6
μ−μ−K Mass (GeV/c²)

Figure 43

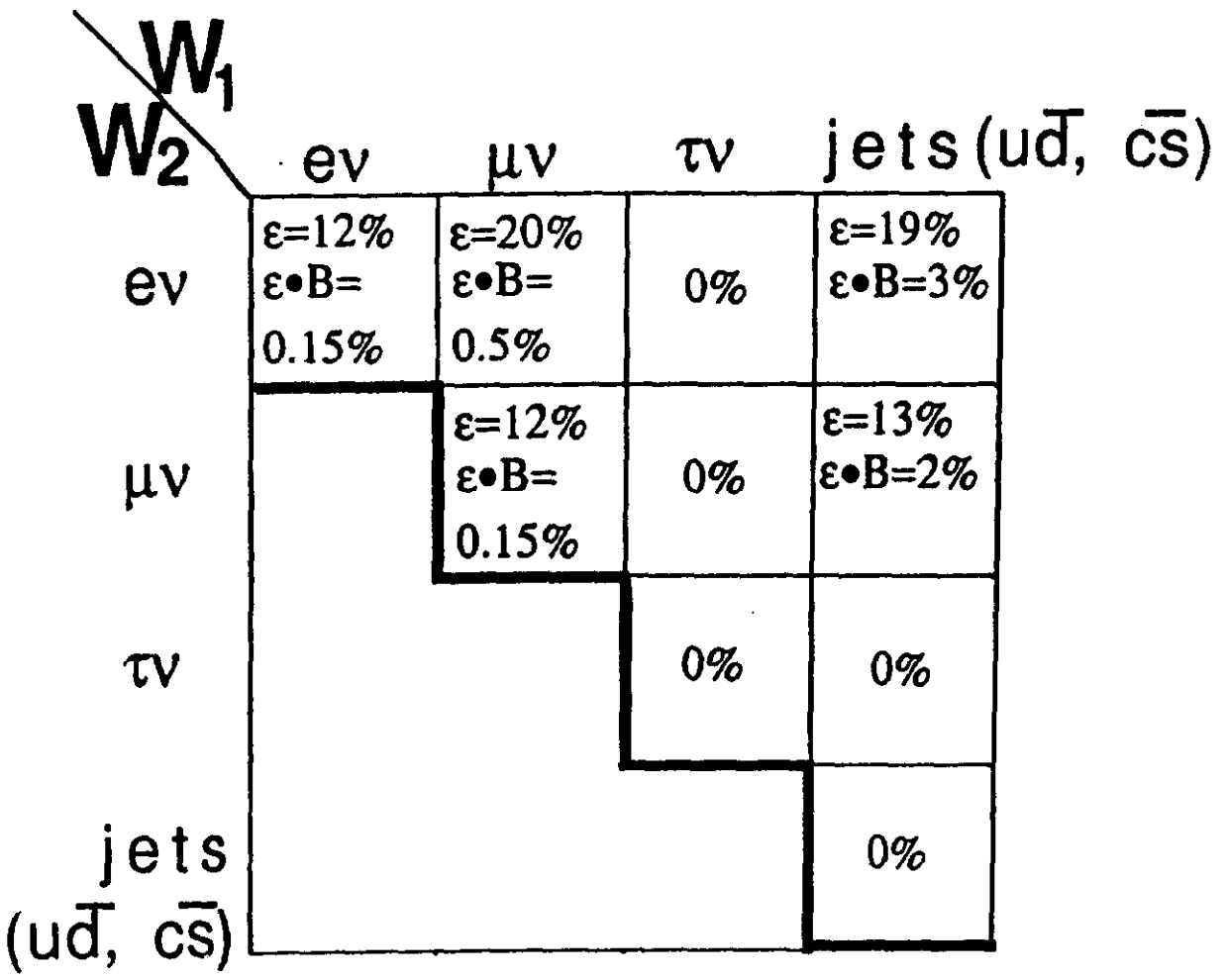
W1
W2
eν
μν
τν
jets (ud̄, cs̄)
ε=12%
ε•B=
0.15%
ε=20%
ε•B=
0.5%
0%
ε=19%
ε•B=3%
ε=12%
ε•B=
0.15%
0%
ε=13%
ε•B=2%
0%
0%
0%

Figure 44

Table I

Sample	Parameter	1 Parameter Fit	2 Parameter Fit
Transverse Mass	m_W (GeV)	80.75 ± 0.31	80.78 ± 0.31
	Γ_W (GeV)	2.1	$1.89^{+0.47}_{-0.40}$
	Conf. Level	84%	89%
P_T(electron)	m_W (GeV)	80.79 ± 0.38	80.83 ± 0.39
	Γ_W (GeV)	2.1	$1.60^{+0.78}_{-0.68}$
	Conf. Level	95%	97%
P_T(neutrino)	m_W (GeV)	80.32 ± 0.41	80.33 ± 0.42
	Γ_W (GeV)	2.1	$2.03^{+0.82}_{-0.73}$
	Conf. Level	83%	88%

Table II

	Model Variation	m_T Fit	$P_T(e)$ Fit	$P_T(\nu)$ Fit
1.	Hadron Resolution/Response and P_T(boson) Distribution	±115	±215	±350
2.	Parton Distributions	±100	±160	±130
3.	Neutrino Scale	±85	–	±170
4.	Electron Resolution	±40	±50	±60
5.	Underlying Event	±30	±50	±20
6.	Fit Procedure	±100	±100	±150
7.	Radiative Decays	+40 ± 40	+60 ± 60	+160 ± 160
	Total	+40 ± 210	+60 ± 300	+160 ± 470

Table III

Uncertainty	Electrons	Muons	Common
STATISTICAL	350	530	
ENERGY SCALE	190	80	80
1. Tracking chamber	80	80	80
2. Calorimeter	175		
SYSTEMATICS	240	315	150
1. Proton structure	60	60	60
2. Resolution, W p_T	145	150	130
3. Parallel balance	170	240	
4. Background	50	110	
5. Fitting	50	50	50
OVERALL	465	620	